DANMARKS OG GRØNLANDS GEOLOGISKE UNDERSØGELSE RAPPORT 2002/44

A1, 2 and 3D backstripping procedure with Application to the Kraka Field

Report for EFP-2001 project: ”Modelling of dynamic Fluid contacts in chalk reservoirs”
ENS J.nr. 1313/01-0004

Ole Valdemar Vejbæk

GEOLOGICAL SURVEY OF DENMARK AND GREENLAND
MINISTRY OF THE ENVIRONMENT

GEUS

DANMARKS OG GRØNLANDS GEOLOGISKE UNDERSØGELSE RAPPORT 2002/44

A1, 2 and 3D backstripping procedure with Application to the Kraka Field

Report for EFP-2001 project: ”Modelling of dynamic Fluid contacts in chalk reservoirs”
ENS J.nr. 1313/01-0004

Ole Valdemar Vejbæk

DANMARKS OG GRØNLANDS GEOLOGISKE UNDERSØGELSE
MILJØMINISTERIET

GEUS

1. Introduction

This report is a contribution to the “modelling of dynamic fluid contacts” project: EFP-2001 (ENS J.nr. 1313/01-0004). The report describes seismic mapping and depth conversion of key horizons covering the Kraka Field (Fig. 1). The purpose of the mapping exercise is to create input for flow modelling, -both representing the present reservoir conditions and at times in the past. For this purpose a first attempt at a backstripping procedure is also developed and applied in 1D, pseudo 2D, and pseudo 3D. The theory is presented together with application/examples of 1-D backstripping of the M-10x well, map based backstripping around the Kraka Field, and a profile on the southeast flank of the Kraka Field. All of these examples are aimed at describing the development of the upper part of the Chalk.

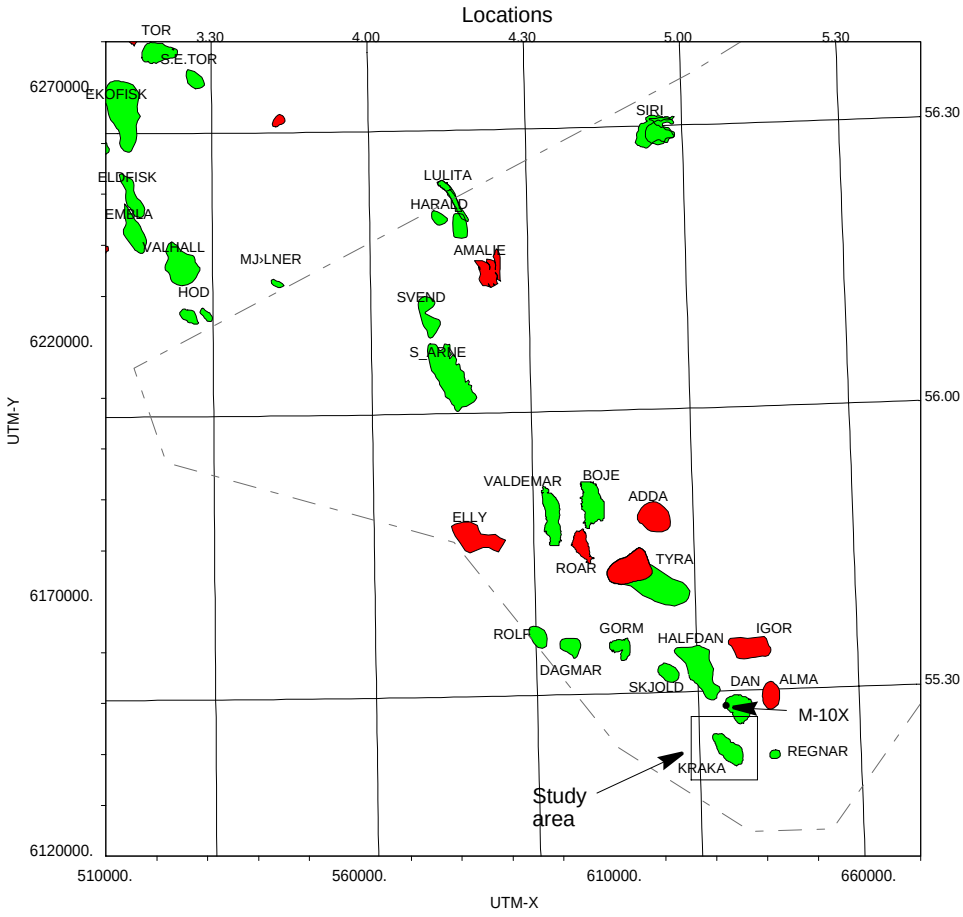

Fig. 1: Location map.

The backstripping procedure describes burial history as well as subsidence compensated for compaction and considering over-pressuring. The porosity development is also described where a boundary condition is the porosity as of today. The backstripping procedure relies on simple analytical methods that allow present porosity to be matched based on simple assumptions on the overpressure development. This approach causes comput-

ing times to be very short and thus allows a high degree of detail in porosity variation to be preserved.
A hypothetical hydrocarbon charging scenario on the Kraka south-east flank is presented as modelled profiles. The model assumes filling at 8 Ma b.p. and discusses subsequent reservoir development. The model is a possibility for testing in the later part of the project.

2. Seismic mapping

The basic seismic data is the merged 3D survey covering the contiguous area (Tredgett and Mooney 1995) This volume is based on a merger of 11 surveys acquired in 1987 to 1993 and covers an area of approximately 1993 km^2. However, only the southernmost part of this survey that covers the Kraka Field, is presented here. An earlier interpretation of the Top Chalk and Top Maastrichtian on these data is expanded and utilised in the present work (Vejbæk 2000). The selection of the Top Maastrichtian by Vejbæk (2000) follows definitions discussed by Kristensen et al. (1995). In addition six reflectors in the Post Chalk succession have been interpreted to support analysis of the Post Chalk subsidence history. Altogether ten horizons have been interpreted in the area (Table 2.1).
The polarity of the seismic data follows the SEG standard with compression pulses corresponding to downward increasing acoustic impedance recorded with negative numbers. Compression pulses and negative numbers for seismic reflections are displayed in red and positive as blue. The term "positive reflection" used below corresponds to a compressional pulse.

Relector name	**Stratigraphy**	**Age**	**Comments**
ovv_Lcen-6	Intra Pliocene	3.5	Estimated age based on position
ovv_ILPlio	Upper Miocene	6	Estimated age
ovv_NTMIO	Near Base Messinian	7.12	Located app. 1 cycle above Near base Messinian in regional 2D (Rasmussen & Dybkjær pers.com.)
ovv_NTMMio	Near Base Tortonian	11.20	Located 1-2 cycles below Base Tortonian in regional 2D (Rasmussen & Dybkjær pers.com.)
ESR_T_Aub	LOD C. aubryae	14.6	Tied from regional 2D (Rasmussen & Dybkjær pers.com.)
ESR_T_Aceras	LOD *C. aceras*	21.1	Tied from regional 2D (Rasmussen & Dybkjær pers.com.)
ovv_t_ch	Top Chalk (Top Ekofisk Formation	61.0	Seismic tie based on Nielsen and Japsen (1990) and completion logs, Age according to Gradstein & Ogg (1996)
ovv_Ttor	Top Tor Formation	65.0	Interpretation based on detailed log correlation (see below)
ovv_Tma4	Top Maastrichtian Unit 4	68	Interpretation based on detailed log correlation (see below)
ovv_buc	Base Chalk	98.9	Seismic tie based on Nielsen and Japsen (1990) and completion logs, Age according to Gradstein & Ogg (1996)

Table 2.1: Interpreted reflectors, statigraphic position, and age in Ma. LOD = last occurrence datum.

The top and base Chalk Group have been interpreted on the basis of well tie information (Nielsen and Japsen 1991). The Top Maa Unit 4 is correlated from a Dan Field interpretation (Kristensen et al. 1995; Vejbæk 2000); and the Top Tor reflector is based on well ties partly from completion report information and earlier regional mapping (Vejbæk 2000). The two latter reflectors are quite difficult to pick in the seismic data due to weak and variable reflection strength and phase and are likely to be revised in the future. The reflectors located in the Cainozoic succession are selected in order to provide a structural overview of Cainozoic subsidence. These reflectors are selected from or correlated to a detailed stratigraphic breakdown of the Cainozoic by Erik Skovbjerg Rasmussen (pers. comm.) under considerations of seismic continuity. As may be evident from table 2.1, only Cainozoic reflectors in the Neogene have been mapped. However, the unresolved Palaeogene interval generally constitutes less than 500 msec of the Cainozoic succession or ¼ of the post chalk interval (see below) and the interval is characterised by relatively slow sedimentation rates. Further subdivision has not been considered to add more information due to uncer-

tainties with reconstructing palaeo-structural configurations in the Palaeogene (see discussions below).
Except the base Chalk map, all structure and isopach maps are depth converted according the approach detail in section 3. The presented maps are listed in Table 2.2.

2.1 Intra Pliocene reflector

This reflector is mapped under the name ovv_Lcen-6 and is located halfway between two reflectors mapped regionally by E. S. Rasmussen (pers. comm.). The latter two reflectors are assigned the ages 1.77 and 5.32 Ma. Based on this, an estimated age of 3.5 Ma is tentatively assigned to the ovv_Lcen-6 reflector. It is thus located within the Pliocene. The reflector is picked at a very continuous positive reflection corresponding to downward increasing acoustic impedance. The reflector pattern above and below display very low-angle west- to southwestward sigmoidal progradation and the surface may display channel like features. For this reason, it is rather unlikely that the reflector was completely horizontal at the time of deposition.

2.2 Upper Miocene reflector

The reflector ovv_ILPlio is located halfway between two reflectors mapped regionally by E. S. Rasmussen (pers. comm.). The latter two reflectors are assigned the ages 5.32 and 7.12 Ma. Based on this, the ovv_ILPlio 6 reflector is assigned an estimated age of 6 Ma which places it within the Late Miocene. The reflector is picked at a very continuous positive reflection corresponding to downward increasing acoustic impedance. The reflector is very suitable to autotracking owing to a very continuous nature. However, a N-S striking narrow zone stretching from the area around the Anne-3 well towards the G-2X well has reduced amplitudes. This is interpreted to reflect lithology changes originating from a laterally varying depositional environment. The reflector is located within a larger package with a low-angle northeast- to northwest-wards sigmoidal progradational reflection pattern. It is therefore rather unlikely that the reflector represents a horizontal surface at the time of deposition and the use of the mapped surface for palaeo-structural reconstruction should be done with caution.

2.3 Near Base Messinian reflector

This reflector is mapped under the name ovv_NTMIO and is assumed nearly equivalent to the Base Messinian based on a tie to regional mapping by E. S. Rasmussen (pers. comm.). The reflectors do not tie exactly. Based on the stratigraphic position the reflector is assigned an age of 7.12 Ma (Gradstein & Ogg 1996). The reflector is picked at a very continuous positive reflection corresponding to downward increasing acoustic impedance. The reflection configuration immediately above and below is generally parallel, but the reflector has scattered channel features apparently cutting into the substratum. The reflector is located within a larger package with a low-angle sigmoidal progradational reflection pattern. It is therefore rather unlikely that the reflector represents a horizontal surface at the time of

deposition and the use of the mapped surface for palaeo-structural reconstruction should be done with caution.

2.4 Near Base Tortonian reflector

This reflector is mapped under the name ovv_NTMMIO and is assumed nearly equivalent to the Base Tortonian based on the approximate tie to regional mapping by E. S. Rasmussen (pers. comm.). The reflectors do not tie exactly. The reflector is often termed “Near Top Middle Miocene” or “Top Overpressure” and is picked at a continuous negative reflection corresponding to downward decreasing acoustic impedance. It is characteristic by separating continuous “railway” reflections above from discontinuous reflections below. The discontinuous reflections below are offset by numerous small-scale faults of little spatial extension, which are assumed a direct indication of over-pressuring. This reflector is therefore interpreted to be at or near the top seal of the over-pressured section below. This pressure “cell” continues downward with the same amount of relative excess pressure to the Top Jurassic, where a further increase occurs. The mapped reflector is itself influenced by the small-scale faulting in the succession below. Slightly irregular (high frequency) curve patterns have, however, been removed by smoothing on the time structure map. The small scale irregularities are not considered to have any bearing on the structural development of the Chalk units. The middle Miocene deposits are interpreted to be pro-delta mud (Michelsen et al. 1998) and may therefore be assumed to have been deposited horizontally albeit in deep waters. For this reason, this reflector is ideal for use in the reconstruction of Palaeo-structural configurations of deeper levels. The reflection configuration above is clearly on- or down-lapping.

2.5 Top Aub reflector

This reflector is located 100-200 msec deeper than the Base Tortonian within the presumably overpressured lower Cainozoic succession. The reflector is picked from a tie to regional mapping by E. S. Rasmussen (pers. comm.). This reflector correlates with the LOD of the dinoflagellate cyst *Cousteaudinium aubryae*, hence the name (K. Dybkjær, pers. comm.). This LOD is located in the lowermost Serravallian corresponding to 14.6 Ma (Mid Miocene; Williams et al. 1998, Gradstein & Ogg 1996). It is a relatively strong positive (red) reflector and is very discontinuous due to some combination of numerous small-scale faults and a possible bad stack caused by a velocity inversion below the Base Tortonian. However, since it is located near the top of the over-pressured section where formation pressure are likely to be closest to the fracture gradient, faulting is a plausible explanation for most of the discontinuous nature of the reflector. The pronounced local (high frequency) topography originating from the discontinuous nature has no direct bearing on the structure of the Chalk horizons. For this reason, heavy smoothing has been applied to the final map to make it useful for backstripping.

2.6 Top Aceras reflector

This reflector is located in the middle of the overpressure section, roughly halfway between the Base Tortonian and the Top Chalk reflectors. The reflector is picked from a tie to regional mapping by E. S. Rasmussen (pers. comm.). The reflector correlates with the LOD of the dinoflagellate cyst *Caligodinium aceras*, hence the name. This LOD is located in the upper Aquitanian corresponding to 21.1 Ma (lower Miocene; Williams et al. 1998). Like the Top Aub, this reflector is also characterised by small-scale high frequency topography due to some combination of numerous small-scale faults and possibly bad stacking. It is, however, somewhat more continuous than the Top Aub, owing to sub-critical over-pressuring and/or lesser problems originating from velocity inversion during stacking. However, strong smoothing has also been applied.

2.7 Top Chalk

This reflector is picked at a generally positive reflection. It is usually strong and continuous and therefore relatively easy to follow. However, in the presence of gas, it looses amplitude and may even obtain reverse polarity. This occurs in the crestal areas of the Dan and Kraka Fields.

2.8 Top Tor reflector

This reflector has a strongly variable nature going from strongly positive to strongly negative. The amplitude changes are mainly related to rock property variations other than fluid content variations. The interpretation is therefore rather tentative; it is subject to rather large uncertainty and is strongly dependent on well tie information. The conformable configuration relative to the Top Chalk and Top Maa Unit 4 reflectors combined with structural considerations reduces the interpretation uncertainty. The amplitude variations are probably caused by minor variations in depositional environment and diagenetic alterations occurring penecontemporaneous with deposition. These variations are probably related to palaeo- bathymetri that for instance may cause hardground formation resulting in a positive reflection. The reflector is important, as it separates Danian Chalk from Maastrichtian Chalk with remarkably different reservoir properties (Engstrøm 1995; Frykman 2001; Vejbæk 2002). The interpretation relies heavily on support from log correlation and synthetic seismic modelling. Autotracking is virtually impossible and thus render mapping very time consuming.

2.9 Top Maa Unit 4 reflector

This reflector is a somewhat weak, but rather continuously positive reflector. It is therefore generally interpreted with higher confidence than the Top Tor reflector. In minor areas, it looses amplitude, but only with local reversals. The interpretation is supported, but only to some extent dependent on well tie information. The reflector is chosen based on the work with the subdivision Dan Field reservoir as presented by Kristensen et al. (1995). This work

presents subdivision using the combined information from log, biostratigraphic and seismic data. As reflectors are assumed to have chronostratigraphic significance, this subdivision provides a good basis for selecting regional correlation. The work of Kristensen et al. (1995) presents a further subdivision of the interval between the Top Maa Unit 4 and the Top Tor reflectors. However, regional seismic correlation of the further subdivision is not considered feasible. Based on log and biostratigraphic data, it may be possible to transfer the subdivision to other fields. The Top Maa Unit 4 reflector is located within the Maastrichtian and in many cases, it represents the boundary between reservoir quality and relatively tighter Maastrichtian Chalk below.

2.10 Base Chalk reflector

This reflector is a relatively strong continuous negative reflector that in general is relatively easy to follow. In wells, the reflector ties with the Cenomanian – Albian boundary equivalent to the base of the Chalk Group. However, in some synclines that probably represent palaeo-bathymetric depressions as suggested by the Chalk isopach map, an alternative interpretation emerges. The alternative appears as a deeper continuous negative reflection, and is unchecked by wells where it exists. However, in this report this alternative has been interpreted as defining the base of a Lower Cretaceous unit that represents the last subsidence caused by abating extensional tectonic movements. Since extensional tectonics is assumed to cease at the Cenomanian - Albian boundary, the shallower option has been chosen (Vejbæk & Andersen 2001).

2.11 Isopach maps

A number of isopach maps have been generated to illustrate the tectonic development (Figs. 12 – 19; Table 2.2). In some cases they may approximate palaeo structural configurations of the lower reflector at the time corresponding to the upper reflector. However, the isopach have not been decompacted, and in some case, the upper reflector was most likely not horizontal at the time of deposition. Except for the Upper Tor and Ekofisk Formation isopachs (Figs. 12 & 13), the isopach maps are contoured with the same range and contour interval to allow direct comparison. Qualitatively the isopach maps may indicate that most of the growth of the Kraka structure occurred in the time interval 61 – 21 Ma b. p. (Fig. 14) and gradually abating until 6 Ma b.p. with only slight additional movement. More detailed estimates on the structural development should, however, encompass backstripping as discussed below.

Fig no.	Interval	C.I.	Text
2	1900-2400	25	Base Chalk time structure map
3	1800-2300	25	Top Maa unit 4 (Mid Tor Formation) depth structure map
4	1700-2200	25	Top Tor depth structure map
5	1700-2200	25	Top Chalk depth structure map
6	1400-1700	15	LOD C. Aceras depth structure map (21.1Ma b.p.)
7	1100-1400	15	LOD C. Aub depth structure map (14.6 Ma b.p.)
8	1100-1400	15	Near Base Tortonian depth structure map (11.2 Ma b.p.)
9	700-1000	15	Near Base Messinian depth structure map (7.12 Ma b.p.)
10	500-800	15	Upper Miocene reflector depth structure map (6 Ma. b.p.)
11	400-700	15	Intra Pliocene reflector depth structure map (3.5 Ma b.p.)
12	30-150	6	Upper Tor Formation isopach map (66-65 Ma b.p.)
13	20-70	2.5	Ekofisk Formation isopach map (65-61 Ma b.p.)
14	0-500	25	Palaeocene-Oligocene isopach map (61-21.1 Ma b.p.)
15	0-500	25	Aquitanian isopach map (21.1-14.6 Ma b.p.)
16	0-500	25	Mid Miocene isopach map (14.6-11.2 Ma b.p.)
17	0-500	25	Tortonian isopach map (11.2-7.12 Ma b.p.)
18	0-500	25	Messinian isopach map (7.12-6 Ma b.p.)
19	0-500	25	Lower Pliocene isopach map (6-3.5 Ma b.p.)

Table 2.2: Depth structure and isopach maps presented in this report.

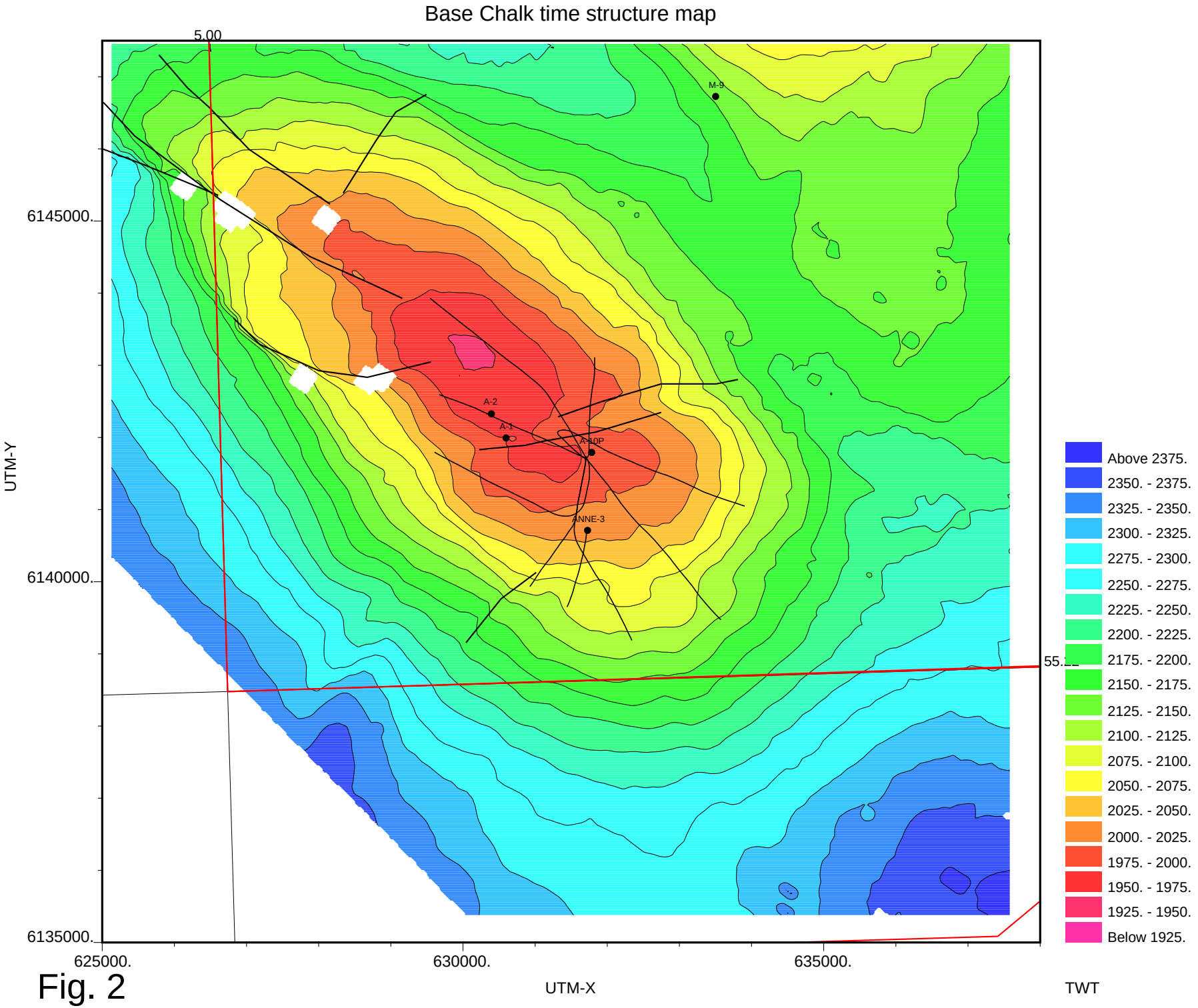
Base Chalk time structure map
5.00
6145000.
6140000.
6135000.
625000.
630000.
635000.
UTM-Y
UTM-X
TWT
M-9
A-2
A-1
A-10P
ANNE-3
55.
Above 2375.
2350. - 2375.
2325. - 2350.
2300. - 2325.
2275. - 2300.
2250. - 2275.
2225. - 2250.
2200. - 2225.
2175. - 2200.
2150. - 2175.
2125. - 2150.
2100. - 2125.
2075. - 2100.
2050. - 2075.
2025. - 2050.
2000. - 2025.
1975. - 2000.
1950. - 1975.
1925. - 1950.
Below 1925.

Fig. 2

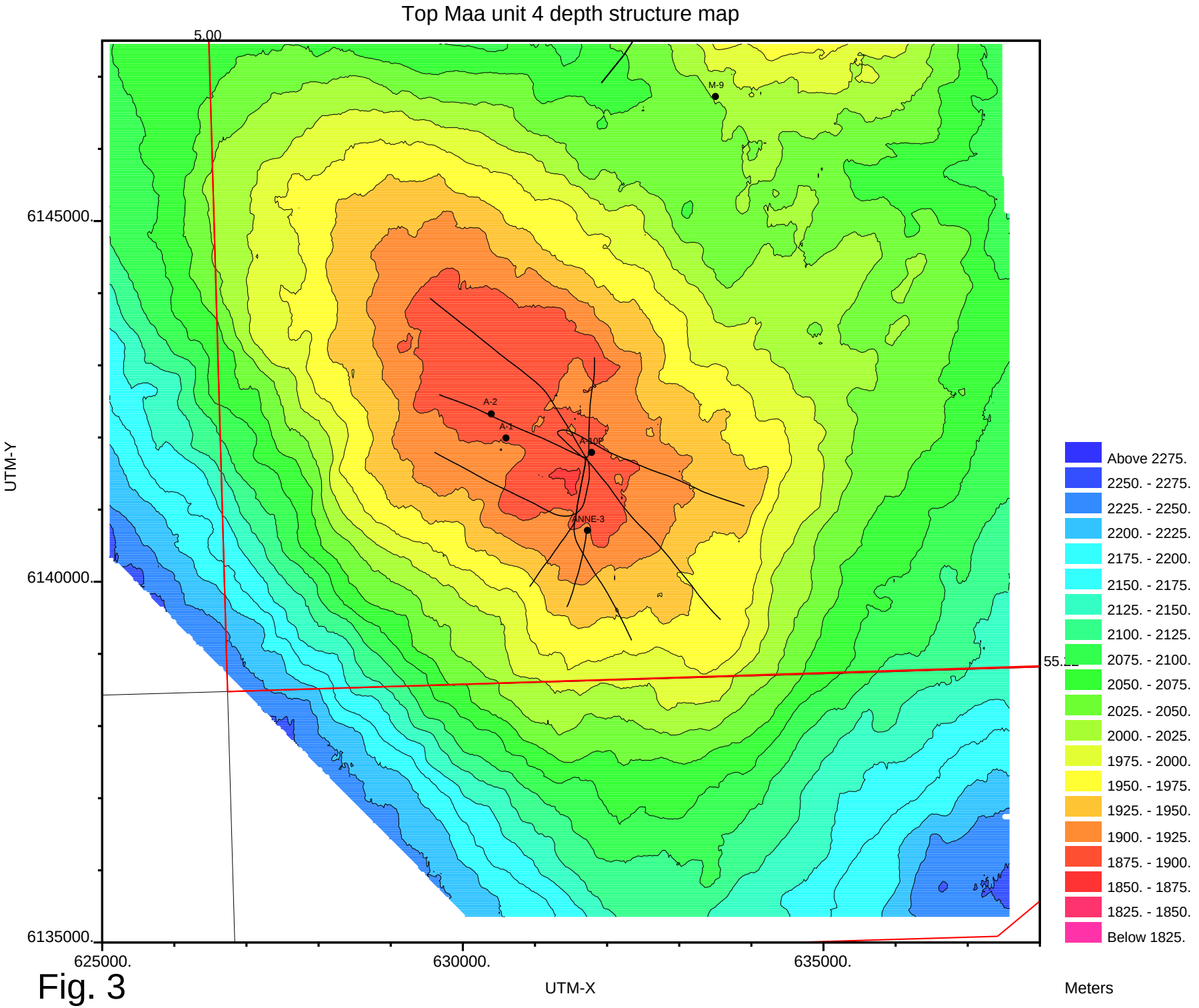
Top Maa unit 4 depth structure map
5.00
6145000.
6140000.
6135000.
625000.
630000.
635000.
UTM-Y
UTM-X
M-9
A-2
A-1
A-10P
ANNE-3
Above 2275.
2250. - 2275.
2225. - 2250.
2200. - 2225.
2175. - 2200.
2150. - 2175.
2125. - 2150.
2100. - 2125.
2075. - 2100.
2050. - 2075.
2025. - 2050.
2000. - 2025.
1975. - 2000.
1950. - 1975.
1925. - 1950.
1900. - 1925.
1875. - 1900.
1850. - 1875.
1825. - 1850.
Below 1825.
Meters

Fig. 3

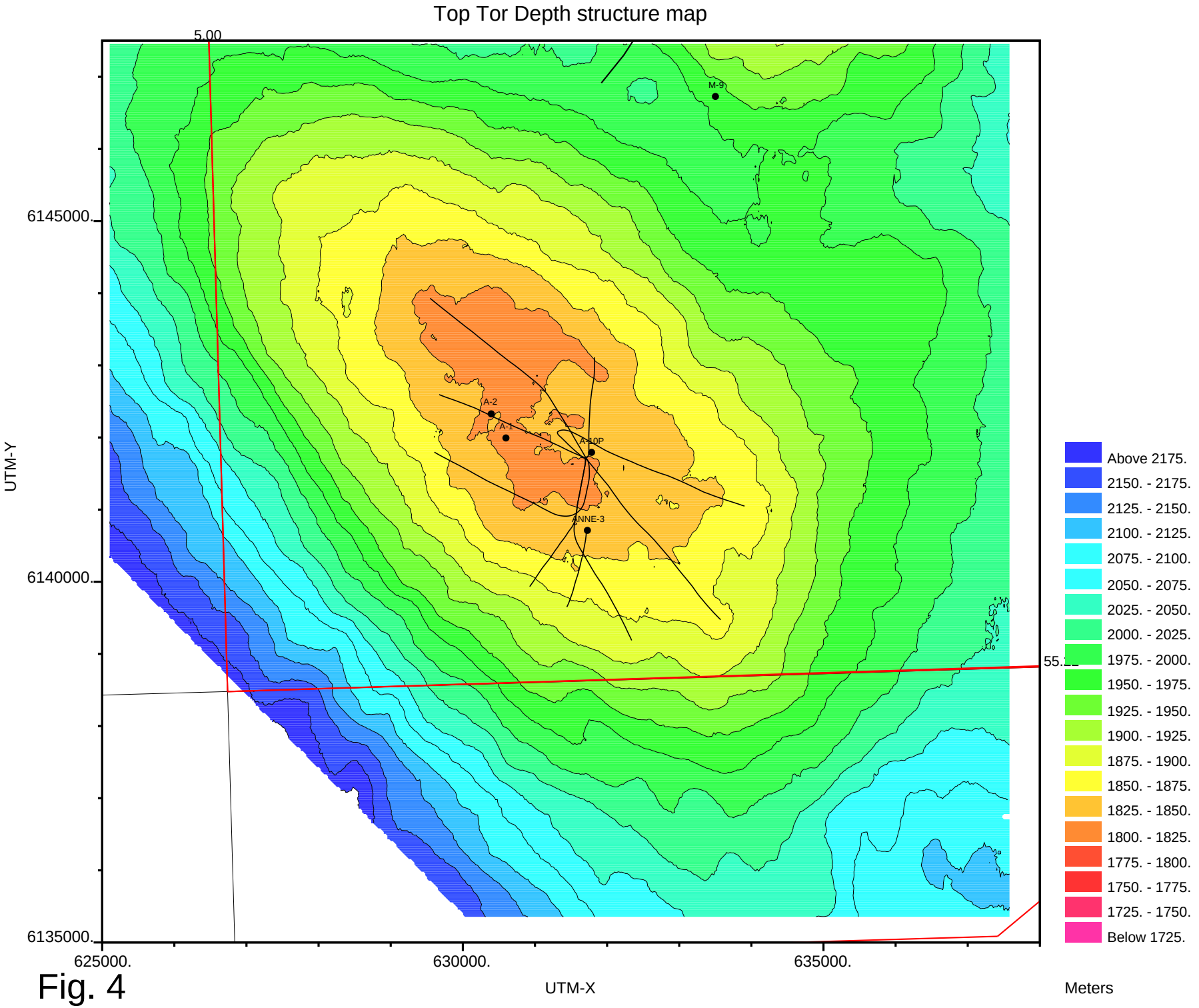
Top Tor Depth structure map
5.00
6145000.
6140000.
6135000.
625000.
630000.
635000.
UTM-Y
UTM-X
M-9
A-2
A-1
A-10P
ANNE-3
Above 2175.
2150. - 2175.
2125. - 2150.
2100. - 2125.
2075. - 2100.
2050. - 2075.
2025. - 2050.
2000. - 2025.
1975. - 2000.
1950. - 1975.
1925. - 1950.
1900. - 1925.
1875. - 1900.
1850. - 1875.
1825. - 1850.
1800. - 1825.
1775. - 1800.
1750. - 1775.
1725. - 1750.
Below 1725.
Meters

Fig. 4

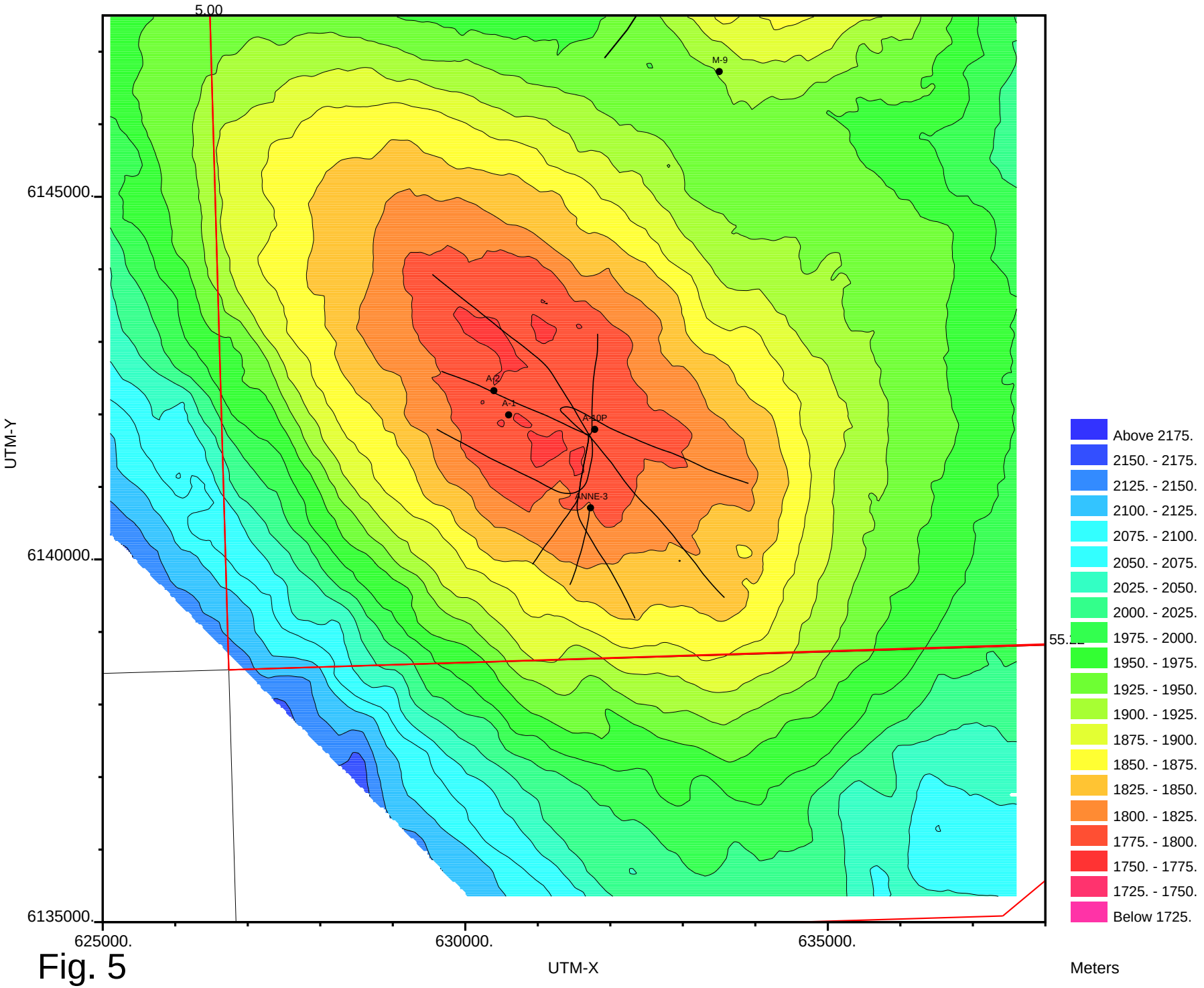
Kraka Field Depth structure map.
5.00
M-9
A-2
A-1
A-10P
ANNE-3
6145000.
6140000.
6135000.
625000.
630000.
635000.
UTM-Y
UTM-X
Meters
Above 2175.
2150. - 2175.
2125. - 2150.
2100. - 2125.
2075. - 2100.
2050. - 2075.
2025. - 2050.
2000. - 2025.
1975. - 2000.
1950. - 1975.
1925. - 1950.
1900. - 1925.
1875. - 1900.
1850. - 1875.
1825. - 1850.
1800. - 1825.
1775. - 1800.
1750. - 1775.
1725. - 1750.
Below 1725.

Fig. 5

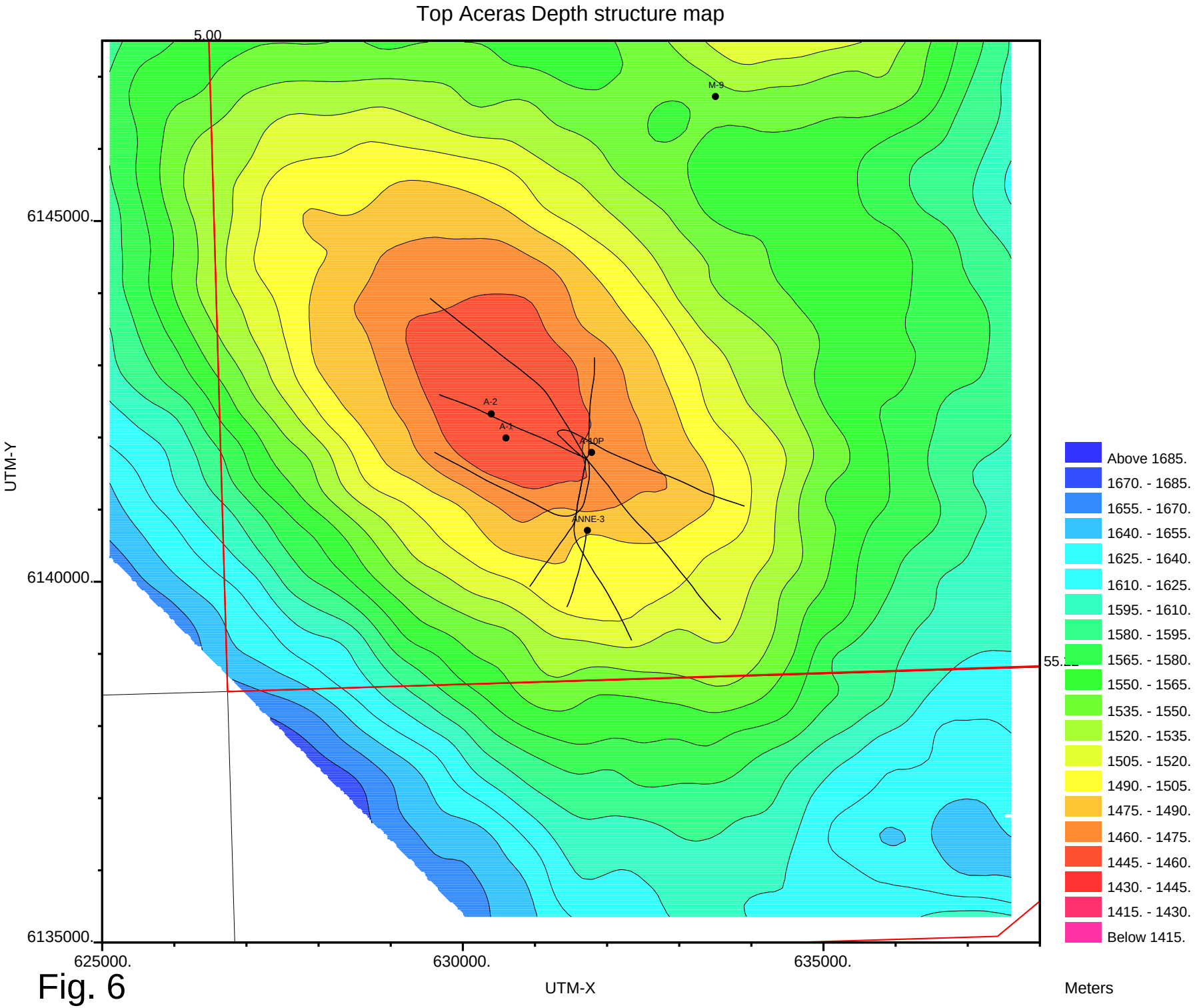
Top Aceras Depth structure map
5.00
6145000.
6140000.
6135000.
625000.
630000.
635000.
UTM-Y
UTM-X
M-9
A-2
A-1
A-10P
ANNE-3
Above 1685.
1670. - 1685.
1655. - 1670.
1640. - 1655.
1625. - 1640.
1610. - 1625.
1595. - 1610.
1580. - 1595.
1565. - 1580.
1550. - 1565.
1535. - 1550.
1520. - 1535.
1505. - 1520.
1490. - 1505.
1475. - 1490.
1460. - 1475.
1445. - 1460.
1430. - 1445.
1415. - 1430.
Below 1415.
Meters

Fig. 6

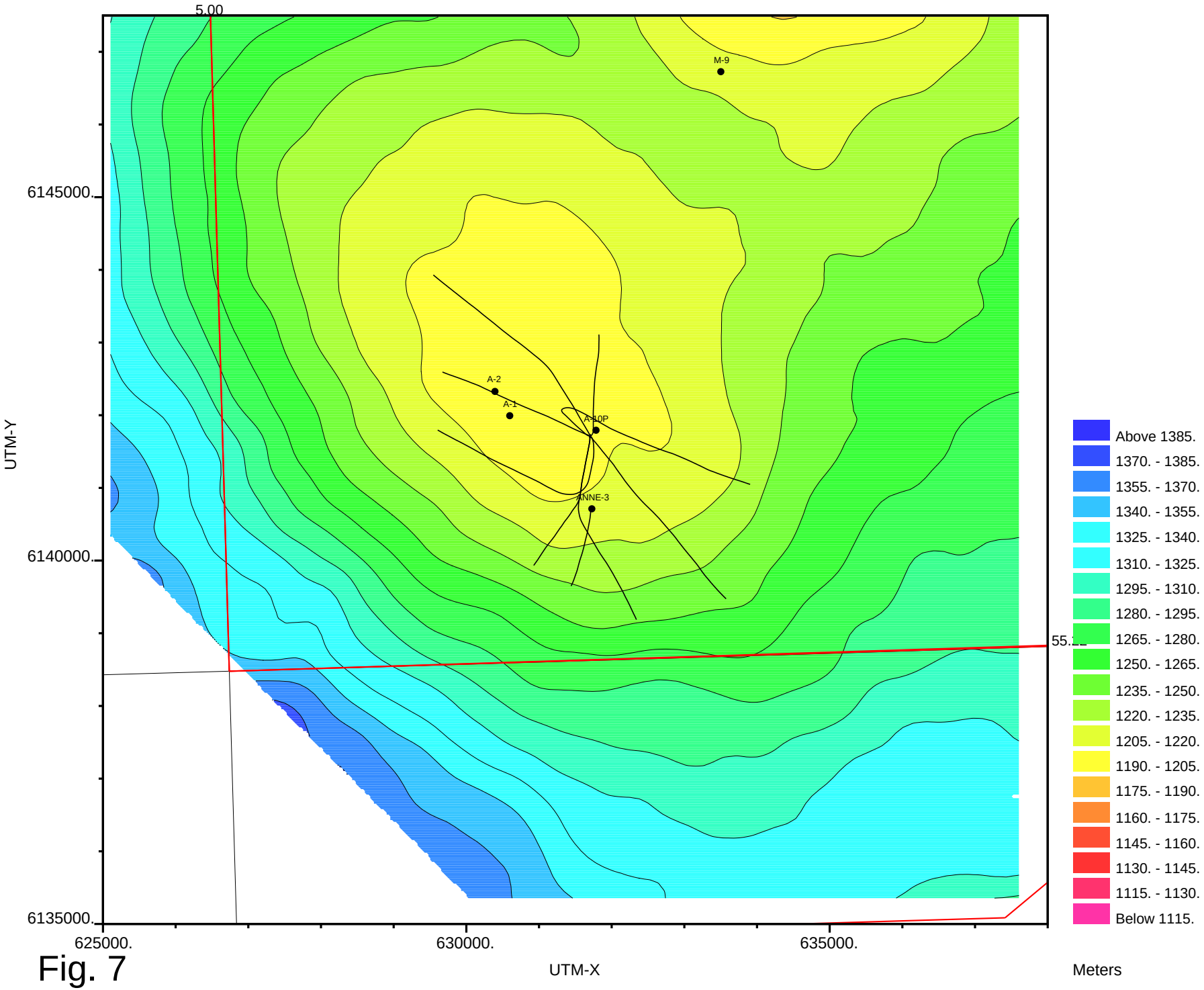
Top Aub Depth structure map (14.6Ma)
5.00
6145000.
6140000.
6135000.
625000.
630000.
635000.
UTM-Y
UTM-X
M-9
A-2
A-1
A-10P
ANNE-3
55.
Above 1385.
1370. - 1385.
1355. - 1370.
1340. - 1355.
1325. - 1340.
1310. - 1325.
1295. - 1310.
1280. - 1295.
1265. - 1280.
1250. - 1265.
1235. - 1250.
1220. - 1235.
1205. - 1220.
1190. - 1205.
1175. - 1190.
1160. - 1175.
1145. - 1160.
1130. - 1145.
1115. - 1130.
Below 1115.
Meters

Fig. 7

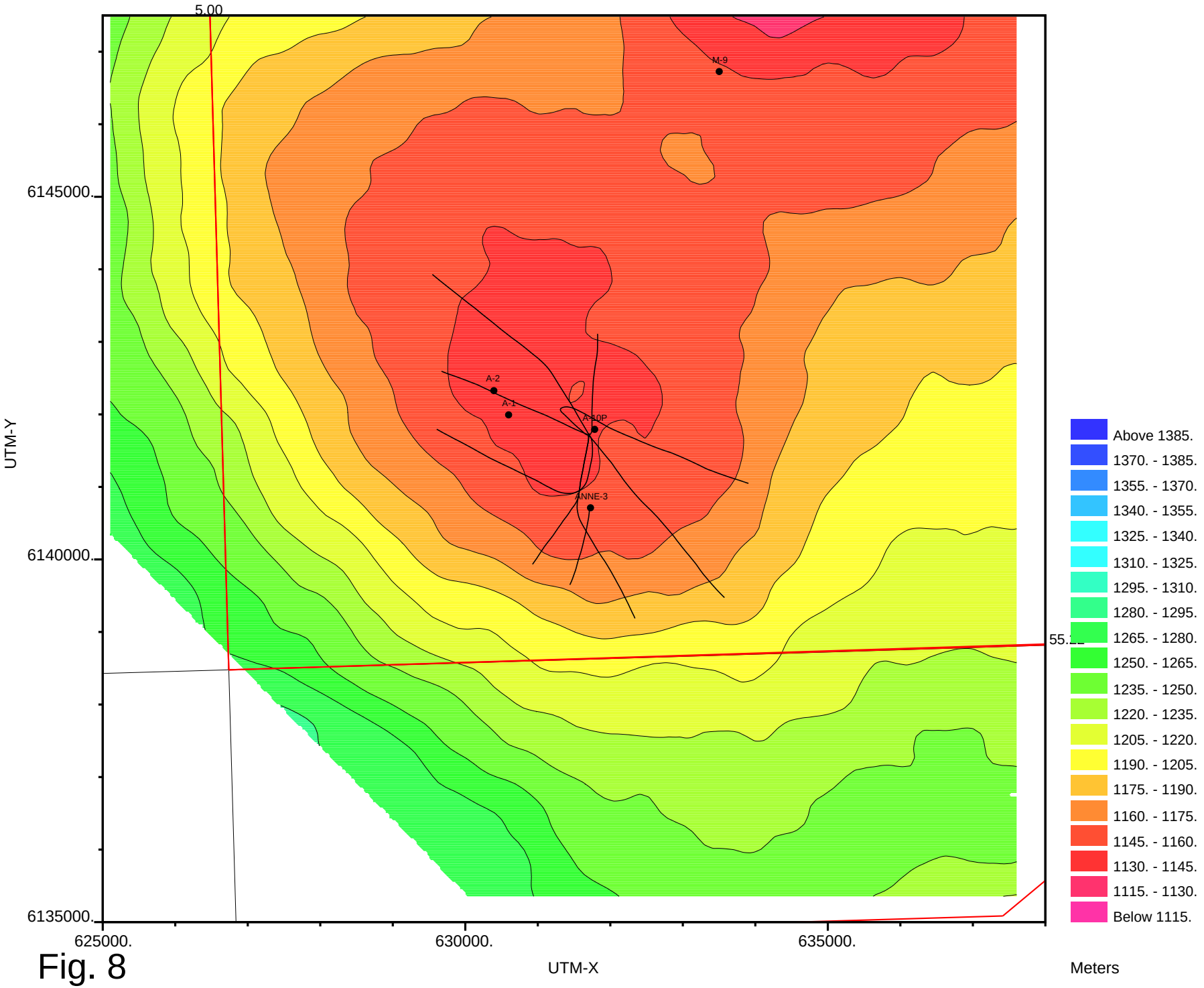
Near Base Tortonian depth structure map (11.2Ma)
5.00
6145000.
6140000.
6135000.
625000.
630000.
635000.
UTM-Y
UTM-X
Meters
M-9
A-2
A-1
A-10P
ANNE-3
Above 1385.
1370. - 1385.
1355. - 1370.
1340. - 1355.
1325. - 1340.
1310. - 1325.
1295. - 1310.
1280. - 1295.
1265. - 1280.
1250. - 1265.
1235. - 1250.
1220. - 1235.
1205. - 1220.
1190. - 1205.
1175. - 1190.
1160. - 1175.
1145. - 1160.
1130. - 1145.
1115. - 1130.
Below 1115.

Fig. 8

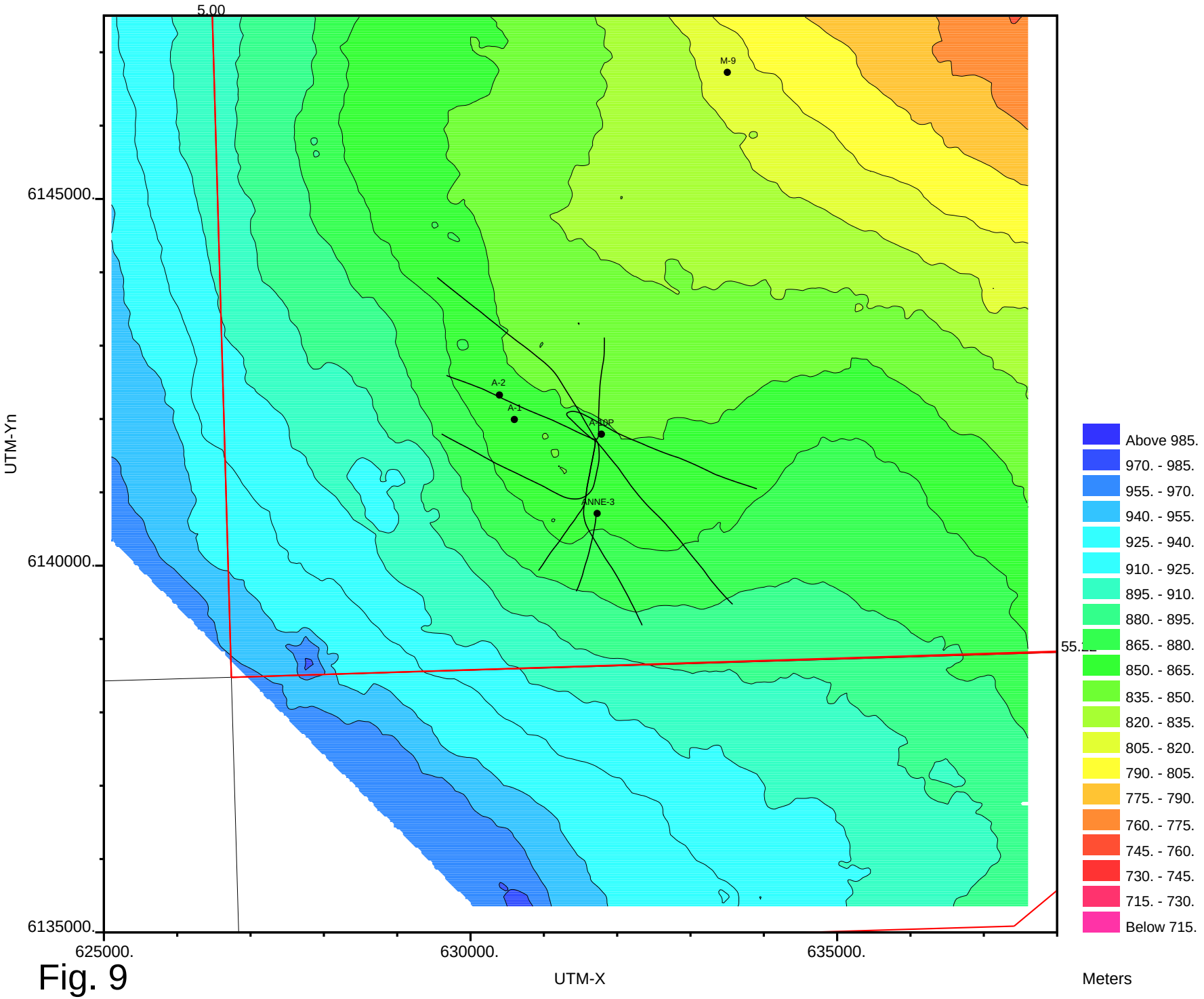
Near Base Messinian Depth structure map (7.12Ma)
5.00
6145000.
6140000.
6135000.
625000.
630000.
635000.
UTM-Yn
UTM-X
M-9
A-2
A-1
A-10P
ANNE-3
Above 985.
970. - 985.
955. - 970.
940. - 955.
925. - 940.
910. - 925.
895. - 910.
880. - 895.
865. - 880.
850. - 865.
835. - 850.
820. - 835.
805. - 820.
790. - 805.
775. - 790.
760. - 775.
745. - 760.
730. - 745.
715. - 730.
Below 715.
Meters

Fig. 9

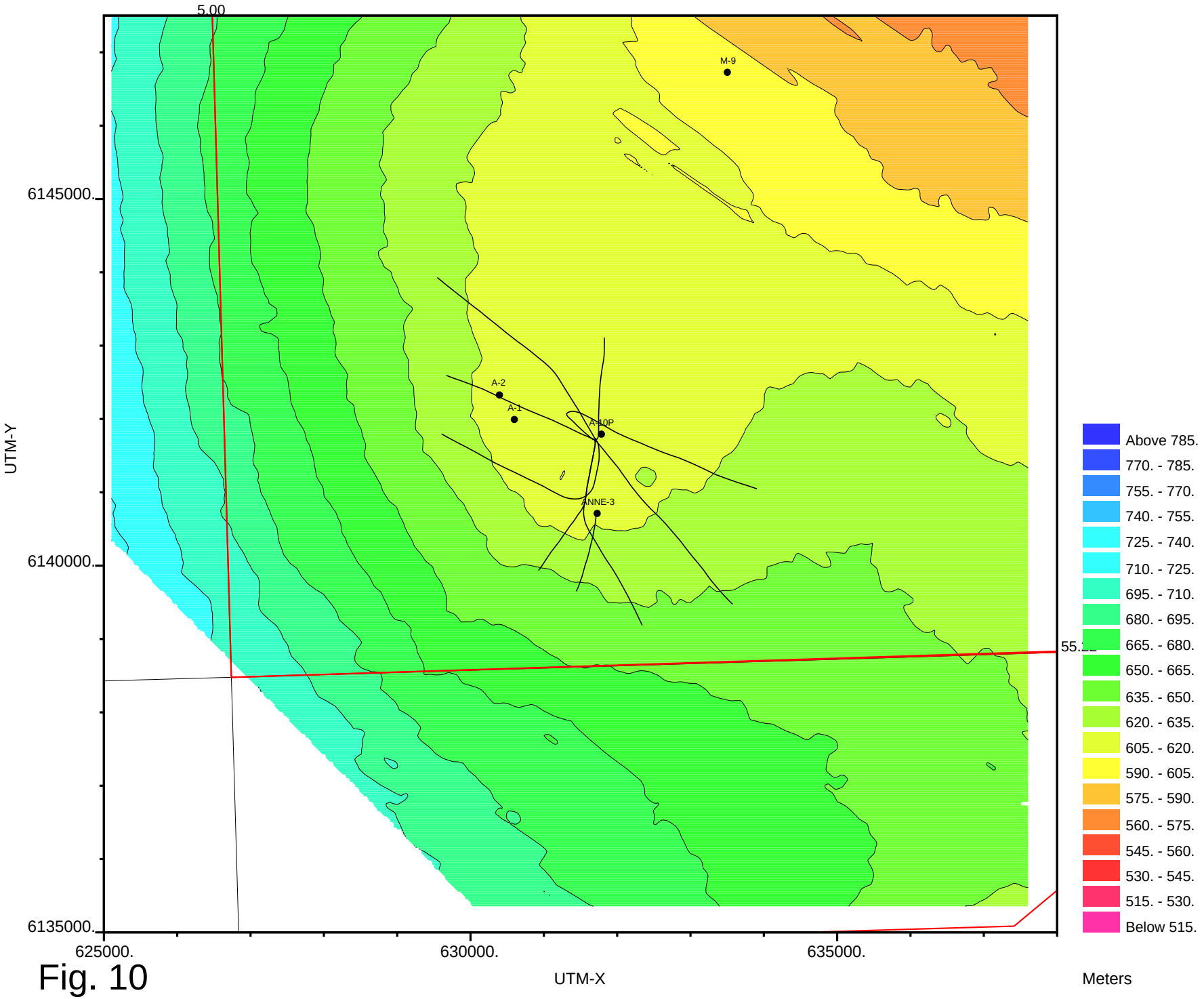
Upper Miocene Depth structure map (6Ma)
5.00
6145000.
6140000.
6135000.
625000.
630000.
635000.
UTM-Y
UTM-X
M-9
A-2
A-1
A-10P
ANNE-3
55.
Above 785.
770. - 785.
755. - 770.
740. - 755.
725. - 740.
710. - 725.
695. - 710.
680. - 695.
665. - 680.
650. - 665.
635. - 650.
620. - 635.
605. - 620.
590. - 605.
575. - 590.
560. - 575.
545. - 560.
530. - 545.
515. - 530.
Below 515.
Meters

Fig. 10

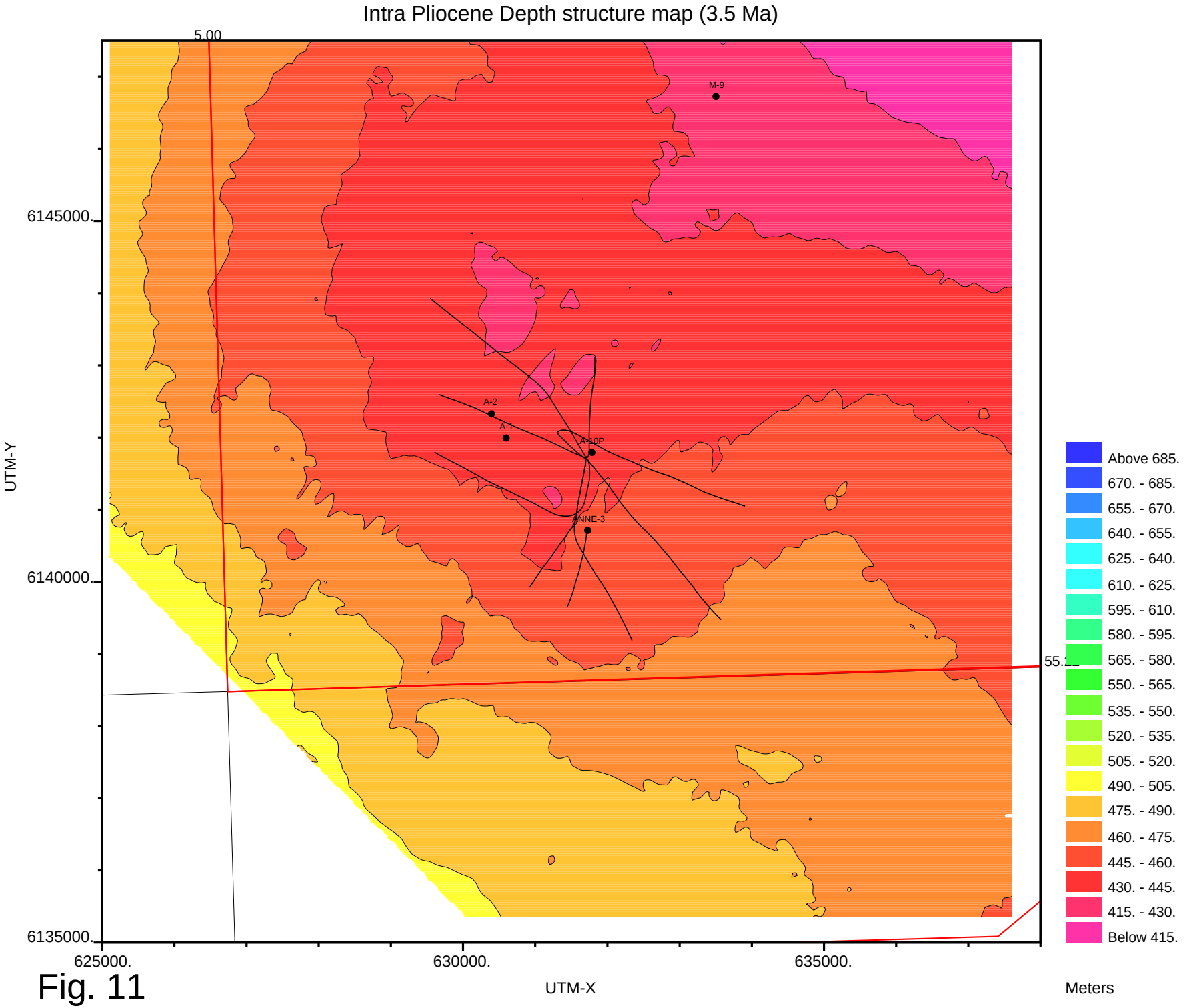
Intra Pliocene Depth structure map (3.5 Ma)
5.00
M-9
A-2
A-1
A-10P
ANNE-3
6145000.
6140000.
6135000.
55.
625000.
630000.
635000.
UTM-Y
UTM-X
Meters
Above 685.
670. - 685.
655. - 670.
640. - 655.
625. - 640.
610. - 625.
595. - 610.
580. - 595.
565. - 580.
550. - 565.
535. - 550.
520. - 535.
505. - 520.
490. - 505.
475. - 490.
460. - 475.
445. - 460.
430. - 445.
415. - 430.
Below 415.

Fig. 11

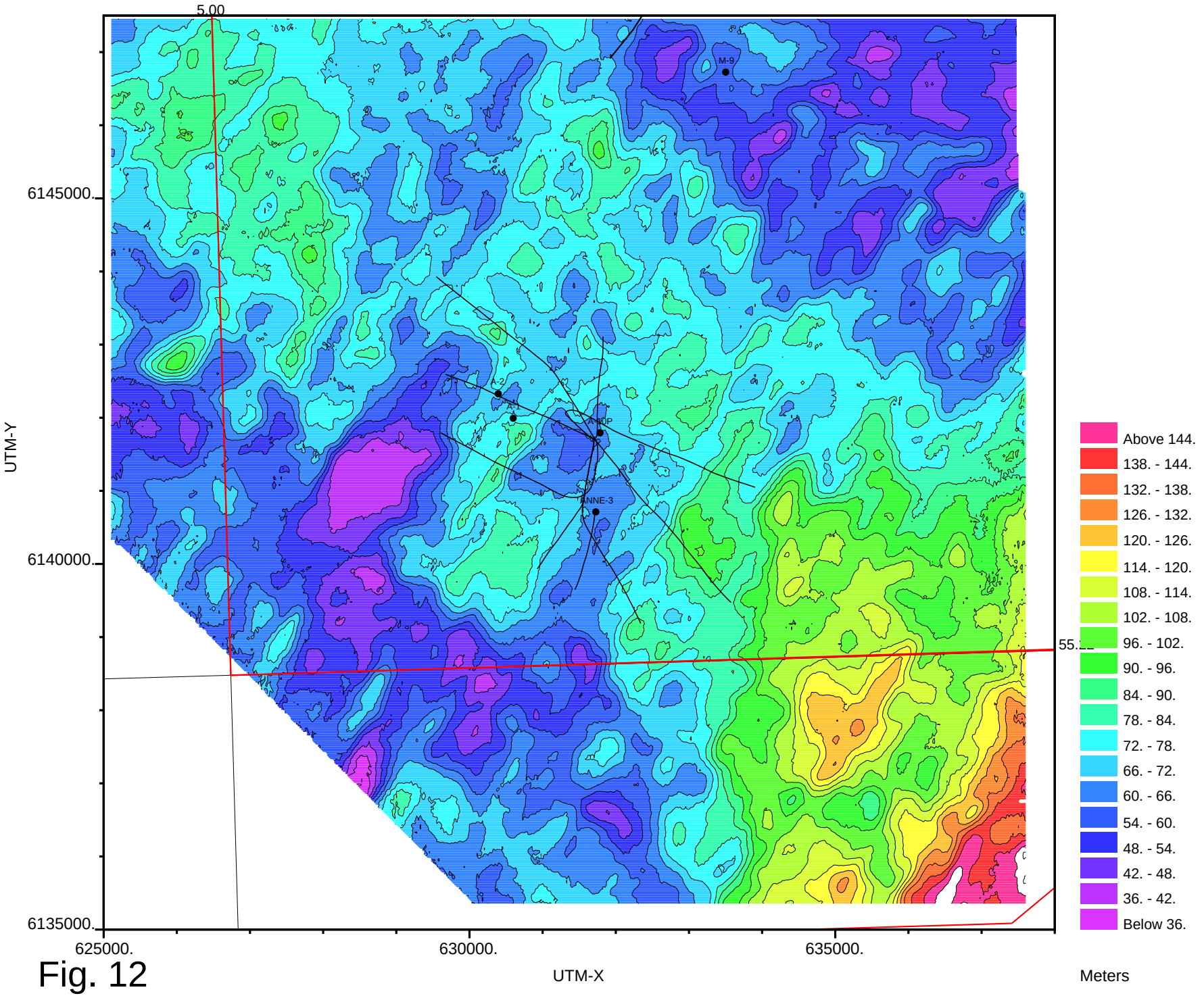
Isopach Maa units 1-3
5.00
6145000.
6140000.
6135000.
625000.
630000.
635000.
UTM-Y
UTM-X
M-9
A-2
A-1
A-3DP
ANNE-3
55.
Above 144.
138. - 144.
132. - 138.
126. - 132.
120. - 126.
114. - 120.
108. - 114.
102. - 108.
96. - 102.
90. - 96.
84. - 90.
78. - 84.
72. - 78.
66. - 72.
60. - 66.
54. - 60.
48. - 54.
42. - 48.
36. - 42.
Below 36.
Meters

Fig. 12

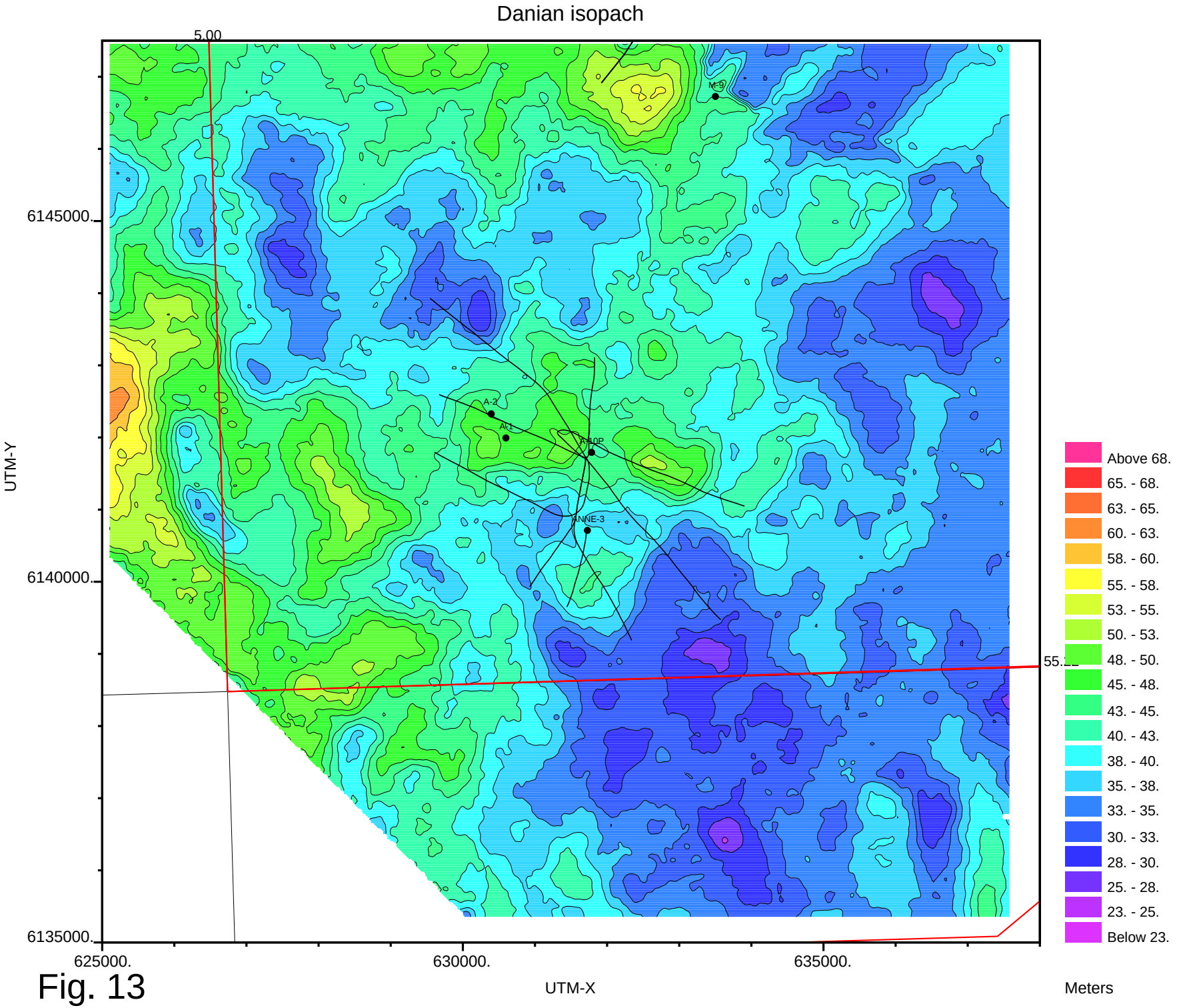
Danian isopach
5.00
6145000.
6140000.
6135000.
UTM-Y
625000.
630000.
635000.
UTM-X
M-9
A-2
A-1
A-10P
ANNE-3
55.
Above 68.
65. - 68.
63. - 65.
60. - 63.
58. - 60.
55. - 58.
53. - 55.
50. - 53.
48. - 50.
45. - 48.
43. - 45.
40. - 43.
38. - 40.
35. - 38.
33. - 35.
30. - 33.
28. - 30.
25. - 28.
23. - 25.
Below 23.
Meters

Fig. 13

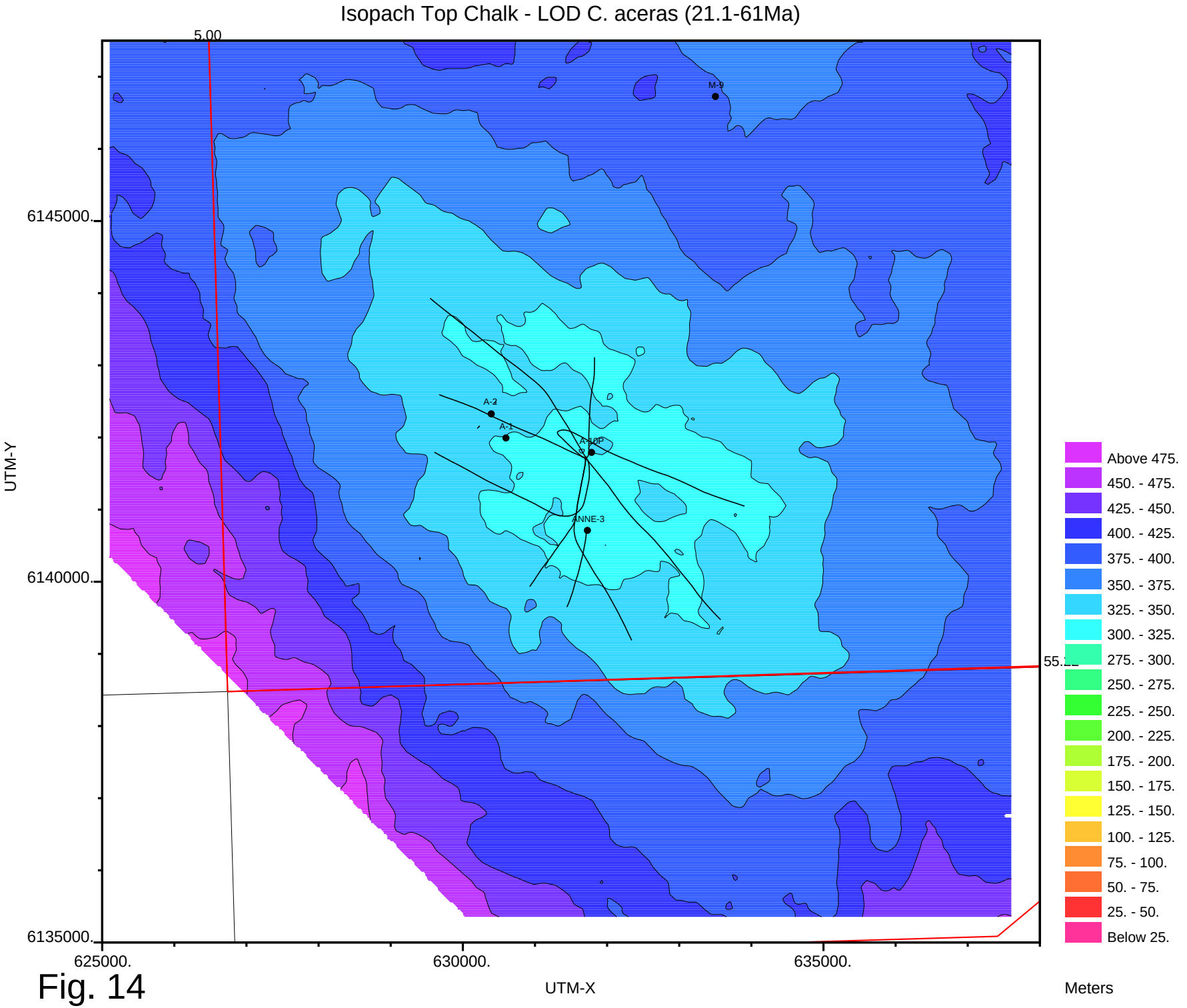
Isopach Top Chalk - LOD C. aceras (21.1-61Ma)
5.00
6145000.
6140000.
6135000.
625000.
630000.
635000.
UTM-Y
UTM-X
M-9
A-2
A-1
A-10P
ANNE-3
55.
Above 475.
450. - 475.
425. - 450.
400. - 425.
375. - 400.
350. - 375.
325. - 350.
300. - 325.
275. - 300.
250. - 275.
225. - 250.
200. - 225.
175. - 200.
150. - 175.
125. - 150.
100. - 125.
75. - 100.
50. - 75.
25. - 50.
Below 25.
Meters

Fig. 14

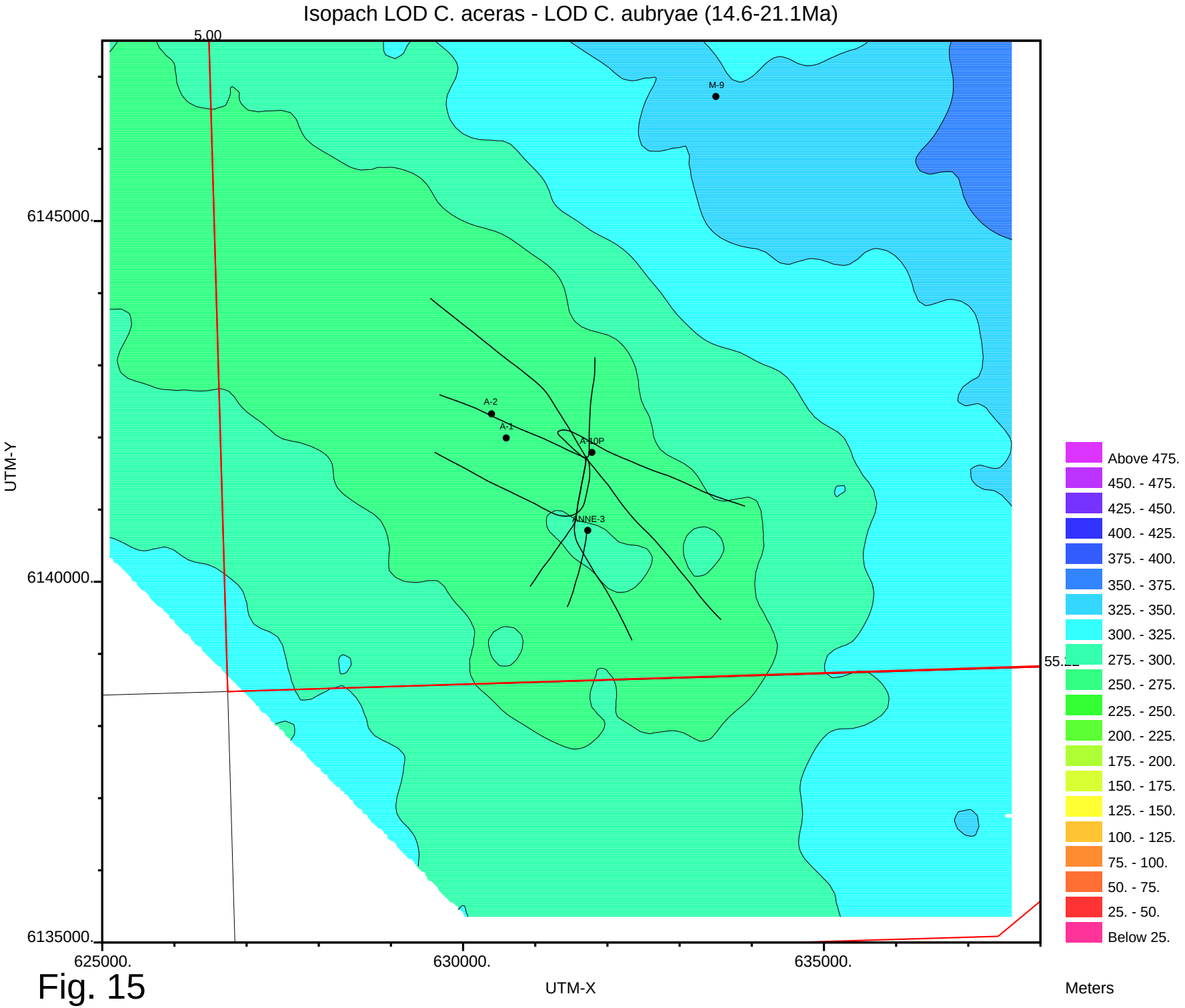
Isopach LOD C. aceras - LOD C. aubryae (14.6-21.1Ma)
5.00
6145000.
6140000.
6135000.
UTM-Y
625000.
630000.
635000.
UTM-X
M-9
A-2
A-1
A-10P
ANNE-3
Above 475.
450. - 475.
425. - 450.
400. - 425.
375. - 400.
350. - 375.
325. - 350.
300. - 325.
275. - 300.
250. - 275.
225. - 250.
200. - 225.
175. - 200.
150. - 175.
125. - 150.
100. - 125.
75. - 100.
50. - 75.
25. - 50.
Below 25.
Meters

Fig. 15

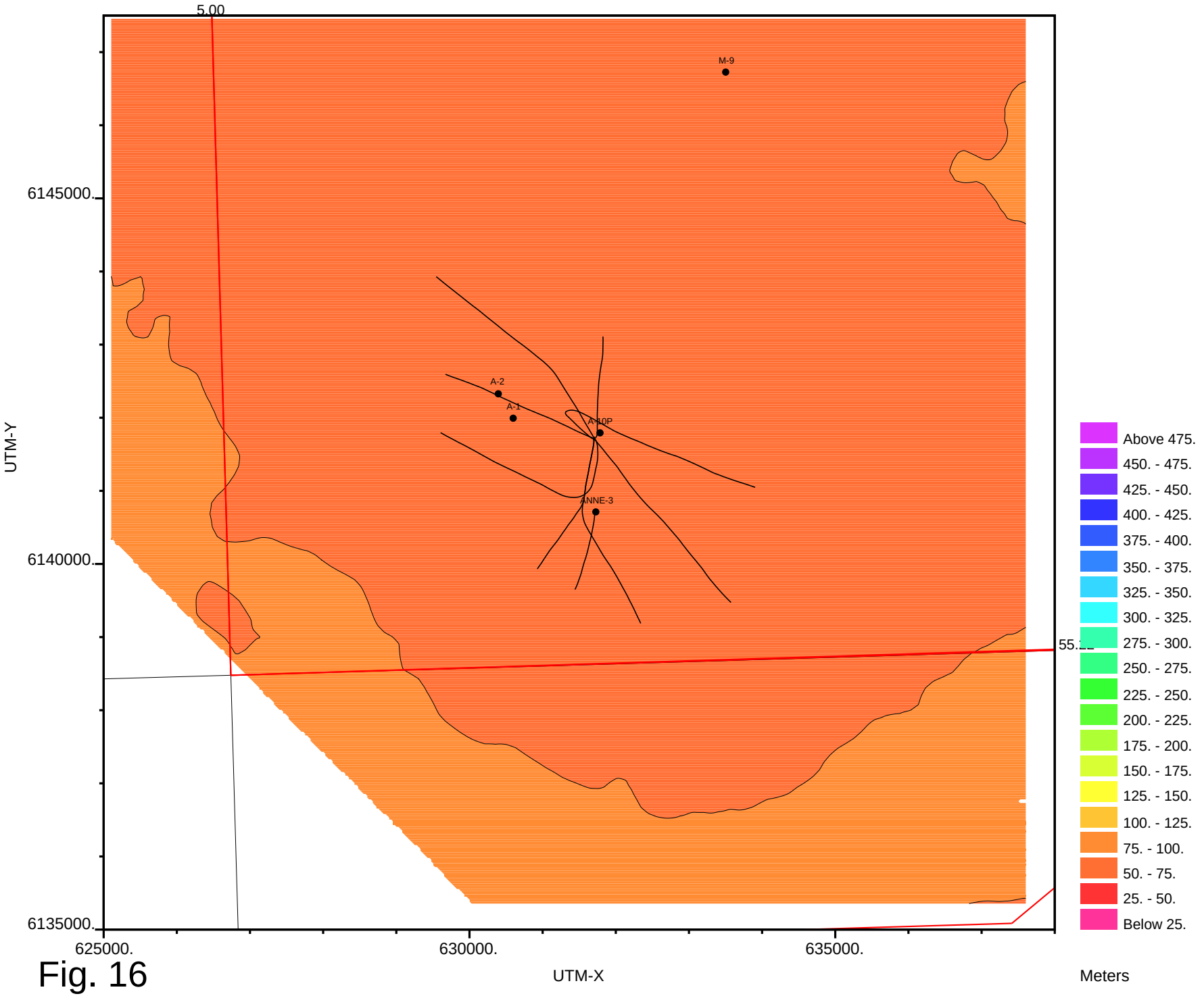
Isopach LOD C. aubryae - N. Base Tortonian (11.2-14.6Ma)
5.00
M-9
A-2
A-1
A-10P
ANNE-3
6145000.
6140000.
6135000.
UTM-Y
625000.
630000.
635000.
UTM-X
Above 475.
450. - 475.
425. - 450.
400. - 425.
375. - 400.
350. - 375.
325. - 350.
300. - 325.
275. - 300.
250. - 275.
225. - 250.
200. - 225.
175. - 200.
150. - 175.
125. - 150.
100. - 125.
75. - 100.
50. - 75.
25. - 50.
Below 25.
Meters

Fig. 16

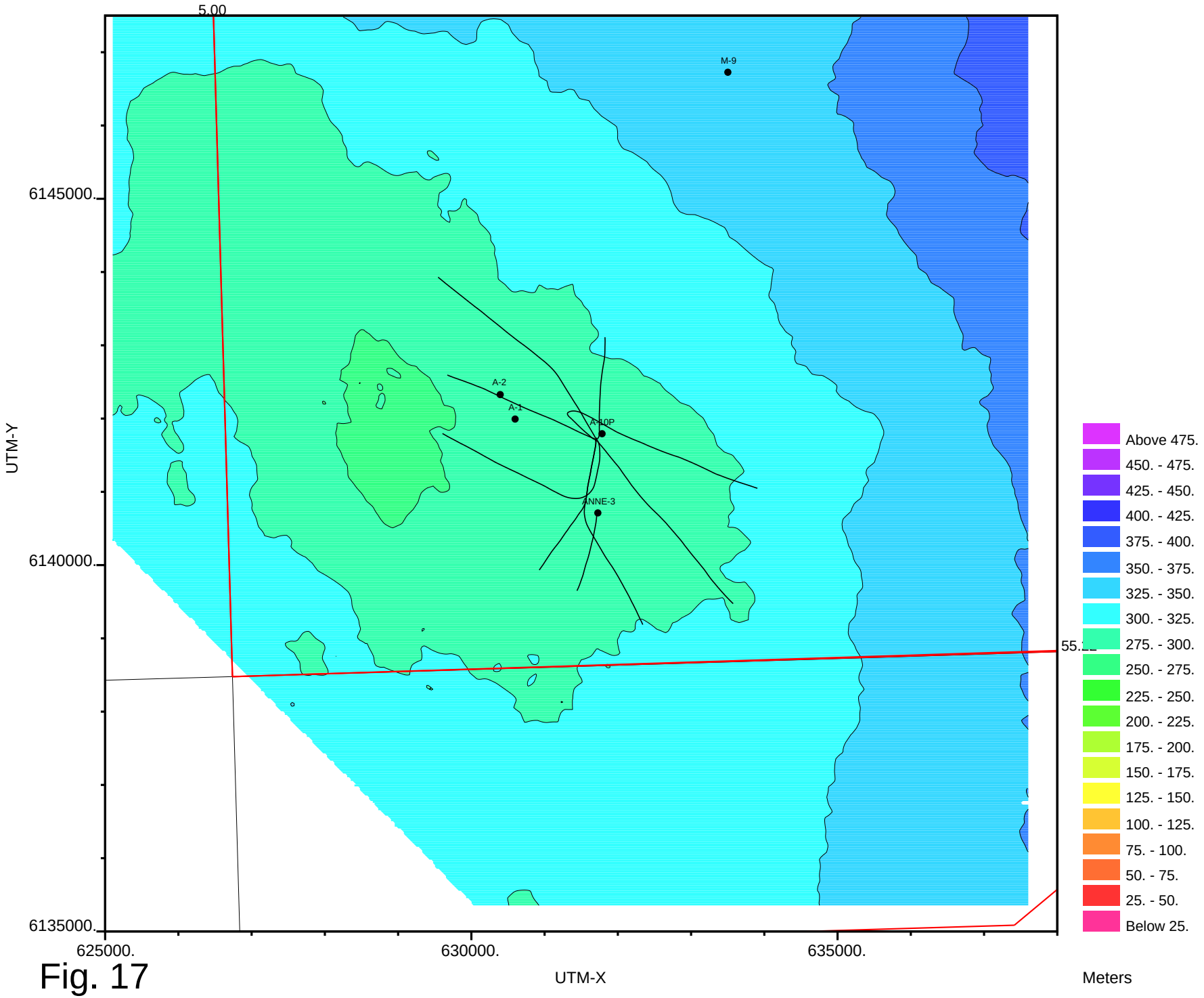
Isopach N. Base Tortonian - N. Base Messinian (7.12-11.2Ma)
5.00
M-9
A-2
A-1
A-10P
ANNE-3
6145000.
6140000.
6135000.
UTM-Y
625000.
630000.
635000.
UTM-X
Above 475.
450. - 475.
425. - 450.
400. - 425.
375. - 400.
350. - 375.
325. - 350.
300. - 325.
275. - 300.
250. - 275.
225. - 250.
200. - 225.
175. - 200.
150. - 175.
125. - 150.
100. - 125.
75. - 100.
50. - 75.
25. - 50.
Below 25.
Meters

Fig. 17

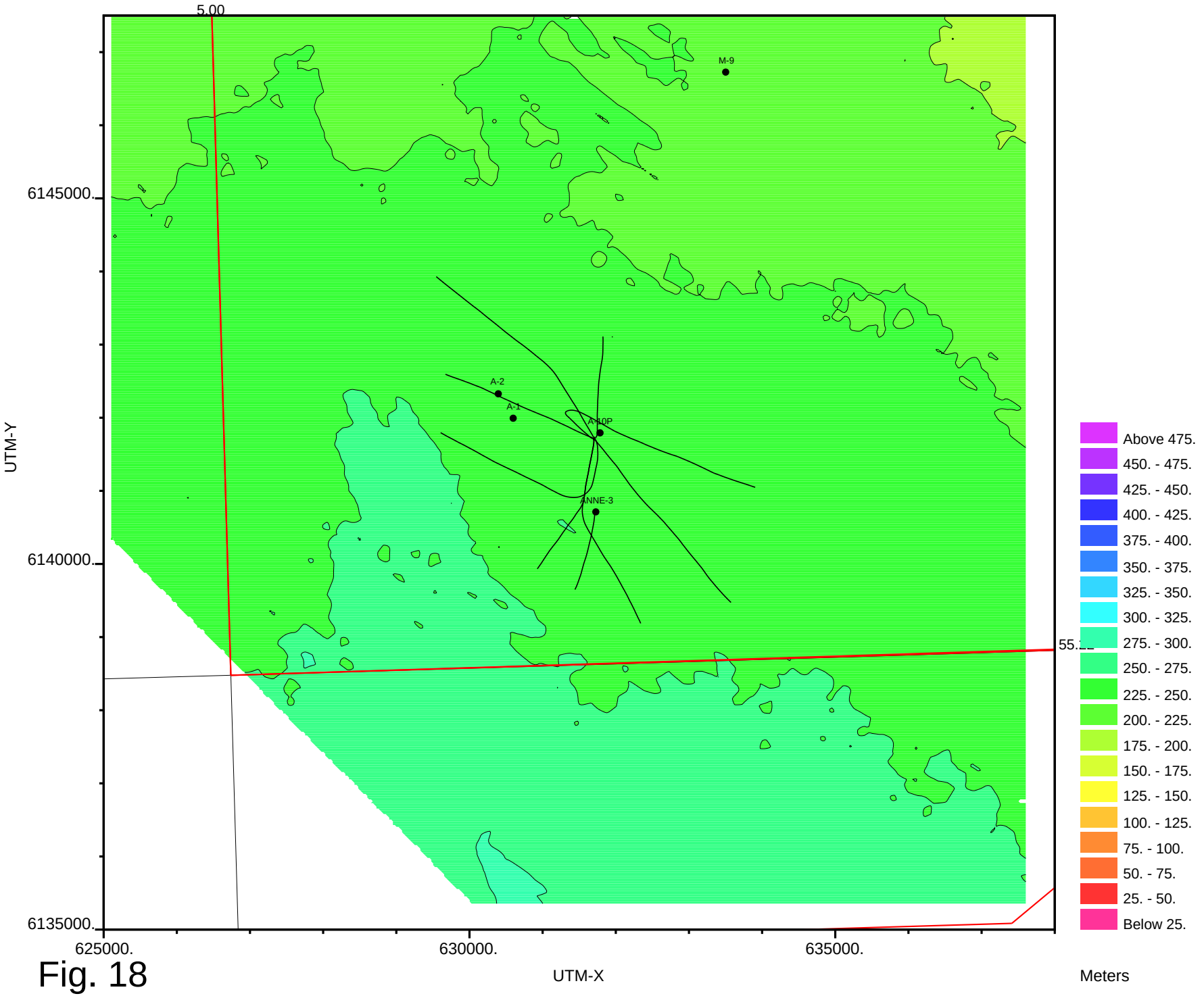
Isopach N. Base Messinian - Upper Miocene (6-7.12Ma)
5.00
6145000.
6140000.
6135000.
UTM-Y
625000.
630000.
635000.
UTM-X
M-9
A-2
A-1
A-10P
ANNE-3
Above 475.
450. - 475.
425. - 450.
400. - 425.
375. - 400.
350. - 375.
325. - 350.
300. - 325.
275. - 300.
250. - 275.
225. - 250.
200. - 225.
175. - 200.
150. - 175.
125. - 150.
100. - 125.
75. - 100.
50. - 75.
25. - 50.
Below 25.
Meters

Fig. 18

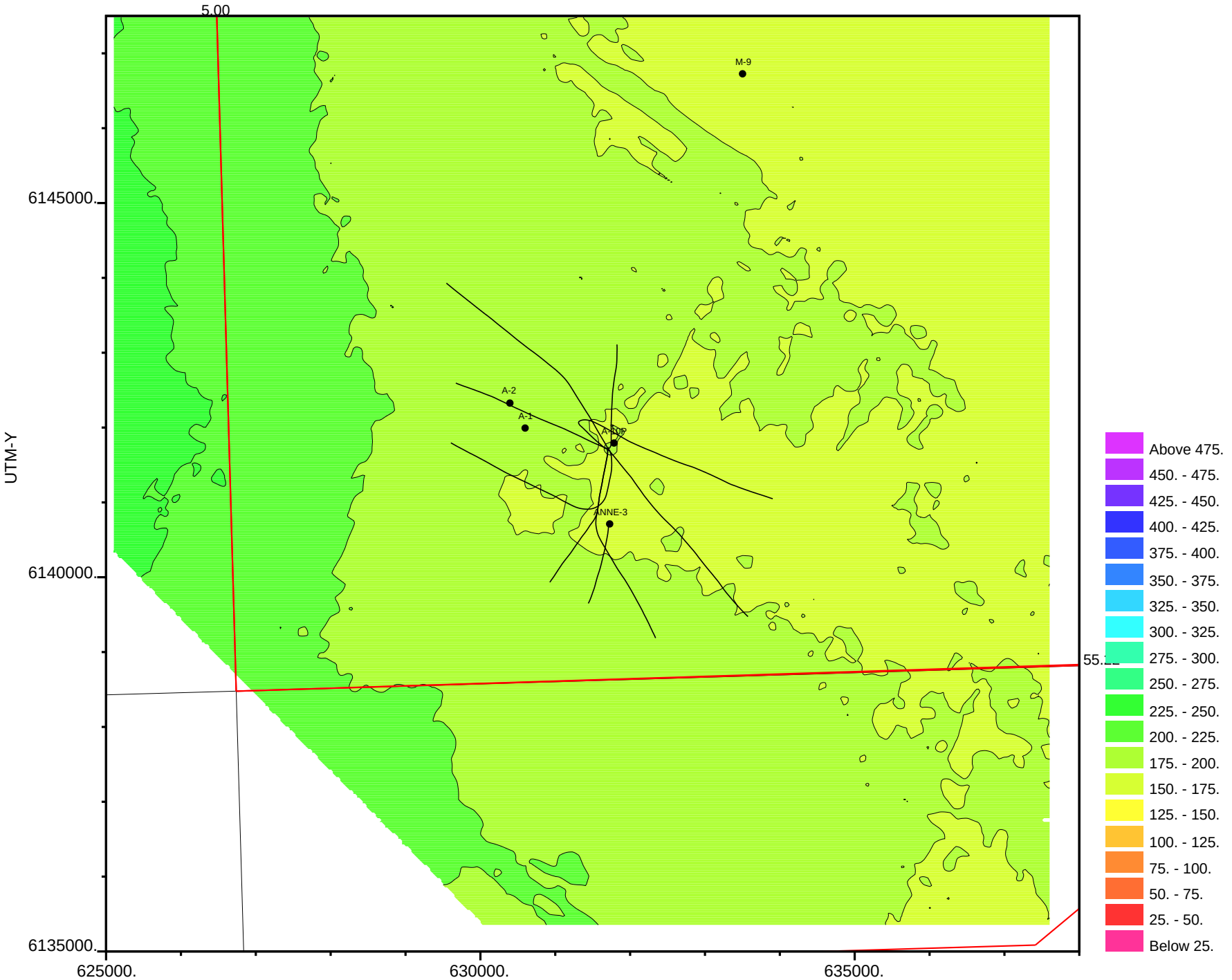
Isopach Upper Miocene - Intra Pliocene (3.6-6Ma)
5.00
M-9
A-2
A-1
A-5DP
ANNE-3
6145000.
6140000.
6135000.
625000.
630000.
635000.
UTM-Y
UTM-X
Meters
Above 475.
450. - 475.
425. - 450.
400. - 425.
375. - 400.
350. - 375.
325. - 350.
300. - 325.
275. - 300.
250. - 275.
225. - 250.
200. - 225.
175. - 200.
150. - 175.
125. - 150.
100. - 125.
75. - 100.
50. - 75.
25. - 50.
Below 25.

Fig. 19

3. Depth conversion

Velocity modelling for depth conversion is performed differently for the Post Chalk Group and for the intra chalk reflectors and seismic samples. The Post Chalk Group velocity models apply linearly depth dependent models as described by Japsen (2000). The Intra chalk velocity models are derived from seismic inversion data.

3.1 Post Chalk Velocity modelling

Depth to the Top Chalk is calculated from average velocities estimated in a regional mapping study (Britze et al. 1995a). The average velocity is calculated using a function of the type:

1) $$V_i = V_0 + dv + k \cdot Z$$

where V_i is the interval velocity, V_0 and dv are surface velocity and associated anomaly (laterally varying), k is the velocity gradient, and Z is depth. The deviations from the average velocity function, the anomaly (dv), is typically obtained from well data (e.g. Japsen 2000). The method is therefore capable of handling anomalies with a larger extent than the well spacing. Local velocity anomalies resulting from e.g. gas clouds or local overpressure release or other phenomena unchecked by wells may therefore result in locally erroneous depth predictions.

The Post Chalk Group is divided at the Near Base Tortonian reflector for depth conversion purposes. This or nearby reflectors are often referred to at “near Top overpressure”, as it is located at the mid Miocene seal below which, fluid pressure exceeds hydrostatic conditions appreciably. At around the Dan Field area, the fluid pressure is roughly 7 MPa above hydrostatic (e.g. Japsen 2000). As the reflector does not correspond exactly to any previously mapped reflector (e.g. Japsen 1992), velocity anomaly mapping has to be re-considered. According to Japsen (19xx), the velocity anomalies in the upper Post Chalk Group are insignificant as compared to the lower Post Chalk Group (Britze et al. 1995a; Japsen, 1998). The velocity anomalies in the Lower Post Chalk Group are mainly attributed to variable degrees of over-pressuring. For these reasons and because no exact well tie data base exist for the interpreted Near Base Tortonian reflector, the following approach was taken:

- The velocity modelling of the Post Chalk Group is divided into two at the Near Base Tortonian.
- All velocity anomalies necessary to match the Top Chalk level are ascribed the velocity model for the lower Post Chalk Group. The upper Post Chalk Group velocity model has no anomalies.
- The Intra Pliocene, the Upper Miocene, the Near Base Messinian, and the Near Base Tortonian are depth converted using the upper velocity model. The ESR_T_Aub, the ESR_T_Aceras, and the top Chalk reflectors are depth converted using the lower velocity model which includes mapping of velocity anomalies (dv).

The general depth conversion parameters for two models in the Post Chalk Group are given in Table 3. The upper Post Chalk Group parameters are from Britze et al. (1995). The Lower Post Chalk Group parameters are converted from the "Shale Trend" equation by Japsen (1999):

2) $ITT = 460 \cdot e^{-z/2175} + 185$

where ITT is integrated transit time with the units $\mu \sec \cdot m^{-1}$ and depth is given in meters. The parameters resulting from the conversion is given in Table 3.1.

	V_0 (m/sec)	k ($\sec^{-1}$)
Upper Post Chalk Group	1725	0.4
Lower Post Chalk Group	1517.2	0.6

Table 3.1: Depth conversion parameters.

WELL.	Alma-1	Alma-2	Anne-3	N-22	E-2	M-1	M-8	M-9	N-1	N-2	O-1	Skj.-Fl	U-1
DZ	478.0	508.8	334.0	619.7	629.1	512.8	372.3	458.4	599.5	579.8	325.5	438.7	675.9
Dv	-275.4	-293.6	-194.6	-364.0	-369.2	-301.7	-216.6	-266.7	-351.4	-341.3	-188.5	-253.9	-395.9

Table 3.2: Velocity anomalies, and calculated burial anomalies.

The Upper Post chalk Group was depth converted first without velocity anomalies. Then velocity anomalies necessary to match the proven Top Chalk at well locations are estimated and mapped. The velocity anomalies at well locations for the lower Post Chalk Group are listed in Table 3.2. The corresponding depth anomaly range from 325 m to 675 m corresponding to an estimated excess fluid pressures in the order of 3.3 to 6.8 Mpa (e.g. Japsen 2000). The resulting velocity anomaly map for the study area is shown as Fig. 21, and the average velocity down to the Top Chalk is shown as Fig. 22. The trend in velocity anomaly map deviate considerably from the expected regional south-east-ward increase in relative velocity corresponding to decreasing fluid pressures. The pattern is clearly affected by the presence of the Kraka Field by locally increasing relative velocity. It must be emphasised, that the velocity anomaly picture only carries a resolution dictated by the well spacing.

The general impression from the average velocity map is that depth is the primary control on velocity variations. The variations are modest, and a constant velocity of 2 Km/sec would only produce errors on depth estimates below 100 m.

3.2 Intra Chalk velocity modelling

In order to get as precise a velocity picture in the chalk as possible, seismic impedance data are employed. For this purpose, data from seismic inversion performed by Mærsk Oil and Gas of the Contiguous area merged 3-D survey are employed (Tredgett and Mooney 1995). The inversion derived seismic impedance provide data also in areas in between wells, and is thus able to catch velocity anomalies that are not documented by wells. For this purpose a relationship between acoustic impedance and velocity is constructed.

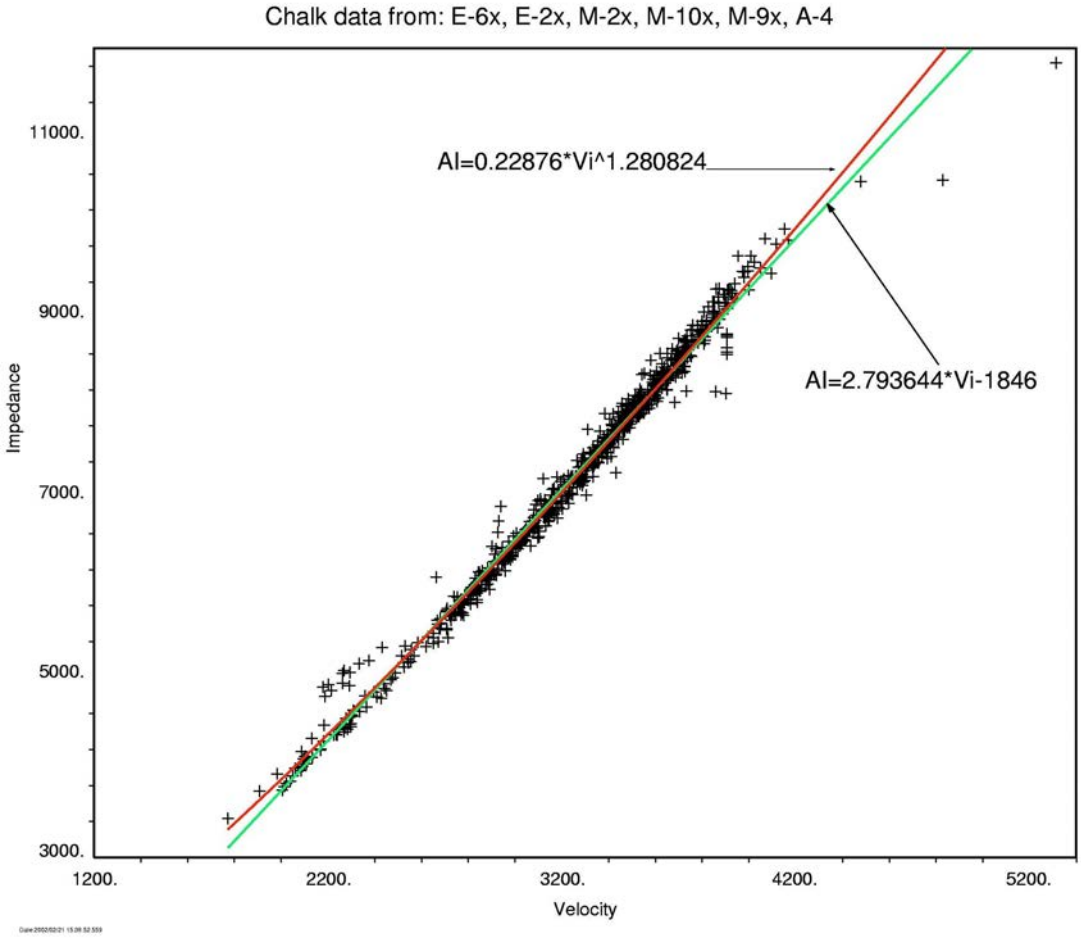

Fig. 20: Seismic impedance versus interval velocity, both derived from well log data.

The relationship is based entirely on well data and produces a very nice correlation (Fig. 20). The correlation coefficient is 0.9932 for the chosen fit type. It must, however, be stressed that the relationship will be applied on a different type of data: the inversion derived seismic impedance. The apparent high degree of confidence suggested by the cross plot of the well data might not be transferable to the data from the inversion. Two types of fit were tried, and the simple linear fit as given by:

3) $Ai = 2.793644 \cdot V_i - 1846 \Leftrightarrow V_i = (Ai + 1846) / 2.793644$

was employed. The parameter Ai and V_i are acoustic impedance and interval velocity respectively. Units are $1000 \cdot Kg \cdot m^{-2} \cdot \sec^{-1}$ and $m \cdot \sec^{-1}$. Resulting interval velocity maps for the upper Tor Formation (between Top Maa unit 4 and Top Tor) and the Ekofisk Formation are shown in Figs. 23, and 24 respectively. The maps shows that velocities are generally lower in the (also more porous) Ekofisk Formation as compared to the upper Tor Formation. Interestingly a low velocity anomaly in the upper Tor Formation is found on the SE flank of the Kraka Field, that would not have been captured by the type of velocity model employed for the Post Chalk Group. Abnormally high velocities indicating tighter chalk is found on the very crest of the Kraka Field in both Tor and Ekofisk Formations. As no significant relative pressure difference exist vertically between the Chalk and the Lower Post Chalk Group, it might be speculated that small DV values on the Southeast flank of the Kraka Field in the lower Post Chalk Group might be an interpolation artefact. This is based on the assumption that velocity anomalies are primarily caused by overpressuring.

Fig no.	Interval	C.I.	Text
21	200-400	10	Velocity anomaly map for the lower Post Chalk Group.
22	2020-2100	4	Average velocity Post Chalk Group
23	2600-4200	80	Upper Tor Fm. Interval velocity
24	2600-4200	80	Ekofisk Formation Interval velocity

Table 3.3: Velocity maps

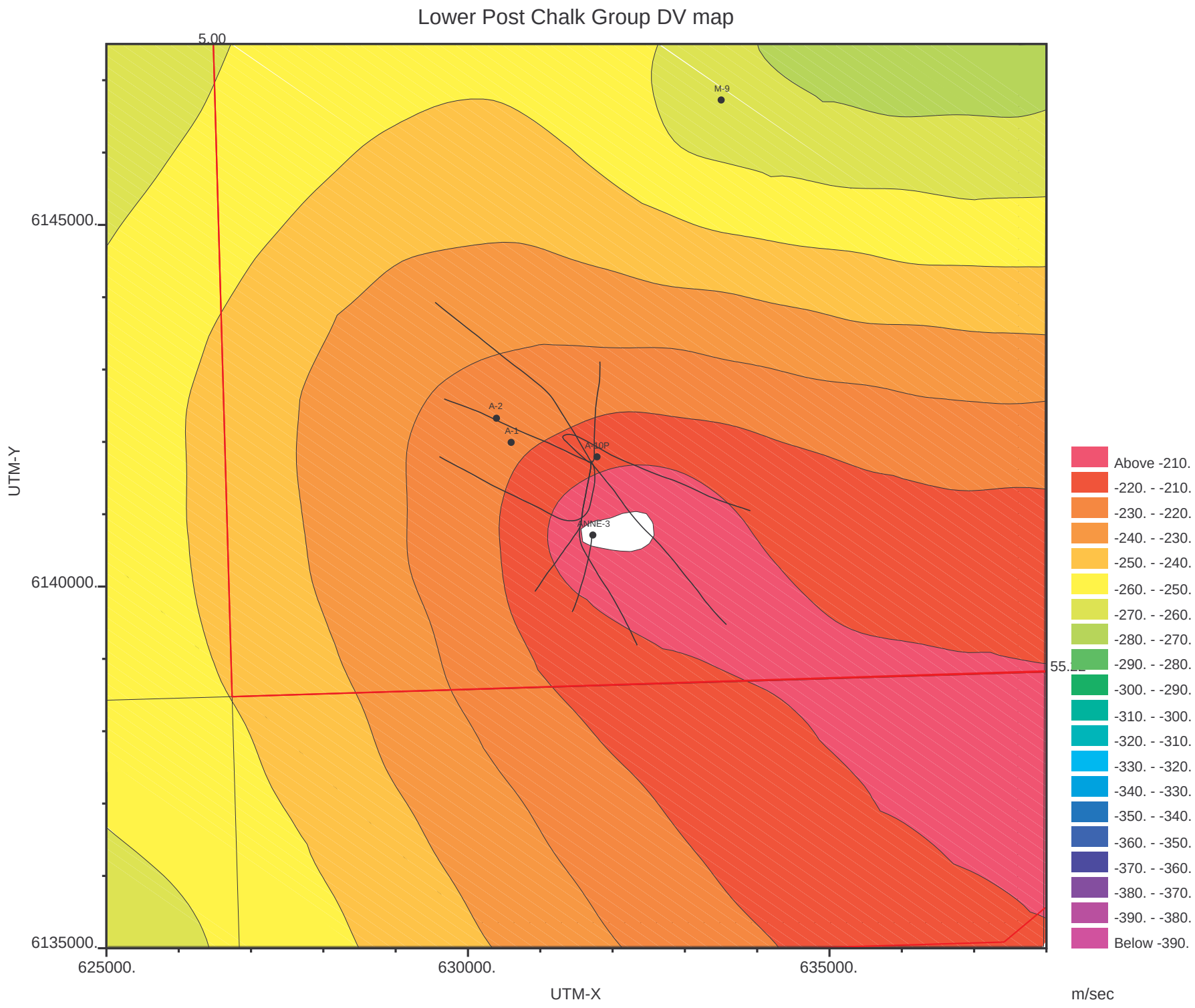
Lower Post Chalk Group DV map
5.00
M-9
A-2
A-1
A-10P
ANNE-3
6145000.
6140000.
6135000.
625000.
630000.
635000.
UTM-Y
UTM-X
Above -210.
-220. - -210.
-230. - -220.
-240. - -230.
-250. - -240.
-260. - -250.
-270. - -260.
-280. - -270.
-290. - -280.
-300. - -290.
-310. - -300.
-320. - -310.
-330. - -320.
-340. - -330.
-350. - -340.
-360. - -350.
-370. - -360.
-380. - -370.
-390. - -380.
Below -390.
m/sec

Fig. 21

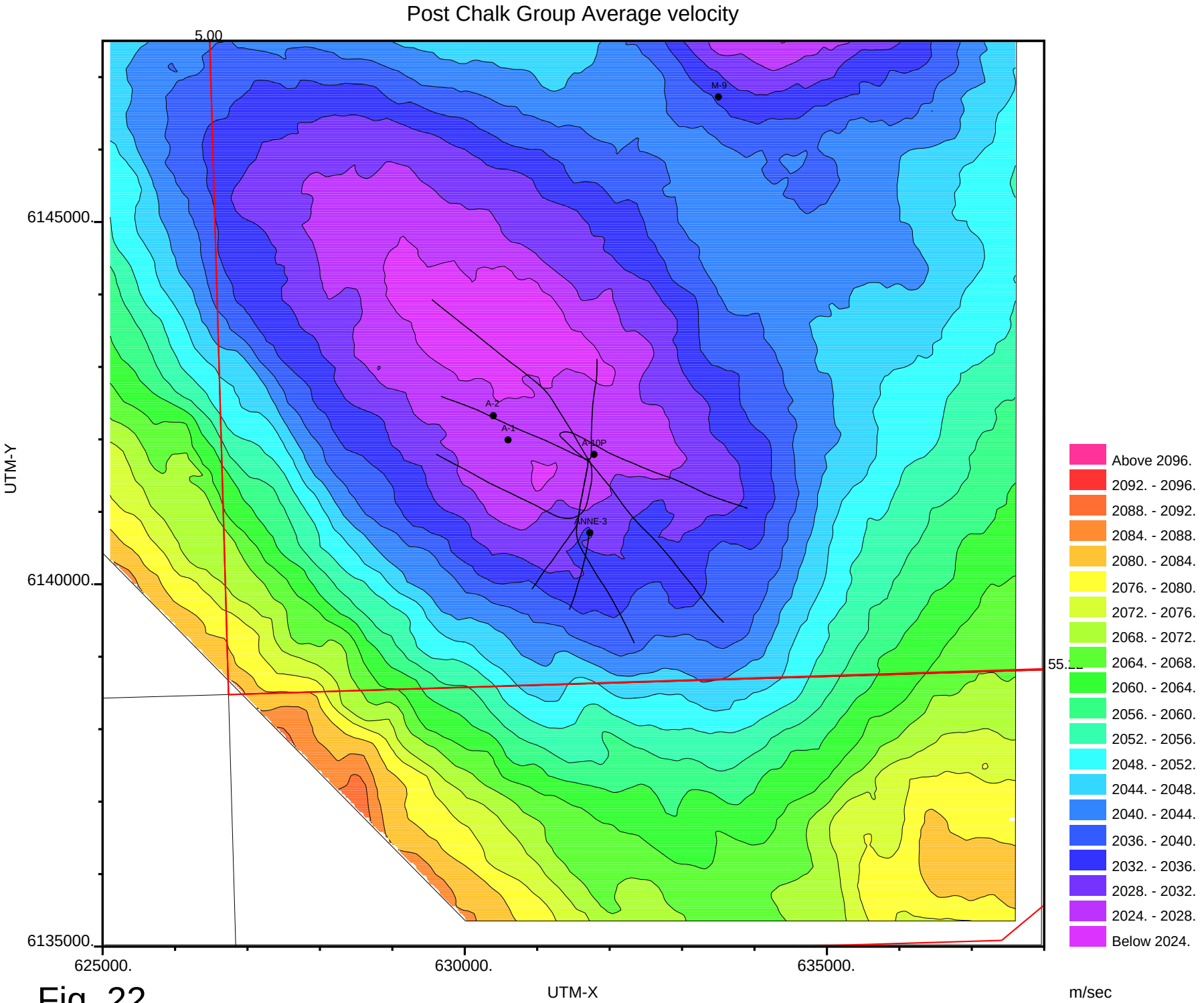
Post Chalk Group Average velocity
5.00
6145000.
6140000.
6135000.
625000.
630000.
635000.
UTM-Y
UTM-X
M-9
A-2
A-1
A-10P
ANNE-3
Above 2096.
2092. - 2096.
2088. - 2092.
2084. - 2088.
2080. - 2084.
2076. - 2080.
2072. - 2076.
2068. - 2072.
2064. - 2068.
2060. - 2064.
2056. - 2060.
2052. - 2056.
2048. - 2052.
2044. - 2048.
2040. - 2044.
2036. - 2040.
2032. - 2036.
2028. - 2032.
2024. - 2028.
Below 2024.
m/sec

Fig. 22

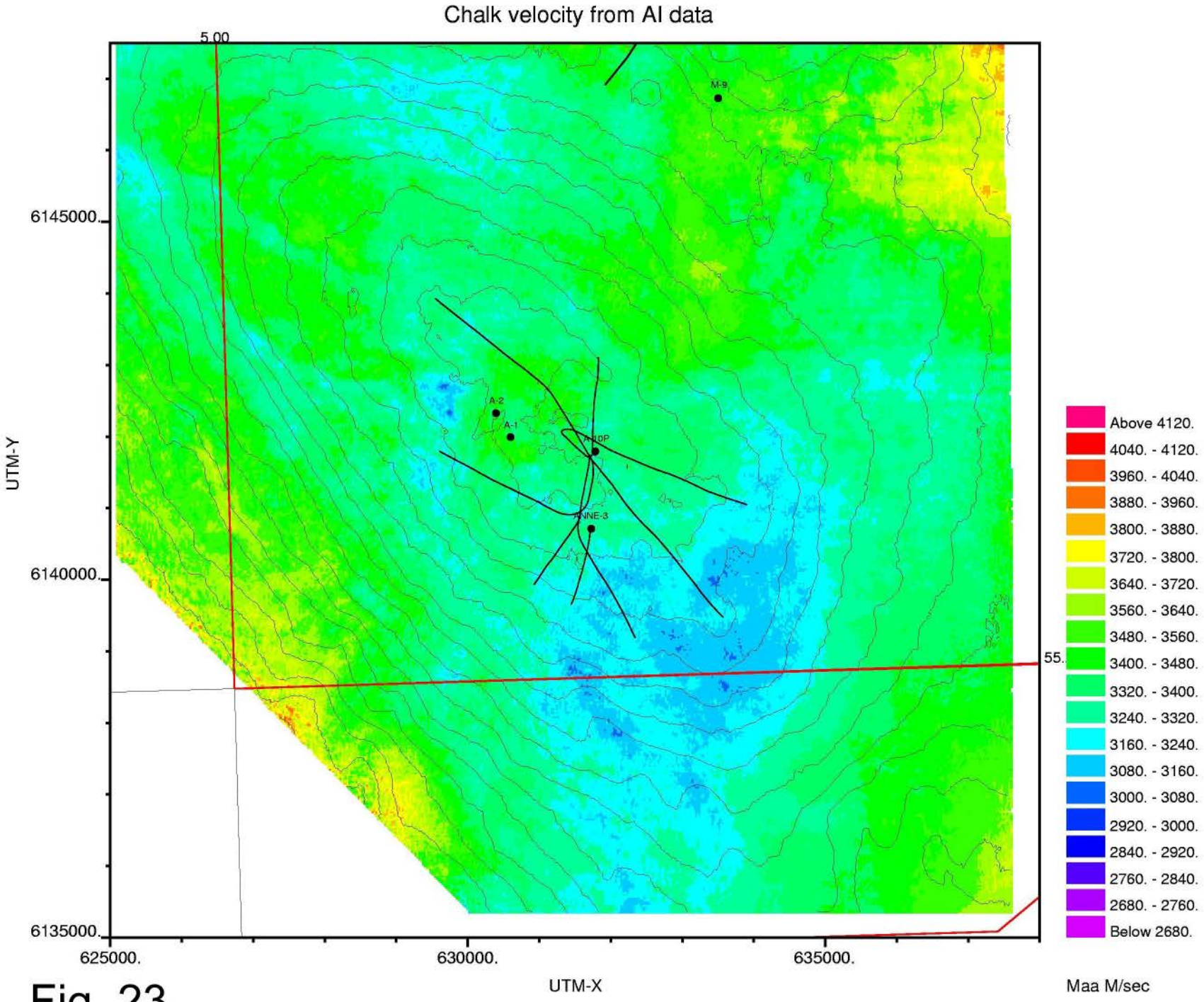
Chalk velocity from AI data
5.00
6145000.
6140000.
6135000.
625000.
630000.
635000.
55.
UTM-Y
UTM-X
M-9
A-2
A-1
A-10P
A-NE-3
Above 4120.
4040. - 4120.
3960. - 4040.
3880. - 3960.
3800. - 3880.
3720. - 3800.
3640. - 3720.
3560. - 3640.
3480. - 3560.
3400. - 3480.
3320. - 3400.
3240. - 3320.
3160. - 3240.
3080. - 3160.
3000. - 3080.
2920. - 3000.
2840. - 2920.
2760. - 2840.
2680. - 2760.
Below 2680.
Maa M/sec

Fig. 23

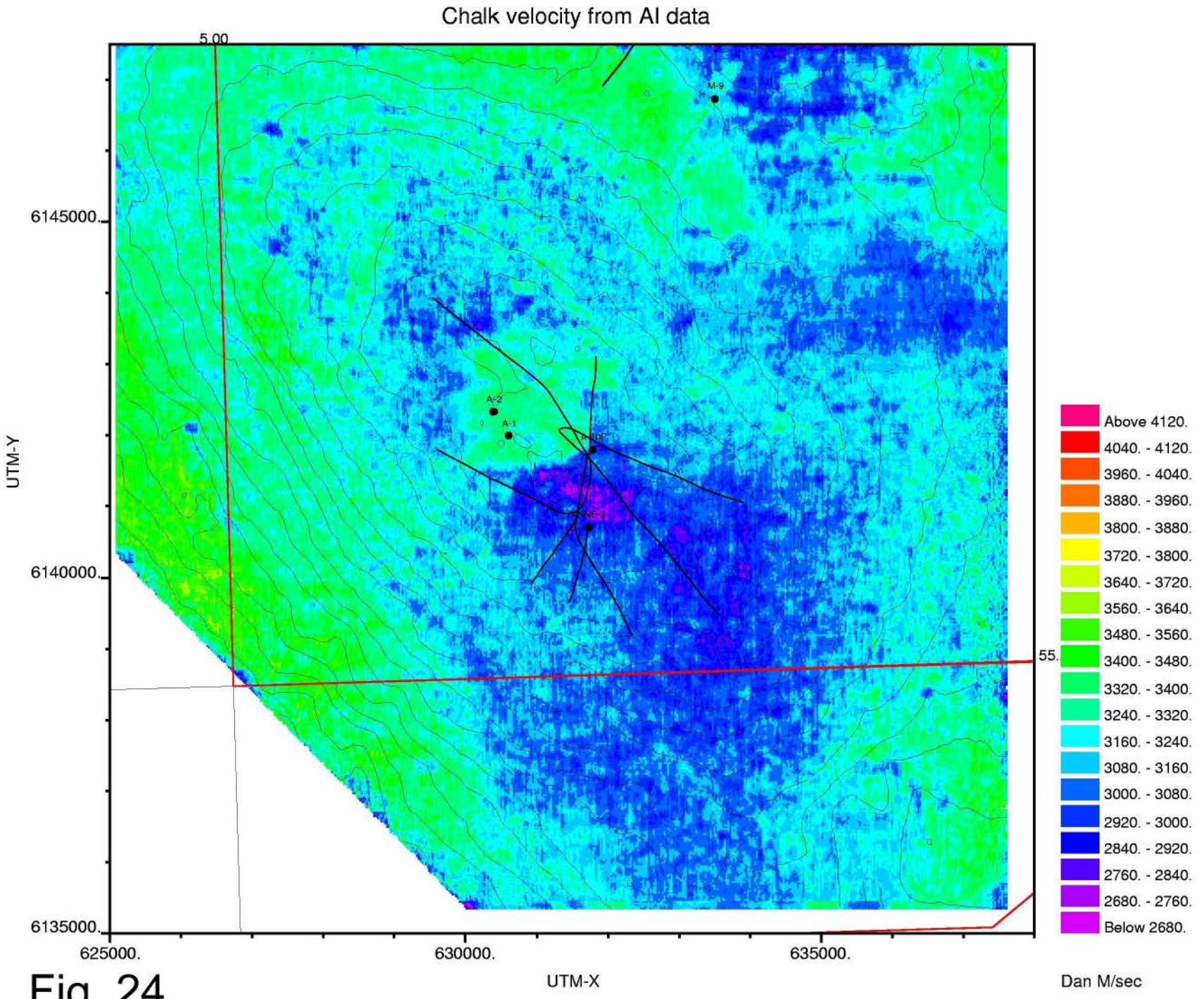
Chalk velocity from AI data
5.00
6145000.
6140000.
6135000.
625000.
630000.
635000.
UTM-Y
UTM-X
55.
M-9
A-2
A-1
A-10F
A-3
Above 4120.
4040. - 4120.
3960. - 4040.
3880. - 3960.
3800. - 3880.
3720. - 3800.
3640. - 3720.
3560. - 3640.
3480. - 3560.
3400. - 3480.
3320. - 3400.
3240. - 3320.
3160. - 3240.
3080. - 3160.
3000. - 3080.
2920. - 3000.
2840. - 2920.
2760. - 2840.
2680. - 2760.
Below 2680.
Dan M/sec

Fig. 24

4. Porosity mapping

Conversion of acoustic impedance derived from seismic inversion to porosity is applied for porosity mapping. In this study, it is only relevant for the Chalk Group layer, as they are the only part of the succession that is entered into flow simulation procedures. Even though the employed seismic impedance data for porosity mapping are not derived from petrophysical logs, but from seismic inversion, the porosity – impedance relationship is established on the basis of log data alone. The resulting porosity maps must therefore be used with caution, as original data, the tools, underlying assumptions, and resulting resolution of seismic inversion derived impedance is quite different than impedance from petrophysical logs.
To investigate the relationship between acoustic impedance and porosity, log data from 4 wells have been employed (Fig. 25).

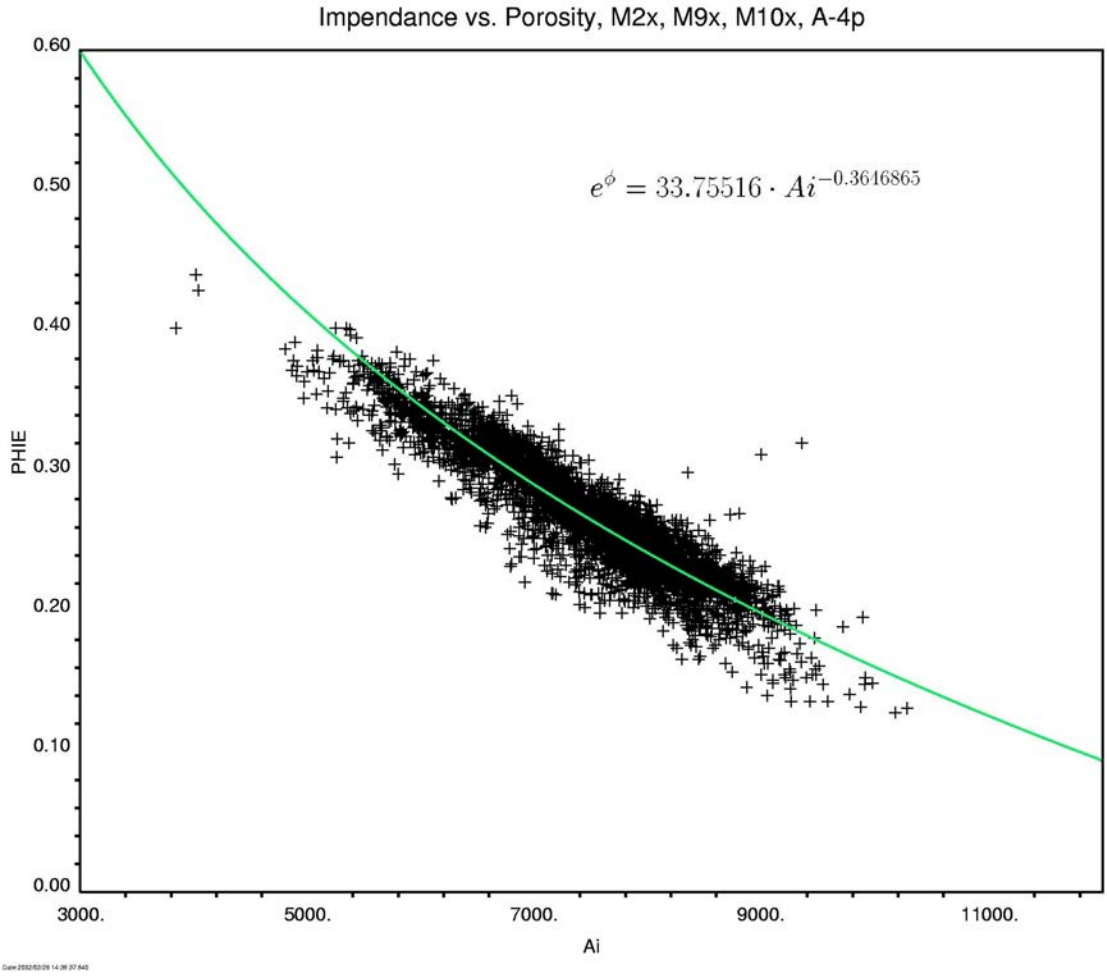

Fig. 25: Acoustic impedance versus porosity. Both quantities are derived from well log data from the entire chalk group.

After a number of trials, an equation of the form:

4) $\phi = Log(33.75516) - 0.3646865 \cdot Log(Ai) \Leftrightarrow e^{\phi} = 33.75516 \cdot Ai^{-0.3646865}$

was adopted. The variables ϕ and Ai are porosity and impedance respectively. Porosity is given in fractions, and acoustic impedance is given in $1000 \cdot Kg \cdot m^{-2} \cdot \sec^{-1}$. Points are based on log readings from the chalk section in three Dan Field wells and one Kraka Field well. Due to the considerable scatter and narrow control range given by these data points, a number of different types of equations may be considered. At a first glance, a simple linear function may do just as well. However, to achieve realistic extrapolation beyond data control points, acoustic impedance at 0% (matrix properties) and 100% (fluid properties) have been calculated and added to the data base before least squares approximation of the above equation (Table 4.1). As may be evident, the function cannot be simply linear.

Porosity (ϕ)	Density (ρ)	P-velocity (V_p)	Bulk Modulus (K)	Shear modulus (G)	Impedance (Ai)
Units	Kg/m^3	$m/\sec$	GPa	GPa	$1000 \cdot Kg \cdot m^{-2} \cdot \sec^{-1}$
0%	2700	5810	59.0	24.0	15674.82
100%	1010	1490	2.25	0	1506.66

Table 4.1: Supporting constructed data for porosity end-points for application in least squares fit of porosity versus acoustic impedance data.

The artificial end-point data are based on an assumed clay content of between 4 and 5%, North Sea RFT data (to derive brine density), and literature data (e.g. Walls et al. 1998). The artificial data requires the relationship to be linear.

Based on equation 3, the vertical average porosity of the Upper Tor (between Top Maa unit 4 and Top Tor) and the Ekofisk Formation are calculated shown in Figs. 26 and 27 respectively. Evidently, the Ekofisk Formation has higher porosity than the upper Tor Formation, which is counteracted by poorer reservoir properties (e.g. permeability, capillary entry pressure) at any particular porosity level. Both maps show that porosity is not decaying monotonically with depth, and a positive anomaly exists on the Southeast flank. Interesting patterns of abnormally high porosity suggests a linkage to fault and fracture zones. This is discussed further in section 6. It must be emphasised that these maps are derived from inversion derived acoustic impedance, and may deviate from reality. For instance:

- Some of the high porosity in the Ekofisk Formation may be caused by interference from the much lower impedance Balder Formation, which due to frequency limits affects the Ekofisk signal.
- The high porosity on the flanks of the Kraka Field may originate from an erroneous low frequency model in the inversion procedure. This is particularly a concern of relevance at the edges of the seismic survey due to reduced CDP coverage and reduced migration quality.

Fig no.	Interval	C.I.	Text
26	0.20-0.40	0.01	Upper Tor Fm. av. Porosity from seismic impedance
27	0.20-0.40	0.01	Ekofisk Formation av. Porosity from seismic impedance

Table 4.2: Porosity maps generated from seismic impedance.

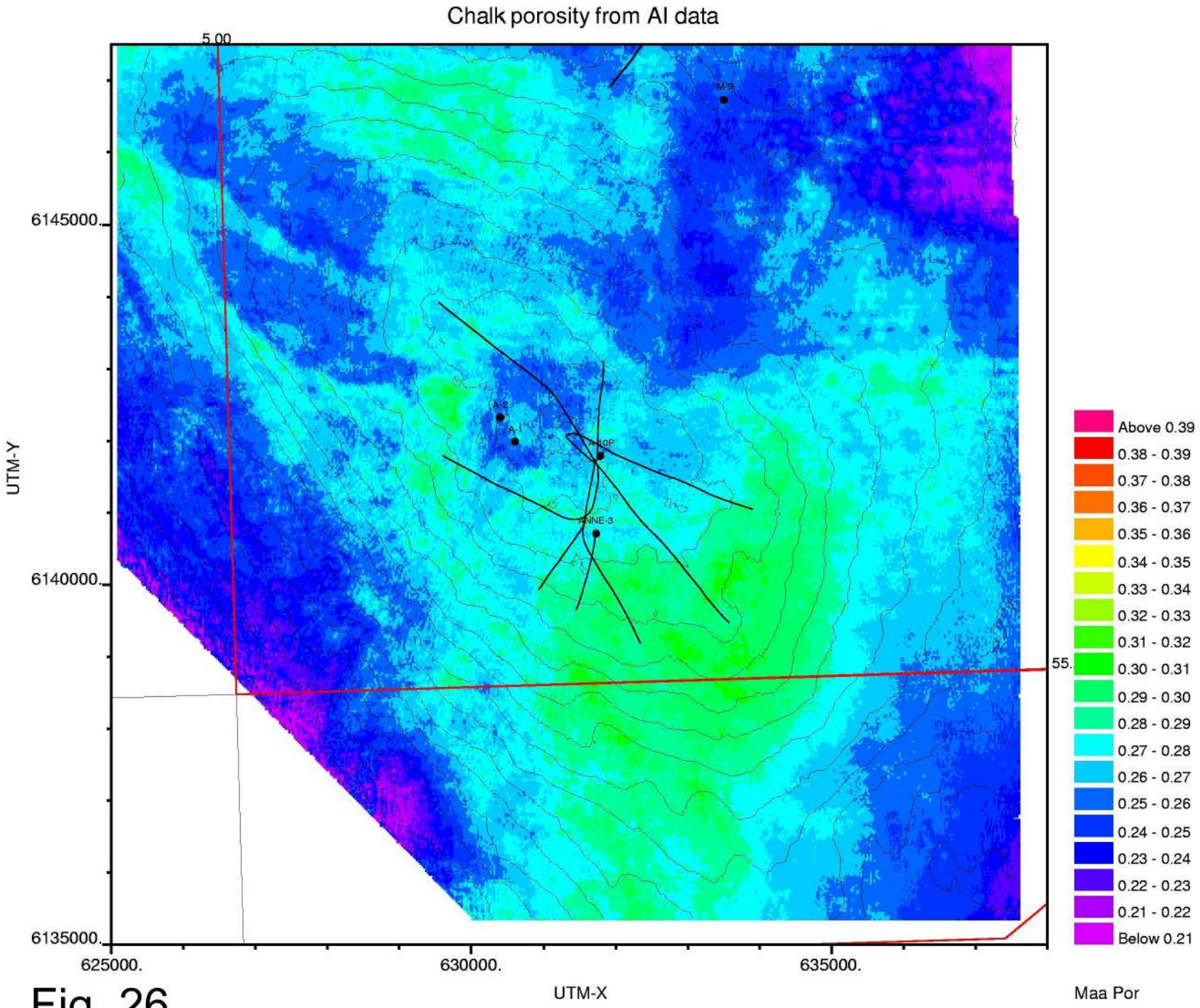
Chalk porosity from AI data
5.00
6145000.
6140000.
6135000.
625000.
630000.
635000.
UTM-X
UTM-Y
55.
M-9
A-2
A-1
A-10P
ANNE-3
Above 0.39
0.38 - 0.39
0.37 - 0.38
0.36 - 0.37
0.35 - 0.36
0.34 - 0.35
0.33 - 0.34
0.32 - 0.33
0.31 - 0.32
0.30 - 0.31
0.29 - 0.30
0.28 - 0.29
0.27 - 0.28
0.26 - 0.27
0.25 - 0.26
0.24 - 0.25
0.23 - 0.24
0.22 - 0.23
0.21 - 0.22
Below 0.21
Maa Por

Fig. 26

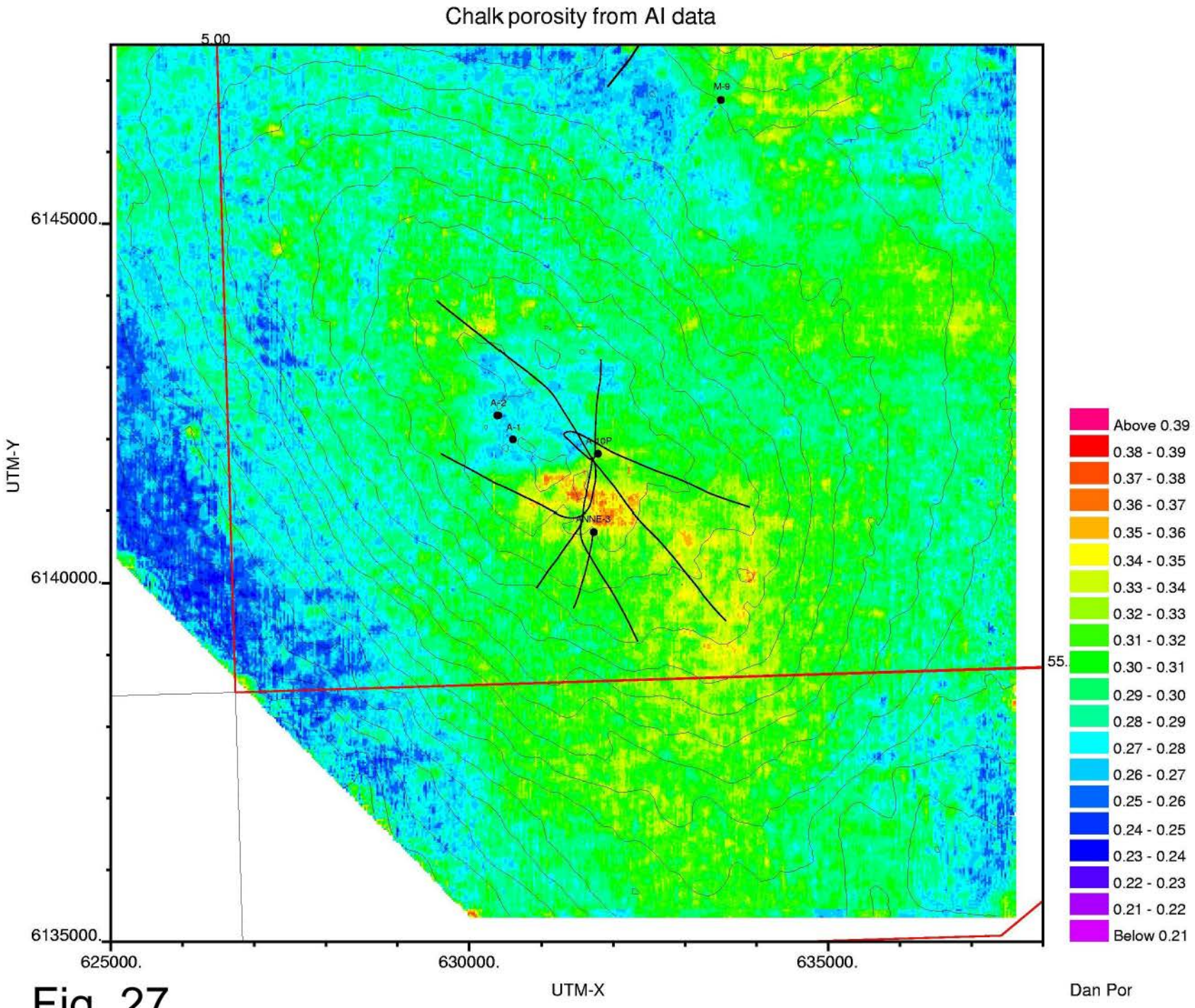
Chalk porosity from AI data
5.00
6145000.
6140000.
6135000.
625000.
630000.
635000.
UTM-X
UTM-Y
55.
M-9
A-2
A-1
A-10P
ANNE-3
Above 0.39
0.38 - 0.39
0.37 - 0.38
0.36 - 0.37
0.35 - 0.36
0.34 - 0.35
0.33 - 0.34
0.32 - 0.33
0.31 - 0.32
0.30 - 0.31
0.29 - 0.30
0.28 - 0.29
0.27 - 0.28
0.26 - 0.27
0.25 - 0.26
0.24 - 0.25
0.23 - 0.24
0.22 - 0.23
0.21 - 0.22
Below 0.21
Dan Por

Fig. 27

5. Backstripping procedures

The goal of the backstripping exercise is to calculate porosity distributions back in time. It is a requirement that the calculated porosity development must fit present day porosity distributions in the chalk as obtained from seismic inversion data.

Basic assumptions are:

- Porosity at present as obtained from conversion of seismic inversion results is a boundary condition.
- In the absence of over-pressuring and early diagenesis, porosity decay follows a simple exponential law according to depth.
- Depth is considered a proxy for effective stress in the absence of overpressure.
- Deviations in porosity from the average function are due to very early diagenesis or later over-pressuring for too tight and too porous intervals respectively.
- The overpressure as of today has not dissipated significantly since onset: Overpressure "arrests" porosity as it is at the time of onset.
- Very tight chalk has been cemented shortly after burial, and follows a lower porosity decay curve than standard.

The basic approach is given earlier by e.g. Sclater and Christie (1980) and Jensen et al. (1984), and is repeated here. New developments, however, are equations necessary to handle the over-pressuring and anomalously tight units.

Porosity decay with depth (z in meters) according to Sclater and Christie (1980) is:

5) $\phi = \phi_0 \cdot e^{-a \cdot z}$

where ϕ_0 is the surface porosity in fractions and the a is decay parameter. In the case of chalk ϕ_0 is 0.7 and a is 0.00071 m^{-1} according to Sclater and Christie (1980) where the reciprocal of the decay parameter, the decay length (reduction to 37% of surface por.), is equal to 1408.5 *m*.
This equation can be developed into the general decompaction equation:

6) $$z_{2n} - z_{1n} = (z_2 - z_1) - \frac{\phi_0}{a} \cdot \left[e^{-az_1} - e^{-az_2}\right] + \frac{\phi_0}{a} \cdot \left[e^{-az_{1n}} - e^{-az_{2n}}\right]$$

where z_n is a new depth after decompaction, and subscripts 1 and 2 refer to tops and bottoms respectively (Jensen et al. 1985). This equation may be rearranged into:

7) $$z_{2n} + \frac{\phi_0}{a} \cdot e^{-az_{2n}} = (z_2 - z_1) + \frac{\phi_0}{a} \cdot \left[e^{-az_2} - e^{-az_1} + e^{-az_{1n}}\right] + z_{1n}$$

As can be seen, the new depths cannot be isolated on one side, and the equation needs to be solved by iteration. The equation applies to periods after sedimentation of a unit has ceased.

During a sedimentation interval, the particle velocity as a function of depth is:

8) $$v(z) = v_0 \frac{1-\phi_0}{1-\phi_0 \cdot e^{-az}}$$

where v_0 is the surface velocity. The time necessary for a certain depth to be reached is:

9) $$t = \int_0^z \frac{1}{v(z')} \partial z' \Rightarrow t = \frac{1}{v_0(1-\phi_0)} \left[z + \frac{\phi_0}{a}(e^{-az} - 1) \right]$$

Again z must be found by iteration. The surface velocity is found from:

10) $$v_0 = \frac{1}{(1-\phi_0)\Delta t} \left[\Delta z + \frac{\phi_0}{a}(e^{-az_2} - e^{-az_1}) \right]$$

where Δt is the duration of sedimentation for the unit, and $\Delta z = z_2 - z_1$ is the present thickness of the unit.

In the case of successions, where erosion has occurred, decompaction is not performed for time intervals where the layer is at shallower depths than previous maximum burial depth: $(z + h)$ where h is the amount of erosion (see Jensen et al. 1984 for further detail on this). This is not relevant for the study area, as no erosion of any significance is assumed to have occurred since Jurassic times.

Over-pressuring is handled by not performing de-compaction during backstripping for depth intervals where the porosity exceeds the porosity expected at the present depth according to the normal compaction trend. In the approach, it is assumed that excess pore pressure has not dissipated at all since onset. The duration of over-pressuring is the shortest possible with this assumption. This method is hereafter called "pressure preserving decompaction".

An alternative approach would be to assume that overpressure, and thus abnormal porosity, has been building up gradually since deposition, hereafter referred to as "gradual pressure build-up decompaction".

The two assumptions may be considered as end-members of possible actual scenarios, but neither handles the case where higher overpressure in the past has dissipated to some extent.

Since burial graphs show rapid burial rates only in the Neogene and very modest burial rates in Cretaceous – Palaeogene times (see below), the observed excess pore pressure is assumed to have been generated very late, and only few million years before present. The pressure preserving de-compaction approximation therefore seems to be the best choice as the short time available reduces the problem of pressure dissipation.

In the case of over-pressuring, the average observed porosity (ϕ_{obs}) in the interval today is higher than predicted by the standard porosity decay function (equation 1). The porosity is assumed preserved since onset of over-pressuring. The over-pressuring as of today is entered into the program in the form of the observed elevated average porosity for the interval. We need to find the position of the base of the layer (z_b) at the time of onset of

over-pressuring to allow decompaction to start at the right time during backstripping. The exact depth where ϕ_{obs} is on the normal compaction curve occurs is (from eq. 5):

11) $z_{obs} = \frac{1}{-a} Log\left(\frac{\phi_{obs}}{\phi_0}\right)$

Since half of the cumulated pore space for the layer occurs above this depth, the base of the layer is found from:

12) $z_b = \frac{1}{-a} Log\left(\frac{-a \cdot c}{\phi_0} + 1\right) \wedge c = \frac{\phi_0}{-a}(e^{-az_{obs}} - 1) + \frac{\Delta z \cdot \phi_{obs}}{2}$

where c is the cumulated pore space from the surface down to the base of the layer at the time of onset of overpressure. This value therefore represents the hypothetical situation where the layer extends to the surface. This is, however, only a calculation trick to obtain the distance from z_{obs} to z_b. The parameter Δz is the present thickness of the layer. This thickness has been maintained since the time of overpressure onset, and is used to find the top of the layer.

In the case of too tight chalk (porosity lower than the normal depth trend), the surface porosity is changed according to an observed porosity (ϕ_{obs}), where this porosity is compared to the expected average porosity at the depth of interest according to equation 5. The average expected porosity in an interval is given by:

13) $\phi_{mean} = \frac{\phi_0}{z_2 - z_1} \int_{z_1}^{z_2} e^{-az'} \partial z' = \frac{\phi_0}{-a \cdot (z_2 - z_1)}(e^{-az_2} - e^{-az_1})$

where z_1 and z_2 are depths to top and bottom respectively. In the sedimentation period the equation reduces to:

14) $\phi_{mean} = \frac{\phi_0}{-a \cdot z}(e^{-az} - 1)$

With these equations, we can now correct the surface porosity for the tight unit on the basis of the difference between the observed mean porosity and the normal compaction mean porosity in the interval:

15) $\phi_0^{'} = \phi_0 - \left[\frac{\phi_0}{-a \cdot (z_2 - z_1)}(e^{-az_2} - e^{-az_1}) - \phi_{obs}\right]$

where $\phi_0^{'}$ is the new surface porosity. Due to the non-linear porosity decay, this is not equivalent to shifting down the porosity with the same amount over the whole depth interval. The decay factor (a) therefore also have to be adjusted:

16) $a' = \frac{Log(\phi_{obs} / \phi_0^{'})}{-z}$

where a' is the new decay parameter.

In the equations above overpressure information is entered in the form of an observed porosity. An alternative way of entering overpressure is to give a burial anomaly value. The burial anomaly is the difference between the actual depth, and the depth corresponding to the effective overburden stress which may be lowered by excess pore pressure. The burial anomaly is here assumed identical to the difference between the actual depth and the

depth where an observed porosity would be on the normal porosity - depth curve. This way of entering overpressure information may be used, if no observed average porosity value is available but over-pressuring is documented from other sources. Then this anomaly is converted to a porosity anomaly using equation 5, where the present mid-point depth for the layer minus the burial anomaly is entered. This is not precise, but is considered a sufficiently good approximation.

5.1 Decompaction parameters

The main topic for this study, the chalk, has been given different sets of compaction parameters as shown in table 5.1.

Table 5.1: De-compaction parameters. Porosity is in fractions and the decay constant has the unit m^{-1}.

Rock unit	Surface porosity (ϕ_0)	Decay parameter (a)	Decay length ($1/a$)	Source
Chalk (1)	0.70	0.00071	1408.5	Sclater & Christie (1980)
Chalk (2)	0.662	0.0005071	1972	Based on Jakobsen (pers comm)
Chalk (3)	0.968	0.0009715	1029.3	Based on Japsen (pers. Comm)
Palaeogene clay	0.71	0.0005102	1960	Frederiksen et al. (2001)
Neogene	0.56	0.0003906	2560	Frederiksen et al. (2001)

The three chalk models are according to Sclater and Christie (1980), Jakobsen (pers. comm.), and Japsen (pers. comm.). While chalk models 1 and 2 are not very different at the depth of interest in this study, the third model is quite different. However, while the two first are entirely empirical, the third is based on extensive calibration of seismic velocity depth trends (Japsen 1999). As this trend produce burial anomalies calculated from burial modelling (see below) that to some extent agrees with pressure data, it is favoured over the others. Chalk models 1 and 2 produce far too small burial anomalies. The favoured chalk decay constants are based on a least square fit to data deeper that 500 m from the model proposed by Japsen (pers. comm.). His data does not follow the exponential decay exactly as seen on Fig. 28. As the chalk today is found at depths in the order of 1.8 to 3 km (see section on mapping) and as hydrocarbon maturation and migration is likely to be very late in the geological history, it is probably only necessary to model porosity decay deeper than 0.5 km accurately. The estimated surface porosity is obviously ridiculous, and is not assumed to occur in reality, therefore the exponential decay with the suggested parameters is only assumed to be valid below 0.5 km depth. A more ideal approach would be to use a segmented curve where Chalk model 1 or 2 define the shallow part and Chalk model 3 define the deeper part.

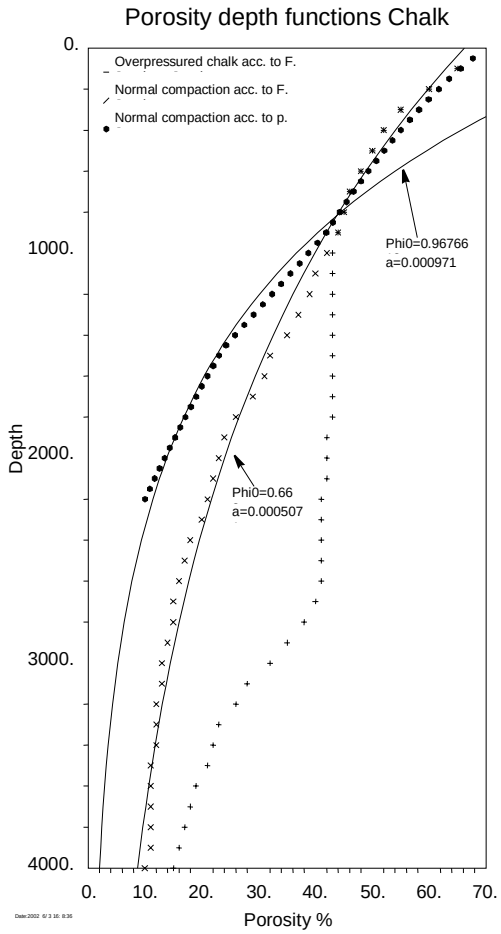

Fig 28: Porosity decay functions for the Chalk. Crosses illustrate a normal compaction and an over-pressured trend as proposed by F. Jakobsen. Dots represent the normal compaction model proposed by P. Japsen.

5.2 1D burial modelling: M-10X.

To test the model presented above, to show the model functionality in 1D, and to illustrate a relevant case from the Danish Central Graben, a modelling of the M-10X well is presented below.

Compaction parameters for the Cainozoic are from Frederiksen et al. (2001) where the parameters for the Neogene units are equivalent to the shaly sand of Sclater and Christie (1980). The chalk parameters are from this study.

It is seen, that overpressure is assumed in the three lower Cainozoic units given as burial anomalies (Japsen 1999) and the upper Chalk units. Although Japsen (1998) also provide burial anomalies for the Chalk (same order of magnitude as the Palaeogene values), these units are handled with porosity anomalies. This is done because the exact porosity as of today must be matched, giving lower priority to pressure. In addition this allows assessment of the validity of the selected normal compaction parameters. Due to the way burial anomalies are handled internally, the burial anomalies and porosity are recalculated for internal consistency.

Unit	Duration (Ma)	Thickness	ϕ_0	a	$1/a$	ϕ_{obs}
U.Pliocene – Recent	3.5	461.49	0.56	0.0003906	2560	-
L. Pliocene	2.5	168.45	0.56	0.0003906	2560	-
Messinian	1.12	204.31	0.56	0.0003906	2560	-
Tortonian	4.08	303.84	0.56	0.0003906	2560	-
Mid Miocene	3.4	64.54	0.56	0.0003906	2560	500
Aquitanian	6.5	290.14	0.71	0.0005102	1960	500
Paleocene – Oligoc.	39.9	310.32	0.71	0.0005102	1960	500
Ekofisk Fm	4	42.40	0.968	0.0009715	1960	0.32
Upper Tor Fm	1	41.82	0.968	0.0009715	1029	0.28
Lower Tor Formation	2	207.12	0.968	0.0009715	1029	0.25
Chalk below T. Hod	27	67.46	0.968	0.0009715	1029	0.20

Table 5.2: M-10X backstripping parameters. Non-equilibrium compaction (last column) is either non-existent, given as observed porosity in fractions (<1) or as a burial anomaly (above 1).

	0-3.5	3.5-6	6-7.12	7.12-11.2	11.2-14.6	14.6-21.1	21.1-61	61-65	65-66	66-68	68-95
Duration	3.5	2.5	1.12	4.08	3.4	6.5	39.9	4	1	2	27
Pal. Depth	40	50	100	300	300	570	600	600	600	600	600
Sea level	0	80	80	100	120	150	190	200	210	230	250

Table 5.3: Palaeo-water depth and relative palaeo-sea-level variation (from Gemmer 2002).

Unit	Burial anomaly	Present porosity
Mid Miocene	500	0.43
Aquitanian	494	0.43
Paleocene –Oligoc.	494	0.36
Ekofisk Fm.	685	0.31
Upper Tor Fm	589	0.27
Lower Tor Formation	592	0.22
Chalk below T. Hod	504	0.19

Table 5.4: Burial anomalies and porosities calculated for the overpressured units. Values differ from input data due to internal consistency calculations and approximations.

Input data to the modelling consists of present thickness, duration, compaction parameters for each unit and optionally a possible burial anomaly or porosity as of today (Table 5.2). In

addition a palaeo water depth (bathymetry) and palaeo-sea-level may be feed into the program in order to get a more realistic subsidence path for the location. In both cases, the compaction calculation refers to the sea bottom. As may be evident from Figs. 29 and 30 the appearance of the subsidence curves is rather different depending on whether or not the burial path is corrected for sea-level and bathymetry or not. Without this correction, subsidence is accelerating already before 22 Ma b.p. After correction a picture emerges of a huge accommodation space that is being filled up by Late Miocene progradation before subsidence accelerates in Pliocene to Recent times. The difference in the picture is the way the underlying tectonic activity is interpreted.

An attempt to visualise the effect of segmenting the porosity – depth model as discussed in the previous section, is illustrated with the dashed curves in Fig. 29. The chalk layers wold follow these curves during burial and then proceed along the full curves after crossing these. This would correspond to a Chalk model 2 (Table 5.1) decompaction for the upper part, and a Chalk model 3 for the lower part. As the intersection times are considered much earlier than the time for hydrocarbon invasion, this possible correction is disregarded.

The burial anomalies and present porosity listed in Table 5.4 for the Palaeogene and Chalk units are program output, which yields burial anomalies and porosity anomalies corresponding to input after minor adjustment for internal consistency. The anomalies suggest over-pressuring in the order of 5 –7 MPa, which is consistent with observations (e.g. Japsen 2000). The adjustments, that account for difference in input and output (Tables 5.2 and 5.4) originate from approximate ways of converting burial anomalies to porosity anomalies and vice-versa. The chalk burial anomalies are somewhat higher than those for the Palaeogene units (Table 5.4). This could be realistic, as over-pressuring by a combination of the presence of hydrocarbons and leakage from the even more over-pressured Jurassic below is likely. The Chalk compaction parameter set 2 (Table 5.1) only produce burial anomalies in the range 68 –391 m (largest in the Ekofisk Formation) corresponding to overpressures of 0.7 – 3.9 MPa and even estimated over-compaction in the lowermost chalk. Chalk model 3 is therefore more compatible with observed pressures and produce less vertical variation in the over-pressured section, also in agreement with pressure data.

The porosity – depth plot in Fig. 31 shows the compaction paths for the four Chalk units. It is interesting, that the present porosity levels (lower end points of the curves) seem to be a roughly downward parallel shift from the normal compaction curve. Only the Ekofisk Formation seems to have slightly higher porosity according to this shift as may be consistent with an overpressure contribution from hydrocarbons in addition to the regional water zone pressures. The time – porosity plot in Fig. 32 shows the overpressure (deviation from normal compaction path) to have started between 6 – 8 Ma b.p. However, the way this is calculated, this estimate is a minimum age for overpressure onset. The early parts of the porosity – time plot (Fig. 32) is unrealistic: The start porosity is in the order of 70% and the time for convergence of a more realistic development with the late part may be estimated from Fig. 29.

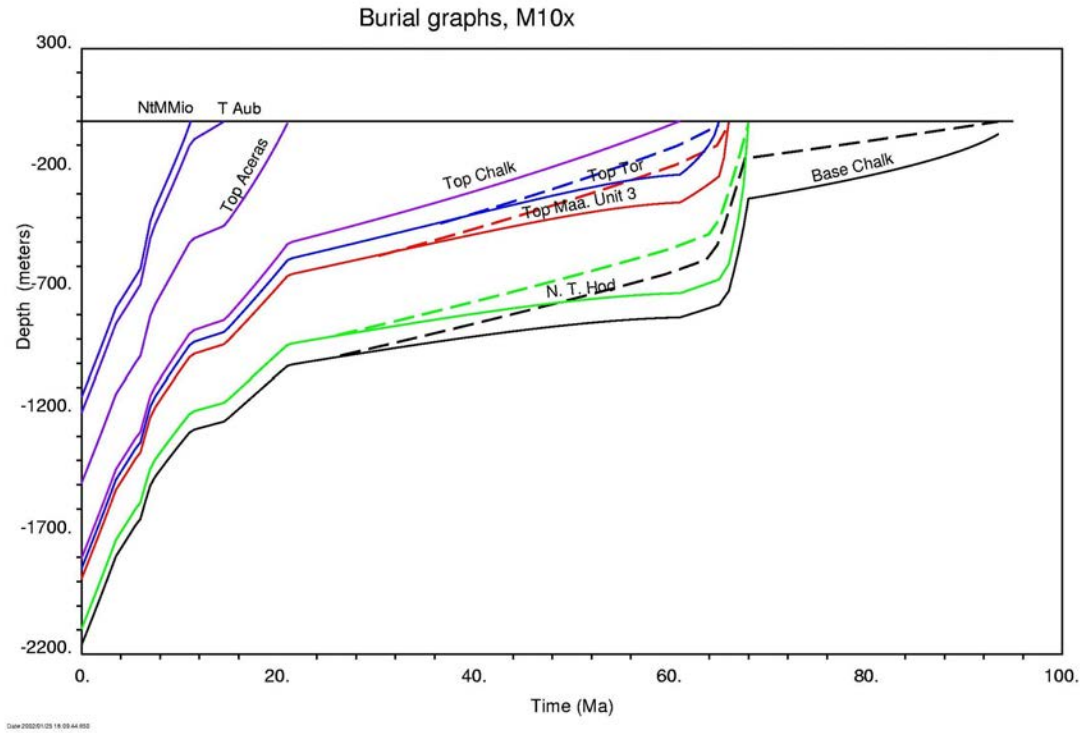

Fig. 29: Burial graph for the M-10x location. Dashed curves represent a more plausible modelling of the shallow/early part (see text).

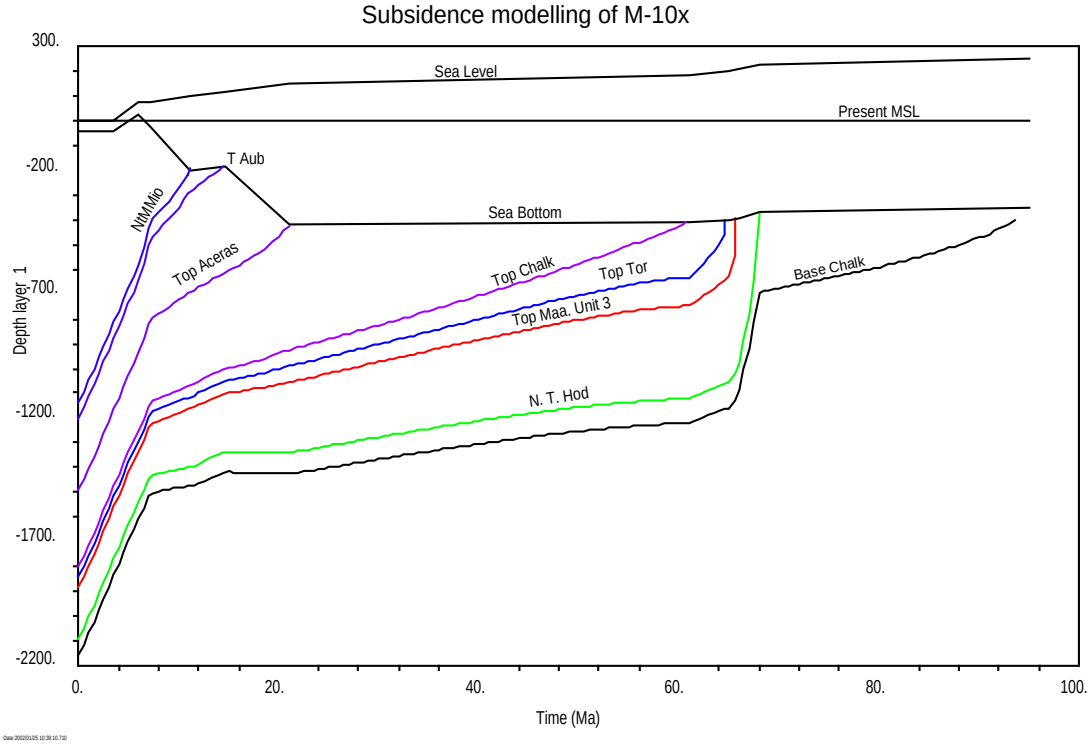

Fig. 30: Subsidence at the M10-X location. The graph is corrected for palaeobathymetry and relative sea-level variations.

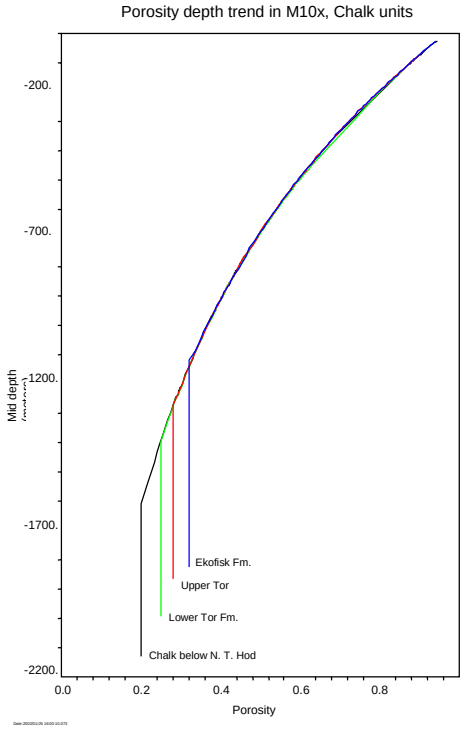

Fig. 31: Calculated porosity – depth development at the M10x location. Lower end-points are the porosity as of today.

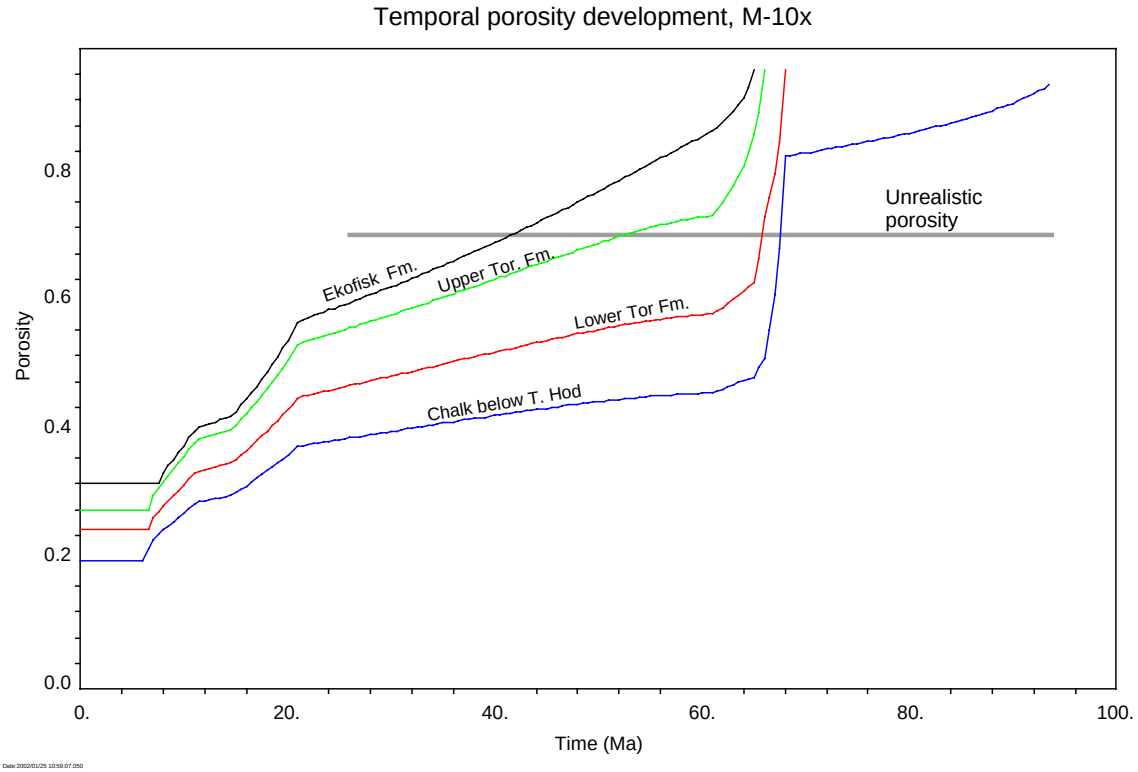

Fig. 32: Porosity – time development at the M-10x location. The development before 50 Ma b.p. is probably rather unrealistic due to the assumed very high surface porosity.

5.3 Pseudo 3D backstripping

Backstripping of maps is done by performing 1D backstripping at all grid points representing the digital maps. The example presented in this section covers the Kraka Field and encompasses 9 units. Pertinent information on these units is given in table 5.5, which is comparable to tables 5.2 and 5.3. As may be evident, palaeo bathymetry information is, as yet, not assumed to vary inside the map area, as only time variation so far is given. This may be of considerable consequence for palaeo structural reconstruction, which is considered particularly relevant for the last 3 units. The overpressure information for the lower Post Chalk Group is given as a burial anomaly, and is assumed uniform within the mapped area. The two Chalk units also suffer over-pressuring, but is given in the form of present day porosity maps as derived in section 4 of this report.

Unit	Duration (Ma)	Pal. Depth (m)	Sea level (m)	ϕ_0	a	ϕ_{obs}
U.Pliocene – Recent	3.5	40	0	0.56	0.0003906	-
L. Pliocene	2.5	50	80	0.56	0.0003906	-
Messinian	1.12	100	80	0.56	0.0003906	-
Tortonian	4.08	300	100	0.56	0.0003906	-
Mid Miocene	3.4	300	120	0.56	0.0003906	500
Aquitanian	6.5	570	150	0.71	0.0005102	500
Paleocene – Oligocene	39.9	600	190	0.71	0.0005102	500
Ekofisk Fm	4	600	200	0.968	0.0009715	Map
Upper Tor Fm	1	600	210	0.968	0.0009715	Map

Table 5.5: General input data for pseudo 3D modelling.

Three input files are required for the modelling:

- Stratigraphic information: Compaction parameters, duration etc. As listed in table 5.5.
- Thickness information: Each line contains coordinates, and present day thicknesses in meters listed from the top down.
- Observed porosity (optional): Contains lines of coordinates and porosities or thicknesses listed from the top down, but only for the layers in the strat. Info. File that are indicated to be supplied with map information for this.

After supplying these files, the user is requested to select which layer to display, and how far back in time, the subsidence simulation needs to go. The program produces 3 files (CPU time roughly 10 min for 250,000 points going back 21 Ma):

- BASINSUB.OUT: Contains maps of Unit tops, thicknesses and porosity at the selected time.
- BASINTIM.OUT: Contains maps of the selected layers that show the time of onset for abnormal porosity (onset of overpressure) and the porosity at that time.
- BASINPRS.OUT: Contains maps for the selected horizons that show the present day burial anomaly (difference between present depth and depth where present porosity is “normal”).

Examples of output are given below.

Figs. 33 and 34 shows the mapped time for when porosity started to deviate from normal compaction according to the model for the upper Tor and Ekofisk formations respectively. This may suggest the approximate time for start of significant over-pressuring and/or the time for invasion of hydrocarbons to preserve porosity. This is suggested to occur some time after deposition has accelerated (compare Figs 29 and 30). Both maps suggest onset time to be somewhat later on the crestal areas of the Kraka Field, which also could be taken as an indication that leakage has allowed compaction to continue a bit further than on the flanks. Similarly, both maps show abnormal compaction to be earlier on the North-east and Southeast flanks. As this onset time is dependent on present observed porosity and this is derived from seismic inversion, the possibility exist that these anomalies rather reflect an error in the inversion. A possible error could likely be in the low frequency model.
Figs. 35 and 36 shows the modelled porosity distribution at 21 Ma b.p. for the upper Tor and Ekofisk formations respectively. The porosity is seen to be solely depth dependent, as expected from the onset time maps. This is because the time is prior to onset of abnormal compaction.
Figs. 37 and 38 shows the isopach of the Upper Tor Formation and Ekofisk Formation respectively at 21 Ma b.p. according to the model. Comparison to the present conditions (Figs. 12 and 13) shows a significant thickness increase exceeding 50%.
Fig. 39 shows a reconstructed Top Chalk Depth structure map at 21 Ma b.p. according to the model. The map cannot be compared directly to the present top structure map, because a considerable water depth is assumed to exist at this time (se Table 5.5). Still the Top Chalk is located roughly 800 m shallower than today.

5.4 Pseudo 2D backstripping

The Southeast flank of the Kraka Field has a porosity anomaly (Figs 26 & 27), which has been studied by the application of pseudo 2D backstripping. A profile crossing the most anomalous parts has been selected as portrayed in Fig. 40.
Pseudo 2D backstripping is carried out as with 1D and 3D in general. However, instead of two or four layers in the Chalk, 40 layers or cells are used with a uniform thickness of 6 meters. These cells roughly correspond to the seismic sample rate. The total number of layers is thus 47, where Post Chalk layers are the same as in 1 and 3D backstripping. As in the 3D backstripping, file information with present porosity as derived from seismic inversion data is fed into the program. The dense layering in the Chalk enables present and “past” profiles to be generated.
Fig. 41 shows the general layering along the profile with a two time vertical exaggeration (above) and the present day porosity as derived from seismic inversion in 4 time vertical exaggeration (below). The other profiles presented below are all with a 4 time vertical exaggeration. The lower profile clearly shows the high porosity streaks in the Tor Formation (at 2 – 4.5 km) and farther up-dip in the Ekofisk Formation. Very high porosity in the uppermost sample in the Danian is probably an error caused by limitations in the high frequency content of the seismic data and/or low frequency model. The upper one or two samples are therefore “contaminated” with low impedance from the lowermost Post Chalk unit (yielding too high porosity).

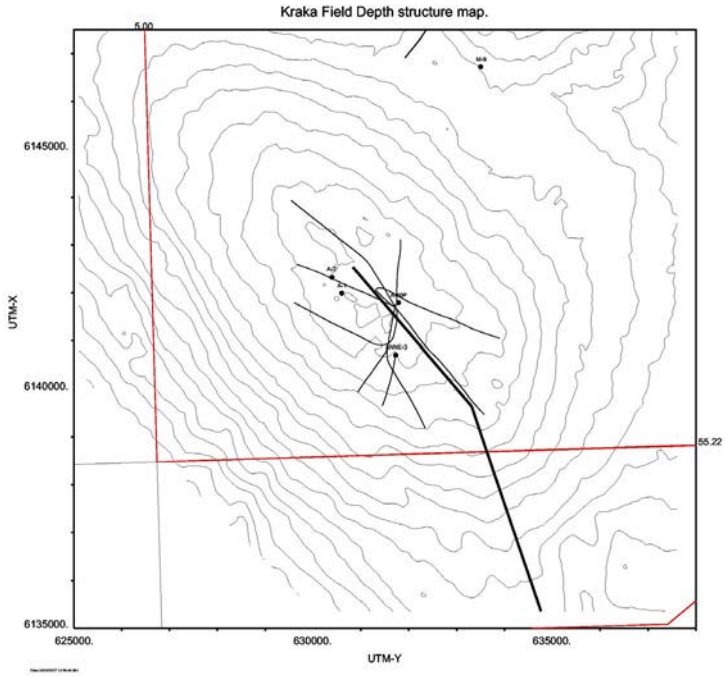

Fig. 40: Location of profile on the SE flank of the Kraka Field. Contours are Top Chalk depth contours repeated from Fig. 5.

Fig. 42 shows four different types of program output in profile. The upper profile shows the calculated burial anomaly as derived from the difference between the present porosity and the assumed normal compaction trend (Fig. 28). A very large burial anomaly is calculated for the upper cells in the Ekofisk Formation, which is due to some combination of upward increasing porosity and artefacts originating from the strong change in general impedance level occurring at the top Chalk transition (see above). The high burial anomaly level is, however, also occurring in the upper Tor Formation. Interestingly, this burial anomaly is much more continuous than the corresponding porosity anomaly in Fig. 41, which suggests that the down-dip decreasing porosity in the high porosity layer is rather a burial effect than caused by changing chalk types and/or other causes for the porosity anomaly.

This picture is to some extent repeated in the second profile, which shows the calculated time for deviation from normal compaction trends. The layered appearance of this "onset time" on the Southeast flank suggests that rock compositional and/or hydrocarbon-charging effects play a role. The layering is impossible to achieve by overpressure alone. This also shows that the employed simplistic backstripping procedure is unable to handle facies variations within the Chalk. Much of the crestal parts of the Kraka field are only slightly more porous than predicted by the assumed normal compaction trend as indicated by the very late "onset time" for under-compaction. Leakage of pore fluids from the crestal areas and/or invasion of fluids to enhance diagenesis are likely causes for this.

The third profile in Fig. 42 shows that the entire chalk package is on the normal compaction trend at 10 Ma b.p. according to the model, as the porosity is everywhere higher than today, and is monotonically deteriorating with depth. The high porosity streak in the Tor Formation is almost vanished at this time.

The fourth profile shows the calculated bed thickness at 10 Ma. The plot illustrates the amount of compaction during the last 10 Ma, as the input bed thickness, the present thickness, is uniformly 6 m. On this plot anomalous high porosity streaks show up as streaks

that have not compacted (retains a 6 m thickness). Parts that are dense today, are predicted to have compacted significantly over the last 10 Ma, hence the larger thickness in the past.

5.4.1 Backstripping "average" properties

The detailed variations in the backstripping output are more likely to reflect facies variations rather than variation in over-pressure effects on a homogeneous chalk medium as assumed implicitly in the backstipping procedure. An alternative approach could be to backstrip using average porosity, and then to retain the local relative porosity variation.

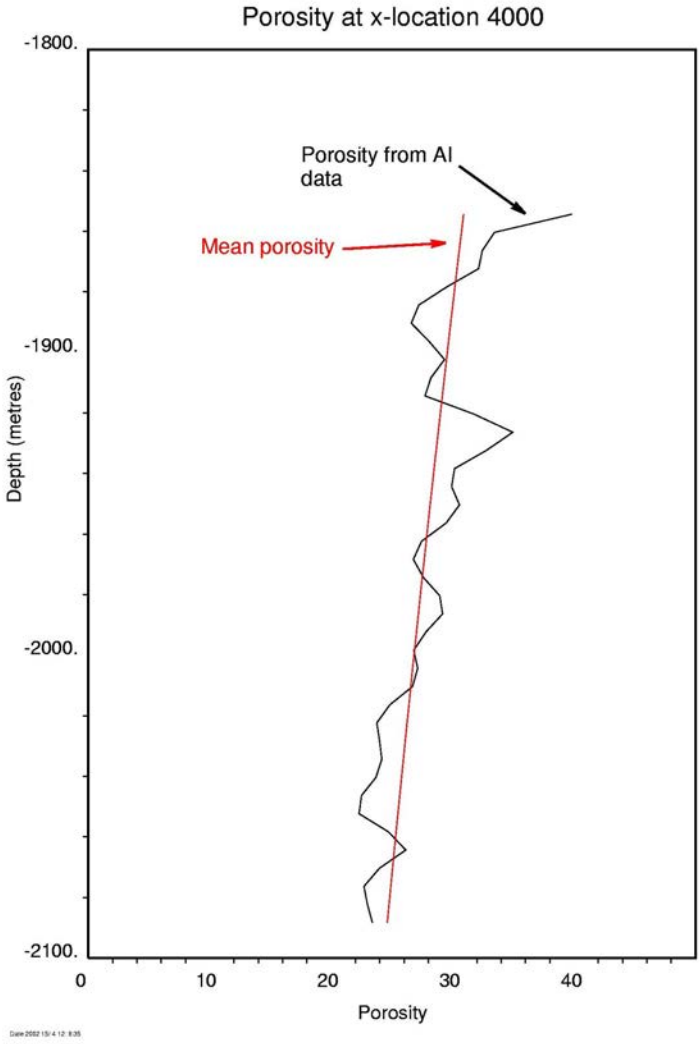

Fig. 43: Chalk porosity at x-location 4000 from profile in Fig. 41. Porosity derived from seismic inversion is in black. The average porosity function at this location (in red) is according to the Chalk model 3 (table 5.1) with a burial anomaly of 680 m.

Arguments for this are:

- Vertical porosity variations are not likely to be caused by variations in timing and degree of overpressure since local pressure differences are likely to dissipate quickly.

- Vanishing vertical porosity variations back in time to yield only depth dependency is unlikely. Or rather; layering is unlikely to be a phenomenon caused only by late over-pressuring.
- Onset time for under-compaction is likely to vary smoothly geographically: The main cause is assumed to be overpressure generated by rapid Neogene deposition.

The burial anomaly is likely to vary smoothly geographically: Excess fluid pressures are assumed to be locally equilibrated.

This approach is implemented by calculating a common burial anomaly for all samples in the chalk at one geographical location. Again: This anomaly is the vertical distance between actual sample depth and the depth where the sample porosity would be on the normal compaction trend. This average anomaly is thus the average of the differences between the present depth and the depth of onset of under-compaction as given by equation 11.

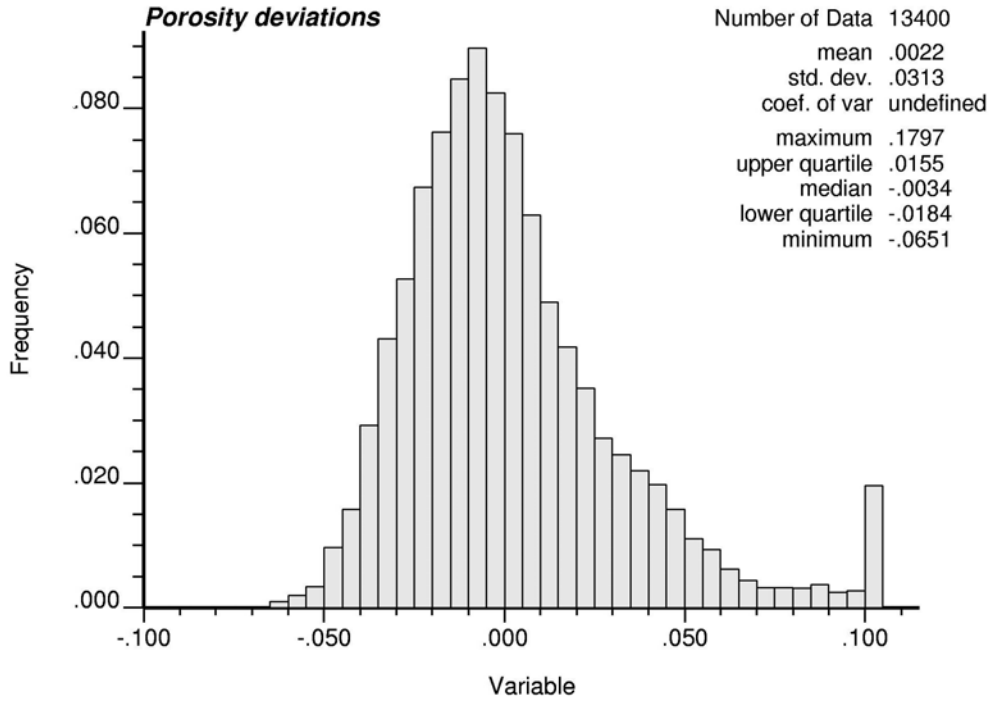

Fig. 44: Histogram of the differences between observed porosity and the calculated average porosity – depth function for all samples in the 2-D chalk model.

The principle of average porosity is depicted in Fig. 43 exemplified with the porosity at x-location 4000 from the profile in Fig. 41. As it is seen, the local deviation relative to the average function (including burial anomaly) is generally less than +/- 5 %. A histogram of all these deviations along the profile shows that approximately 90 % of the data points deviate less than 5% porosity from the average function (Fig. 44). This low deviation is ensured by the laterally varying burial anomaly. The local peak at around +10% porosity is probably mainly erroneous data from the uppermost Danian, where transitional problems originating from seismic inversion are encountered (discussed above).

Examples of application of this approach are shown in Fig. 45. A surprisingly smooth calculated burial anomaly function is shown as a red curve in panel 1. These burial anomalies

and Chalk model 3 (Table 5.1) gives the average porosity depth function displayed in the same panel. The burial anomaly suggests overpressure variations in the order of 4 to 7.5 MPa with the lowest values on the crest of the Kraka Field. This suggests leakage from the central Kraka Field and/or an erroneous low frequency model used in the seismic inversion.

The second panel in Fig. 45 shows the residual porosity, which added to the porosity in panel 1 yields the calculated porosity as of today. An increase in lateral continuity of the anomalies is noted in the second panel. The residual porosity field in panel 2 is added to modelled smooth porosity fields representing the present and past. Such reconstructed porosity profiles in the past are shown as panels 3 and 4 for 10 Ma and 8 Ma b.p. respectively. The lowermost panel in Fig. 45 shows that under-compaction commenced at between 4.5 and 7.5 Ma b.p. The reconstructed porosity profiles in panels 3 and 4 are therefore both normally compacted until then. Any panel younger than 4.5 Ma b.p. will be calculated to be under-compacted and thus display the same porosity as of today. The calculated 4.5 Ma onset of under-compaction could also reflect local leakage of fluids after overpressuring had started. Such more complicated scenarios are not considered possible to model in the present analytical approach.

Fig no.	Interval	C.I.	Text
33	0-10	0.5	Onset time for abnormal porosity Upper Tor Formation
34	0-10	0.5	Onset time for abnormal porosity Ekofisk Formation
35	0.40-0.60	0.01	Porosity at 21 Ma b.p. Upper Tor Formation
36	0.40-0.60	0.01	Porosity at 21 Ma b.p. Ekofisk Formation
37	30-150	6	Upper Tor Fm. isopach at 21 Ma b.p.
38	20-70	2.5	Ekofisk Fm. isopach at 21 Ma b.p.
39	900-1400	25	Top Chalk depth structure map at 21 Ma b.p
41	20 – 40%	1%	Profile with 2 (upper) and 4 times (lower) vertical exaggeration. Lower profile is porosity from seismic impedance.
42	0 – 1000m 2 – 12 Ma 20 – 40% 6 – 8 m	50 m 0.5 Ma 1% 0.1 m	Profiles showing calculated burial anomaly, onset of under-compaction, Porosity at 10 Ma b.p., bed thickness at 10 Ma b.p.
45	20 – 40% -10-10% (second profile)	1%	Porosity profiles showing 1: Average porosity depth function, 2:Porosity deviation from average, 3: Porosity at 10 Ma b.p., 4: Porosity at 8 Ma b.p., 5: calculated onset of under-compaction.

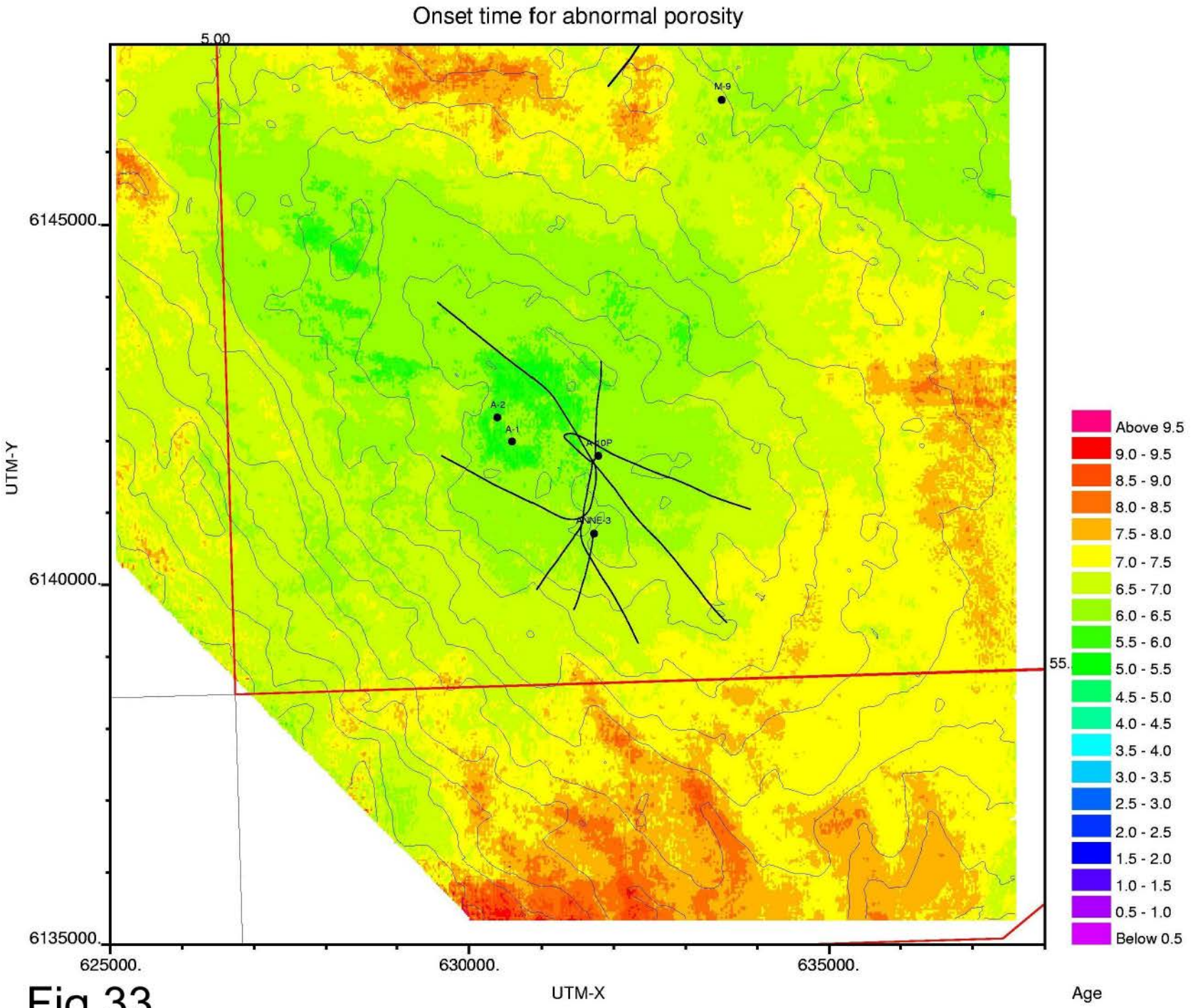
Onset time for abnormal porosity
5.00
6145000.
6140000.
6135000.
625000.
630000.
635000.
55.
UTM-Y
UTM-X
M-9
A-2
A-1
A-10P
A-NNE-3
Above 9.5
9.0 - 9.5
8.5 - 9.0
8.0 - 8.5
7.5 - 8.0
7.0 - 7.5
6.5 - 7.0
6.0 - 6.5
5.5 - 6.0
5.0 - 5.5
4.5 - 5.0
4.0 - 4.5
3.5 - 4.0
3.0 - 3.5
2.5 - 3.0
2.0 - 2.5
1.5 - 2.0
1.0 - 1.5
0.5 - 1.0
Below 0.5
Age

Fig.33

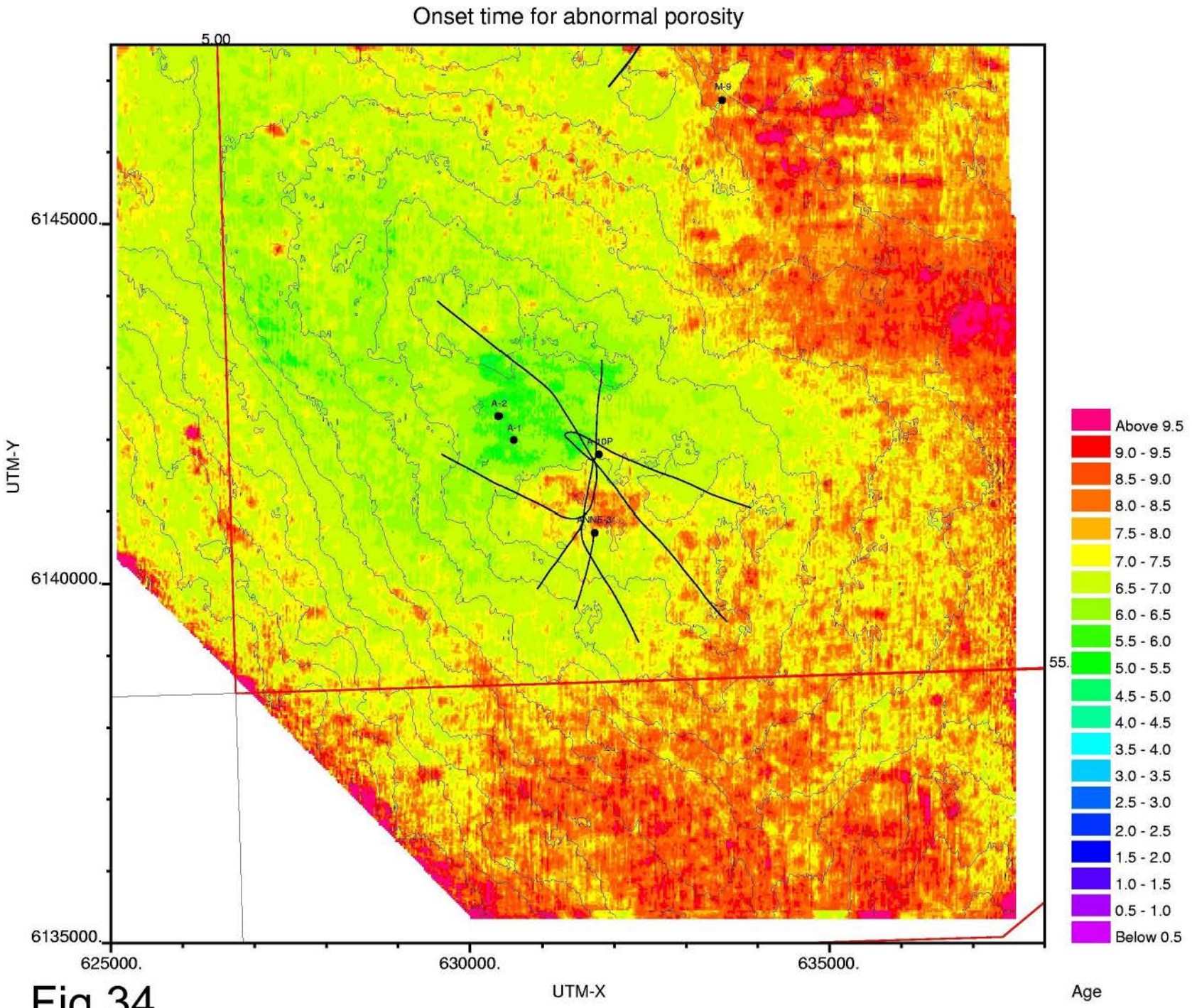
Onset time for abnormal porosity
5.00
6145000.
6140000.
6135000.
625000.
630000.
635000.
UTM-X
UTM-Y
55.
M-9
A-2
A-1
A-10P
ANNE-3
Above 9.5
9.0 - 9.5
8.5 - 9.0
8.0 - 8.5
7.5 - 8.0
7.0 - 7.5
6.5 - 7.0
6.0 - 6.5
5.5 - 6.0
5.0 - 5.5
4.5 - 5.0
4.0 - 4.5
3.5 - 4.0
3.0 - 3.5
2.5 - 3.0
2.0 - 2.5
1.5 - 2.0
1.0 - 1.5
0.5 - 1.0
Below 0.5
Age

Fig.34

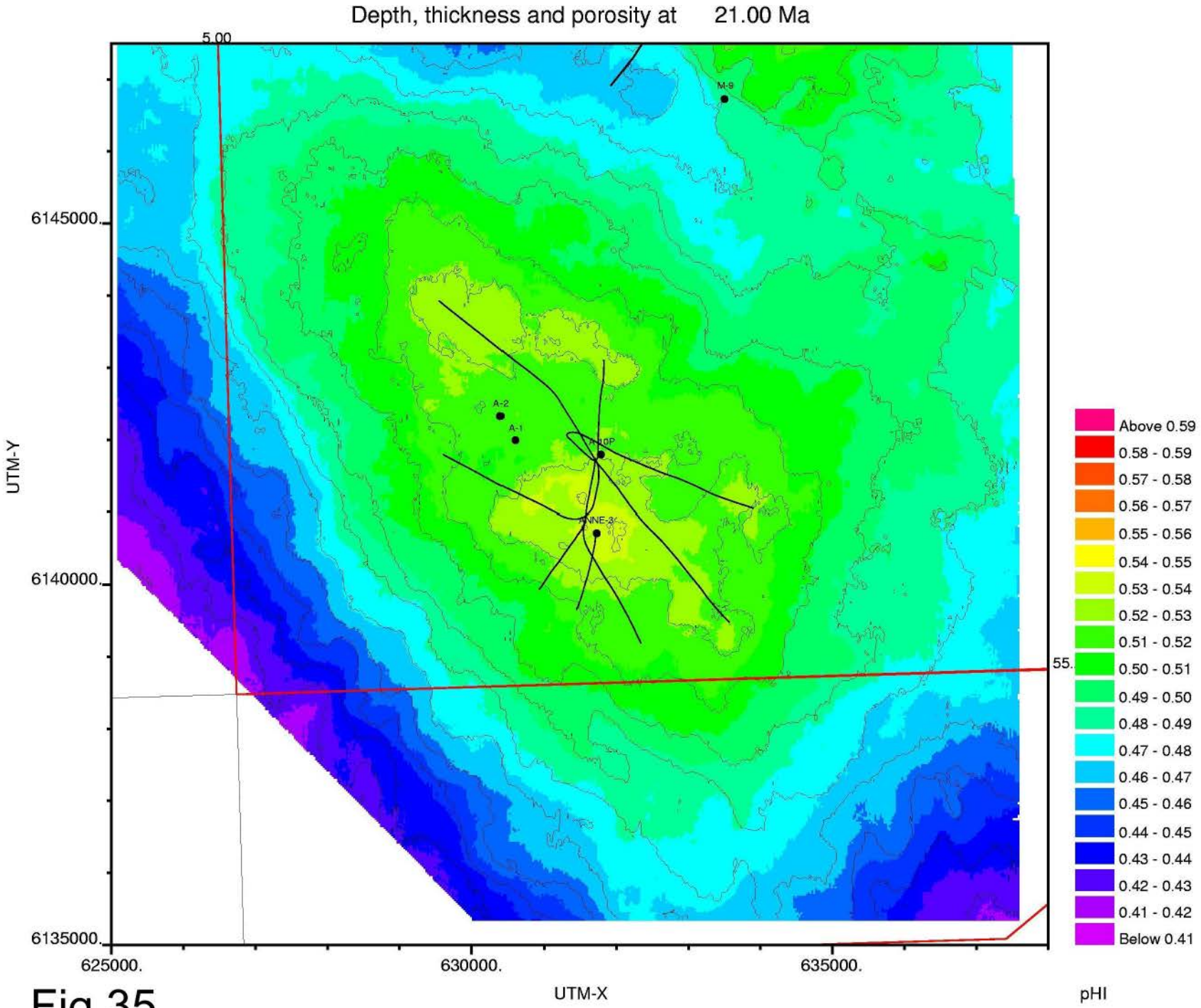
Depth, thickness and porosity at 21.00 Ma
5.00
6145000.
6140000.
6135000.
625000.
630000.
635000.
UTM-X
UTM-Y
M-9
A-2
A-1
A-10P
ANNE-3
55.
Above 0.59
0.58 - 0.59
0.57 - 0.58
0.56 - 0.57
0.55 - 0.56
0.54 - 0.55
0.53 - 0.54
0.52 - 0.53
0.51 - 0.52
0.50 - 0.51
0.49 - 0.50
0.48 - 0.49
0.47 - 0.48
0.46 - 0.47
0.45 - 0.46
0.44 - 0.45
0.43 - 0.44
0.42 - 0.43
0.41 - 0.42
Below 0.41
pHI

Fig.35

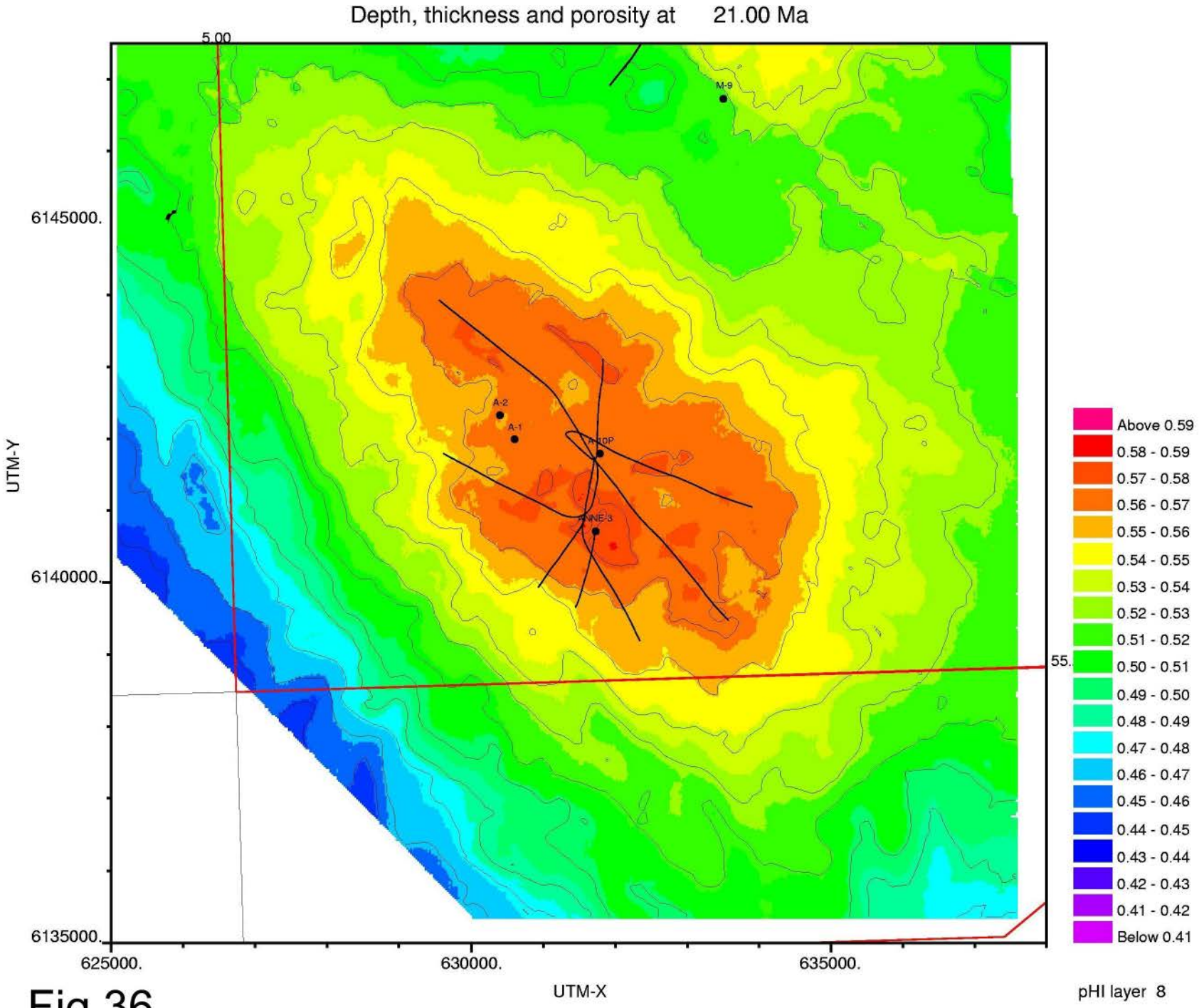
Depth, thickness and porosity at 21.00 Ma
5.00
6145000.
6140000.
6135000.
625000.
630000.
635000.
UTM-Y
UTM-X
55.
M-9
A-2
A-1
A-10P
ANNE-3
Above 0.59
0.58 - 0.59
0.57 - 0.58
0.56 - 0.57
0.55 - 0.56
0.54 - 0.55
0.53 - 0.54
0.52 - 0.53
0.51 - 0.52
0.50 - 0.51
0.49 - 0.50
0.48 - 0.49
0.47 - 0.48
0.46 - 0.47
0.45 - 0.46
0.44 - 0.45
0.43 - 0.44
0.42 - 0.43
0.41 - 0.42
Below 0.41
pHI layer 8

Fig.36

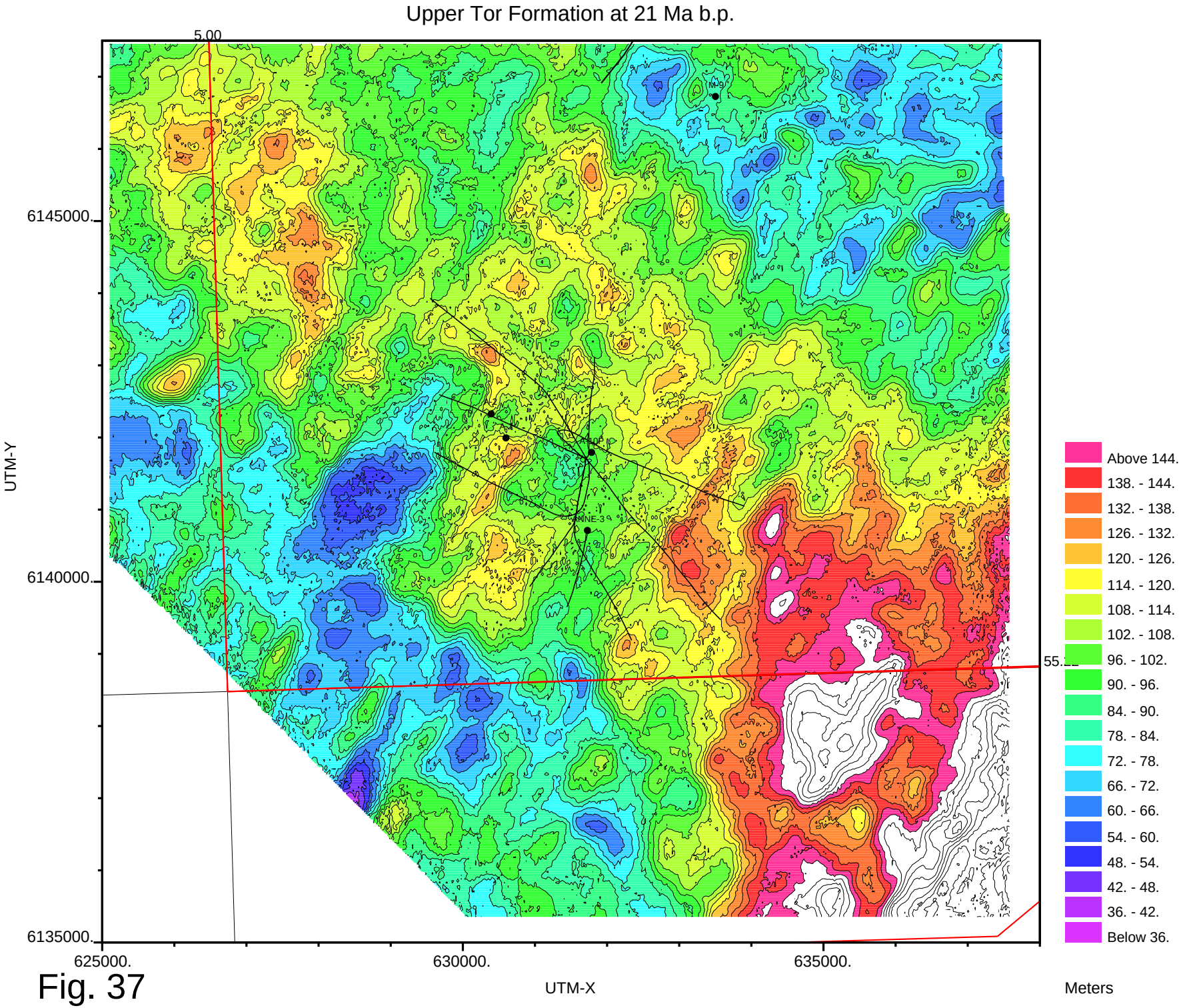
Upper Tor Formation at 21 Ma b.p.
5.00
6145000.
6140000.
6135000.
625000.
630000.
635000.
UTM-Y
UTM-X
55.
Above 144.
138. - 144.
132. - 138.
126. - 132.
120. - 126.
114. - 120.
108. - 114.
102. - 108.
96. - 102.
90. - 96.
84. - 90.
78. - 84.
72. - 78.
66. - 72.
60. - 66.
54. - 60.
48. - 54.
42. - 48.
36. - 42.
Below 36.
Meters

Fig. 37

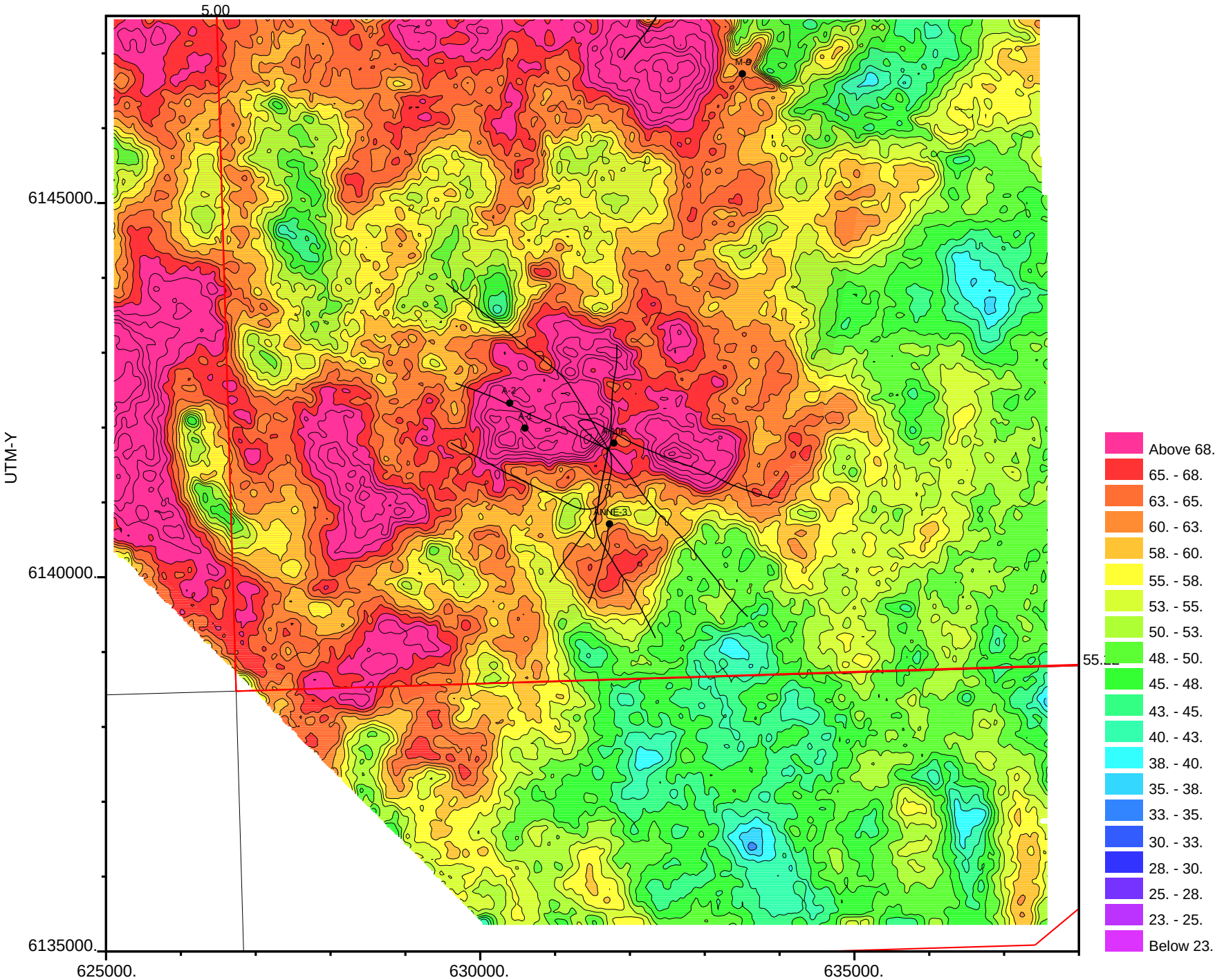
Ekofisk isopach smooth at 21 Ma b.p.
5.00
6145000.
6140000.
6135000.
625000.
630000.
635000.
UTM-Y
UTM-X
M-9
A-2
A-4
A-10P
ANNE-3
55.
Above 68.
65. - 68.
63. - 65.
60. - 63.
58. - 60.
55. - 58.
53. - 55.
50. - 53.
48. - 50.
45. - 48.
43. - 45.
40. - 43.
38. - 40.
35. - 38.
33. - 35.
30. - 33.
28. - 30.
25. - 28.
23. - 25.
Below 23.
Meters

Fig. 38

Top Chalk depth structure map 21 Ma b.p.

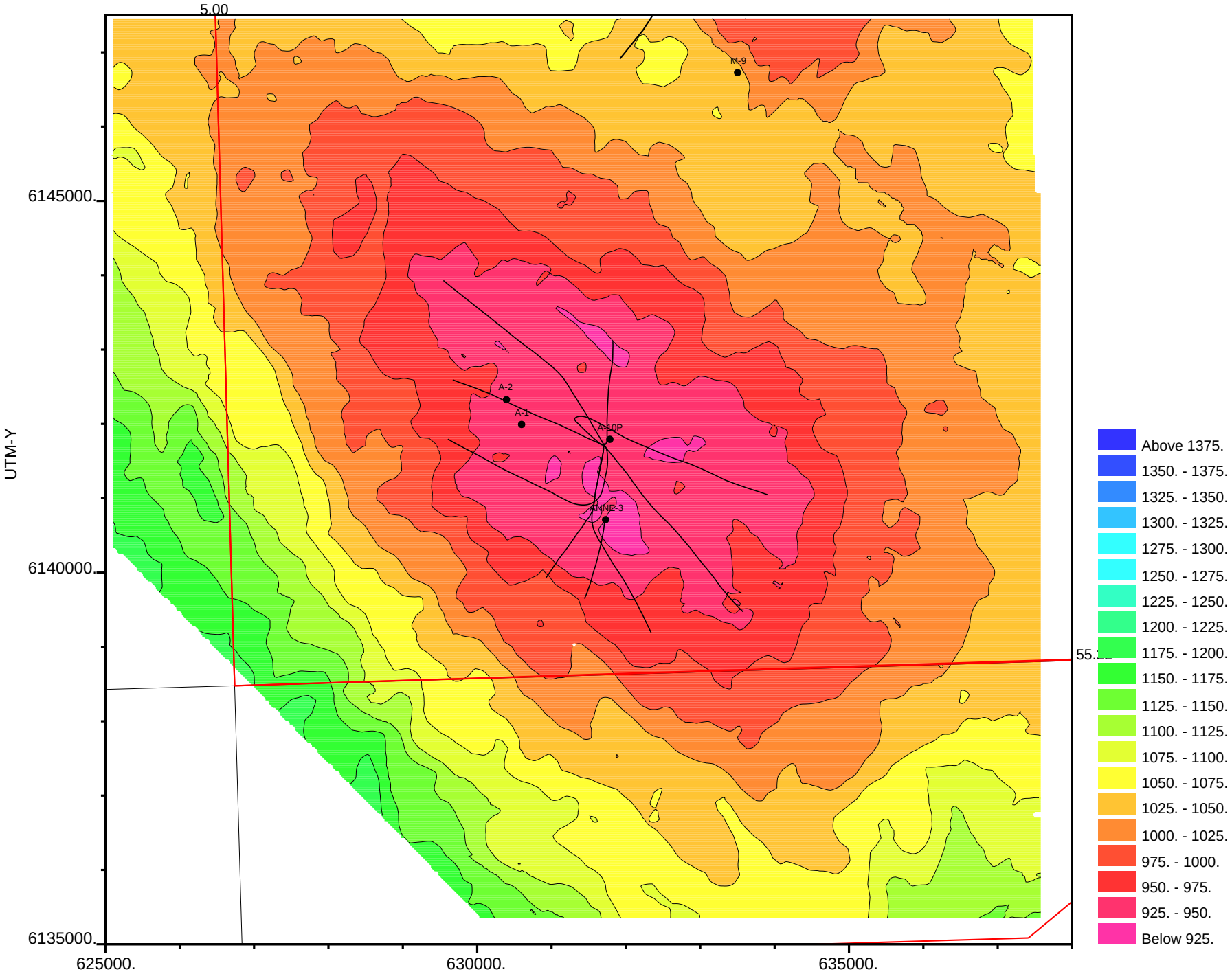

Fig. 39

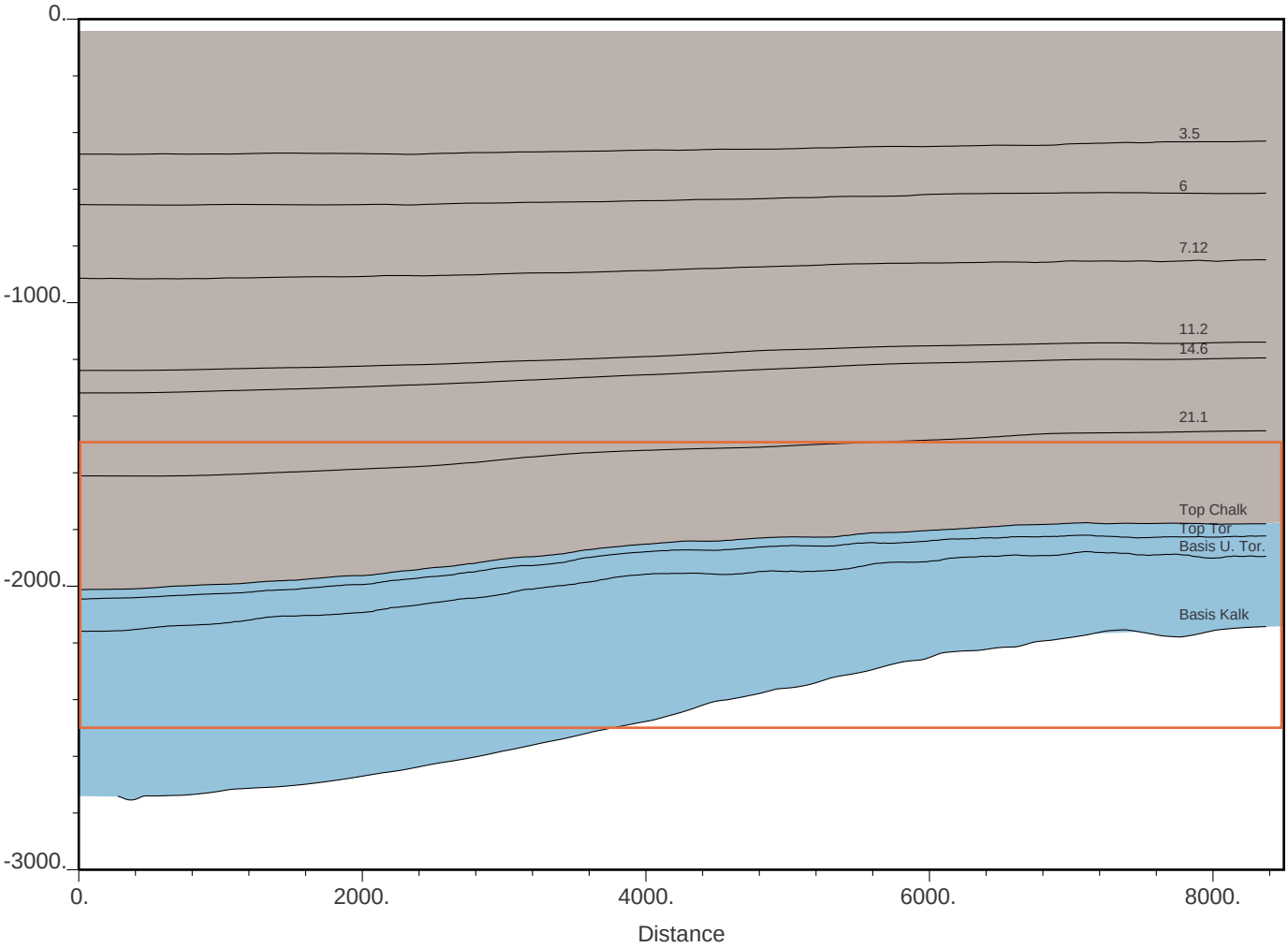

Chalk porosity from AI data

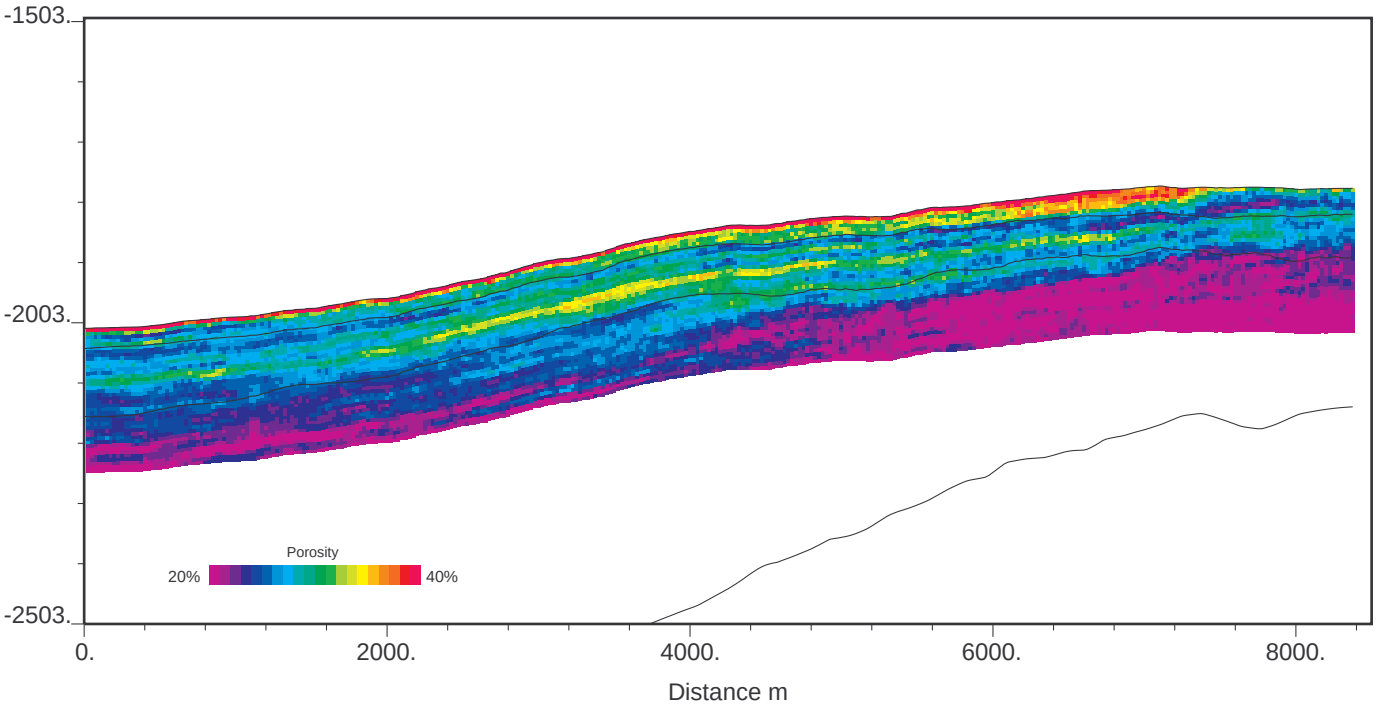

Date:2002/03/22 08:59:39.829

Fig. 41

Burial anomaly data at present

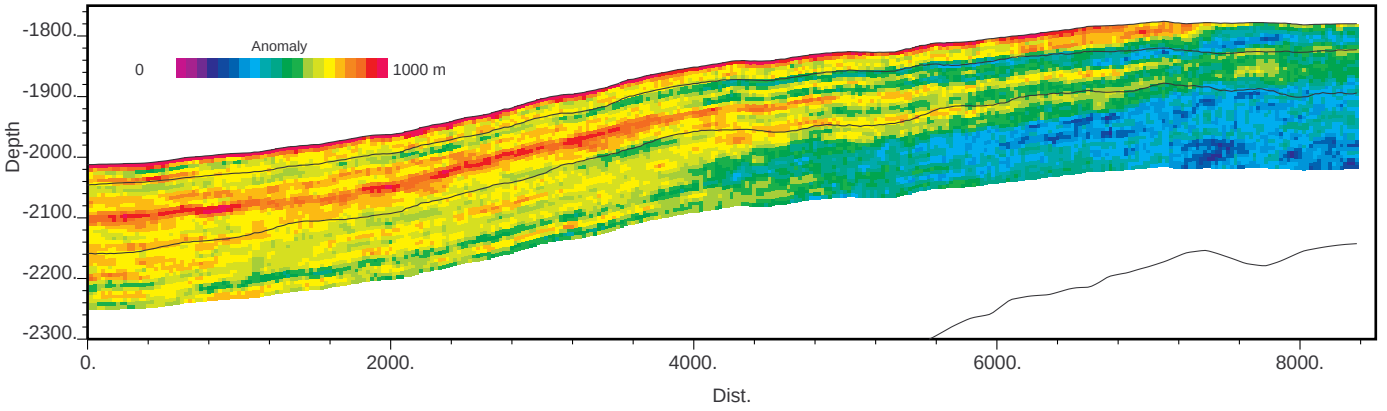

Onset time for abnormal porosity

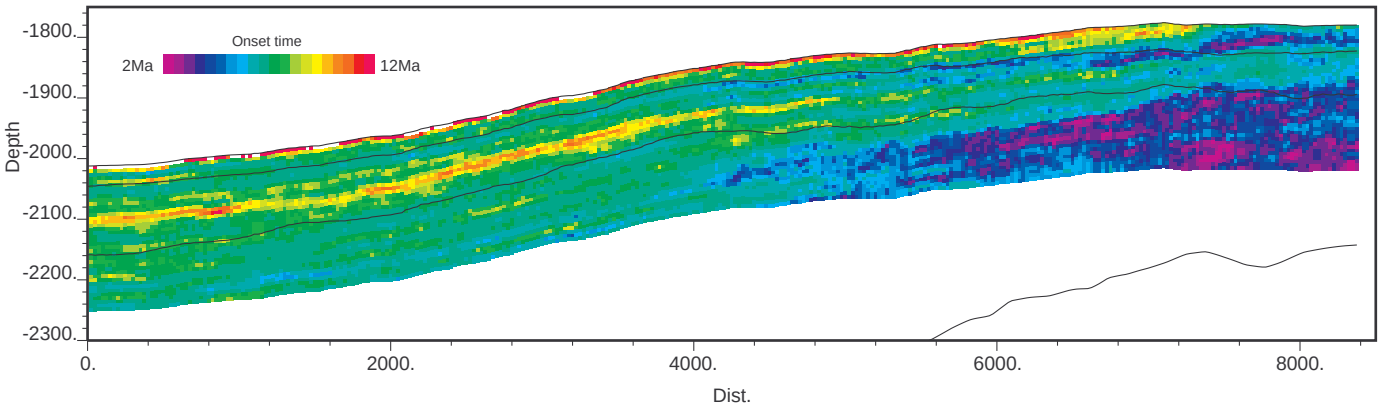

Porosity at 10.00 Ma

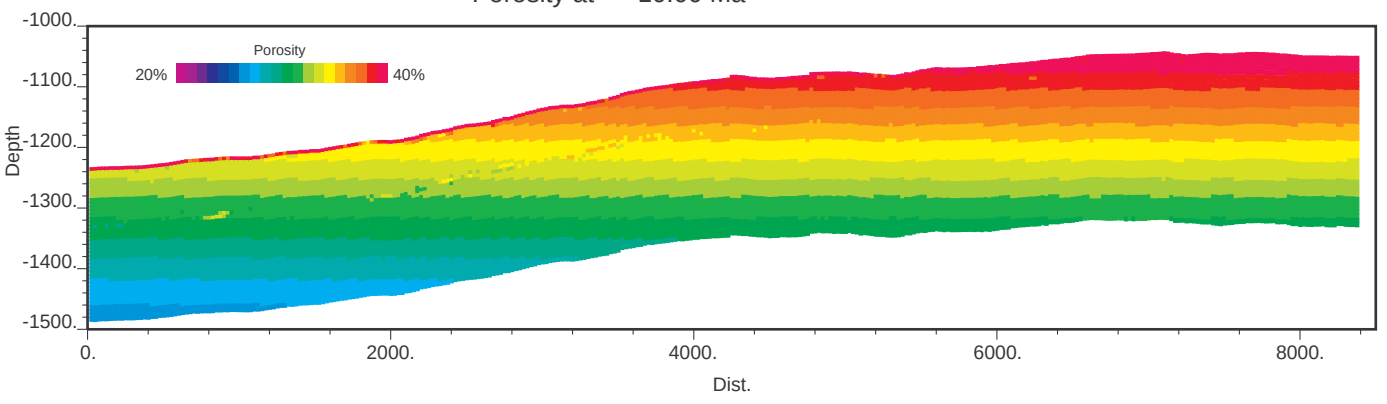

Bed, thickness at 10.00 Ma

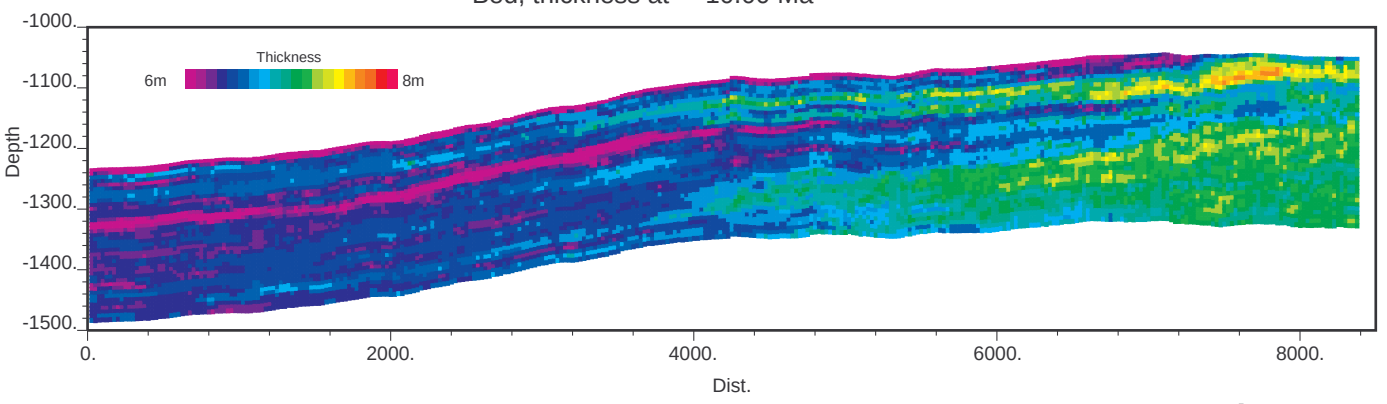

Fig. 42

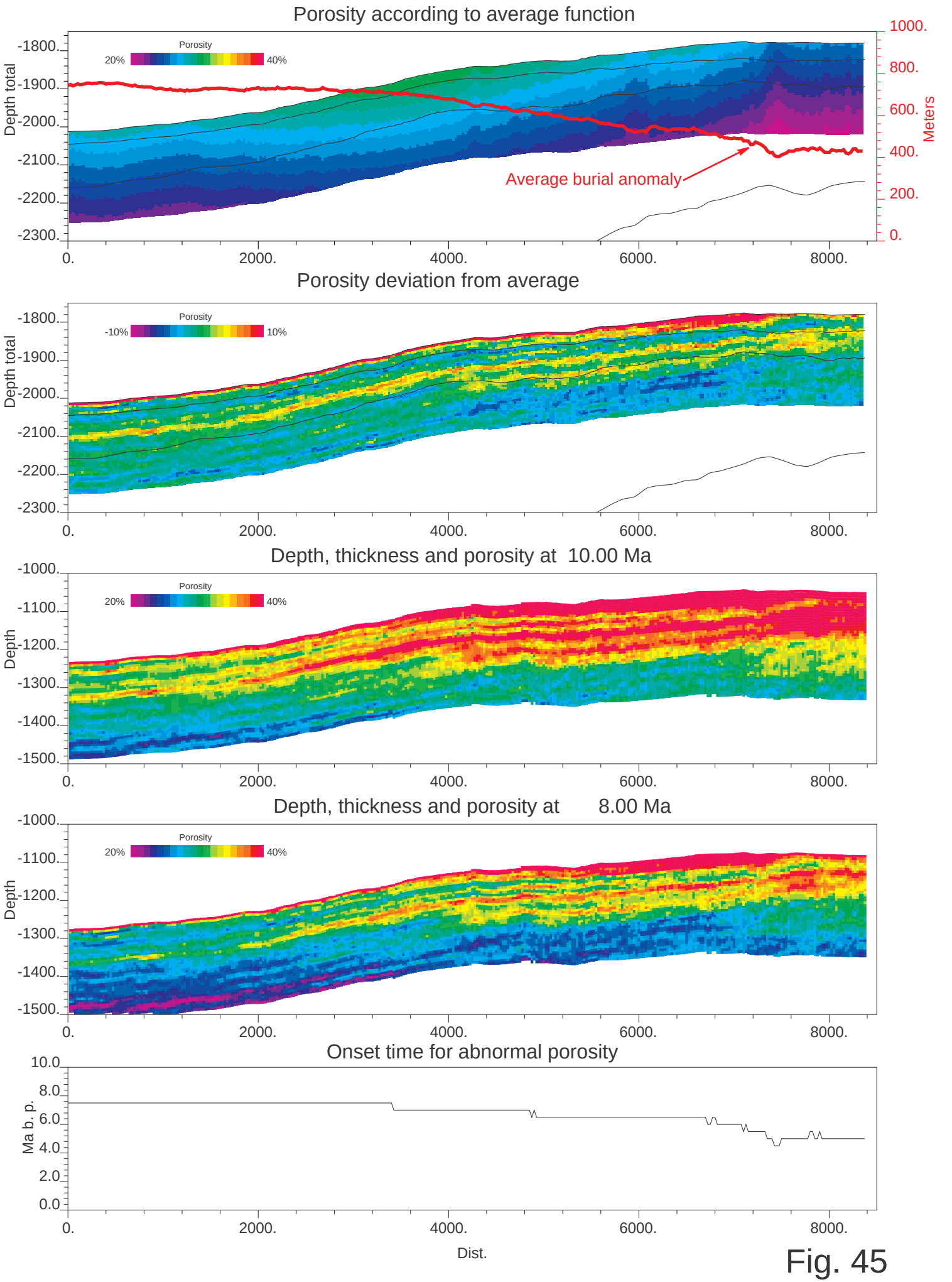
Porosity according to average function
Porosity
20%
40%
Depth total
-1800.
-1900.
-2000.
-2100.
-2200.
-2300.
1000.
800.
600.
400.
200.
0.
Meters
Average burial anomaly
0.
2000.
4000.
6000.
8000.
Porosity deviation from average
Porosity
-10%
10%
Depth total
-1800.
-1900.
-2000.
-2100.
-2200.
-2300.
0.
2000.
4000.
6000.
8000.
Depth, thickness and porosity at 10.00 Ma
Porosity
20%
40%
Depth
-1000.
-1100.
-1200.
-1300.
-1400.
-1500.
0.
2000.
4000.
6000.
8000.
Depth, thickness and porosity at 8.00 Ma
Porosity
20%
40%
Depth
-1000.
-1100.
-1200.
-1300.
-1400.
-1500.
0.
2000.
4000.
6000.
8000.
Onset time for abnormal porosity
Ma b. p.
10.0
8.0
6.0
4.0
2.0
0.0
0.
2000.
4000.
6000.
8000.
Dist.

Fig. 45

6. Discussion

Modelling of porosity development presented in this report suggests that over-pressuring in the Kraka Field area commenced later than 10 Ma b.p.
The Kraka Field has been an anticline through most of the Cainozoic with the main closure at approximately the same position as today (see section 2). It is therefore somewhat puzzling that high porosity anomalies exist on the northern and south- to south-eastern flanks. A possible explanation for this could be that migration from a deep Jurassic source located to the Southeast has been found its way to the Chalk via fractures on the southeast flank. It is thus conjectured that these hydrocarbons could have been pooled locally to cause locally elevated porosity by impeding cementation.
The main reservoir is the upper part of the Danian where permeability may reach 8 mDarcy (Thomasen and Jacobsen (1994). In the aquifer effective permeability is quoted to be around 1 mDarcy. It is likely that the Kraka Field has been sourced from the Upper Jurassic. The area around the Kraka Field attains sufficient maturity for possible HC generation only in the Lola Formation or deeper, and only in the last app. 5 Ma according to basin modelling results (Andersen et al. 1998). Shallower source rocks are immature. Maturity in the Upper Jurassic succession (notably the upper Jurassic Bo member (formerly Hot Unit)) increases to the north, north-west and east. HC invasion is thus likely to have occurred later than 5 Ma b.p., and it is possible that some component of lateral migration must be considered in order to fill the reservoir.

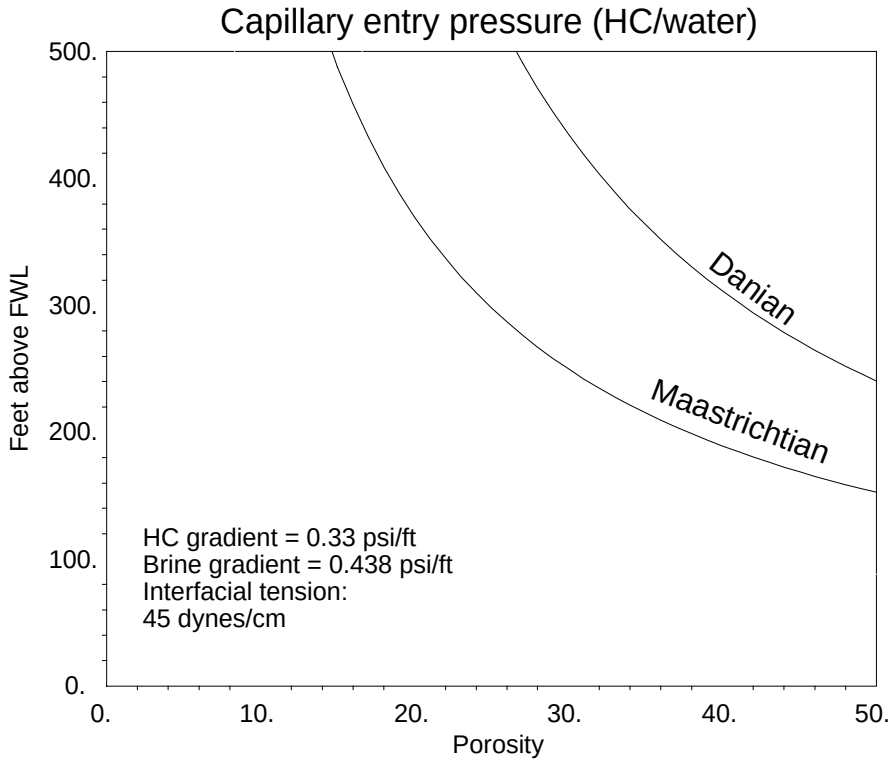

Fig. 47: Calculated entry pressures expressed as height above the free water level.

The base chalk gaussian curvature suggests the presence of sub-seismic fractures (Fig. 46). Gaussian curvature is different from zero where the shape requires plastic deformation if the surface originally was plane. Some high strain zones (shown in red) clearly coincide with standard interpreted faults, but also suggest these to be more extensive than interpreted. On the south-east flank an extensive area shows slightly elevated curvature suggesting extensive sub-seismic fracturing. The gaussian curvature clearly shows that the base chalk surface is marred by fractures/faults on the flanks in all directions. A top Chalk gaussian curvature map suggests fracturing to be insignificant at that level. This indicates that most faults and fractures terminate before reaching the Ekofisk Formation level. In accordance with this, fracture permeability is reported to be insignificant on a reservoir scale, although of local importance (Thomasen and Jacobsen 1994).

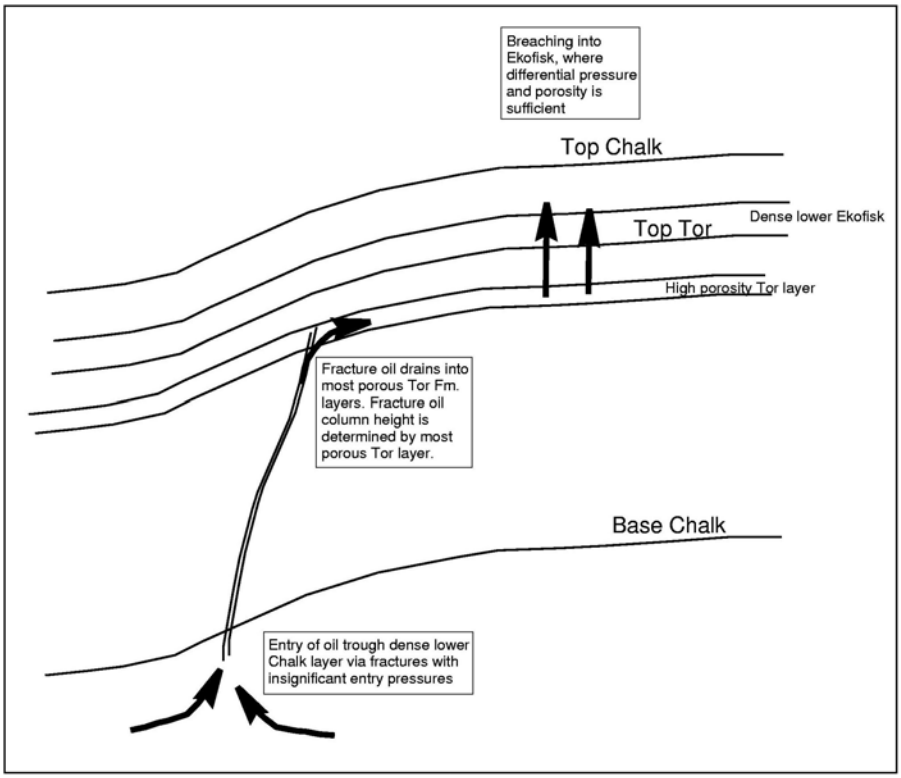

Fig. 48: Sketch of the suggested entry mechanism for the oil migration into the Tor and Ekofisk Formations.

Since a considerable oil column is required for oil to enter water-wet chalk (Fig. 47), simple matrix migration of hydrocarbons through the dense lower Chalk Group is inconceivable. Fig. 47 shows the entry pressures expressed as height above the free water level, plotted versus porosity according to the EQR model by Engstrøm (1995), and using parameters based on experience from the area relevant for Tor and Ekofisk Chalk. The plot shows that 20% porosity Maastrichtian Chalk is capable of providing top seal to a 350’ oil column rendering matrix migration through the dense lower chalk virtually impossible. Instead the faults or fractures may constitute conduits, where oil columns of sufficient height to provide sufficient differential pressure for oil to enter porous sections of the upper Chalk Group is envisaged. Due to lower capillary entry pressures in the Maastrichtian, and due to apparent

lack of seismic evidence for significant fracturing at Top Chalk level, the oil-columns in the fractures are assumed likely to be drained by Maastrichtian carrier beds before reaching the Ekofisk Formation via matrix migration through the lower Ekofisk. The principle is sketched in Fig. 48 and a hypothetical case of oil charging at 8 Ma b.p. is modelled in Fig. 49.

In this model, a non-dynamic (flat) free water level (FWL) is placed at a depth where the resulting differential pressures (between oil and water phases) just allows the lower Ekofisk Formation to be breached (Fig. 49 upper panel). This model is applied to the modelled porosity profile for 8 Ma b.p. (Fig. 45). The second panel (Fig. 49) shows a model of the present HC saturation, if differential pressures (between oil and water phases) have remained unchanged. This is done by keeping the FWL at the same distance below top Chalk during subsidence and compaction. This is equivalent to assuming that compaction has been associated with discharge of both oil and water. However, since capillary entry pressures increase with decreasing porosity, oil saturation goes down during compaction and more oil than water is expelled (lost by re-migration).

An alternative model may be that the amount of oil remains unchanged, since also the sealing capacity of the seals surrounding the accumulation increase with decreasing porosity (unless fracturing occurs). In order to maintain the hydrocarbon volume, the differential pressures (between oil and water phases) must increase to overcome the increasing capillary entry pressure, and the decreasing available pore space. This is done by lowering the FWL with 90 m corresponding to a relative pressure increase in the oil phase of 32 psi (=0.22MPa). This situation is accompanied by a perceptible redistribution of oil (Fig. 49, 3rd and 4th panel). Some of this (but not solely) is due to a reduction in porosity and a constant oil volume. In the event, that the original oil column was determined by the fracture pressure of the top seal, it is likely that further compaction must be associated with leakage of hydrocarbons due to failure of the top seal.

The models assume equilibrium conditions to have been achieved and maintained (flat FWL). However, the modelled permeability profiles in Fig. 50 show quite modest permeability both at present and at 8 Ma b.p. The permeability in the profiles is converted from modelled porosity using:

17) $$K_{air} = a \cdot \phi^{b}$$

where K_{air} is the gas permeability in *mDarcy,* ϕ is porosity in fractions, and a and b are constants as given in table 6.1 (Frykman 2001). This permeability is then converted to fluid permeability using:

18) $$K_{fl} = a \cdot K_{air}^{\ b}$$

	A	B
Danian (por. to perm.)	300	5
Maastrichtian (por. to perm.)	155	3.5
Permeability conversion	0.52	1.083

Table 6.1: Conversion parameters for porosity – permeability conversion and air to fluid permeability conversion (from Frykman 2001).

Even at 8 Ma.b.p. the fluid permeability rarely exceeds 2 mDarcy. To approximate buoyancy driven migration as well as re-migration, flow velocity has been estimated. The smoothed local gradient of the Top Chalk surface on the presented profile is shown as the 3rd panel in Fig. 50. The 4th is then the calculated flow velocity for oil assuming a permeability of 1 mDarcy (Thomasen and Jacobsen 1994), and a differential gradient between oil and water of 0.11 psi/ft. Flow rates only reach a maximum of 5 km/Ma, which makes it likely that some degree of non-equilibrium dynamic conditions exist today. Some dip on the FWL along matrix migration conduits towards possible fracture entry points must be assumed.

Fig no.	**Text**
46	Gaussian curvature at Base Chalk level. Contours are Base Chalk TWT iso lines with an interval of 25 msec.
49	Calculated HC saturations modelled for using porosity models shown in Figs. 41 (2nd panel) and 45 (4th panel).
50	Modelled Permeability based on porosity models shown in Figs. 41 (2nd panel) and 45 (4th panel).

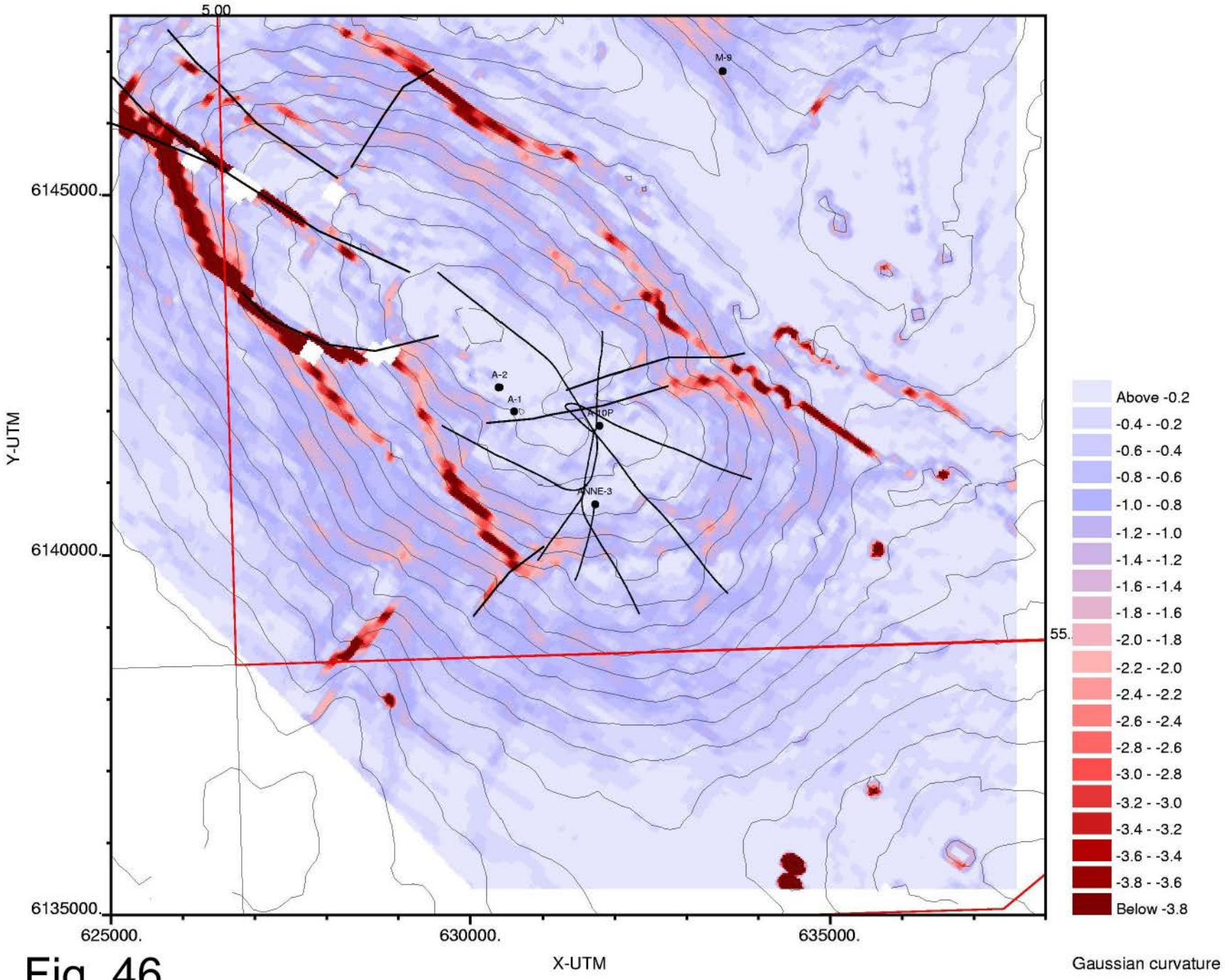
5.00
6145000.
6140000.
6135000.
625000.
630000.
635000.
X-UTM
Y-UTM
55.
M-9
A-2
A-1
A-10P
ANNE-3
Above -0.2
-0.4 - -0.2
-0.6 - -0.4
-0.8 - -0.6
-1.0 - -0.8
-1.2 - -1.0
-1.4 - -1.2
-1.6 - -1.4
-1.8 - -1.6
-2.0 - -1.8
-2.2 - -2.0
-2.4 - -2.2
-2.6 - -2.4
-2.8 - -2.6
-3.0 - -2.8
-3.2 - -3.0
-3.4 - -3.2
-3.6 - -3.4
-3.8 - -3.6
Below -3.8
Gaussian curvature

Fig. 46

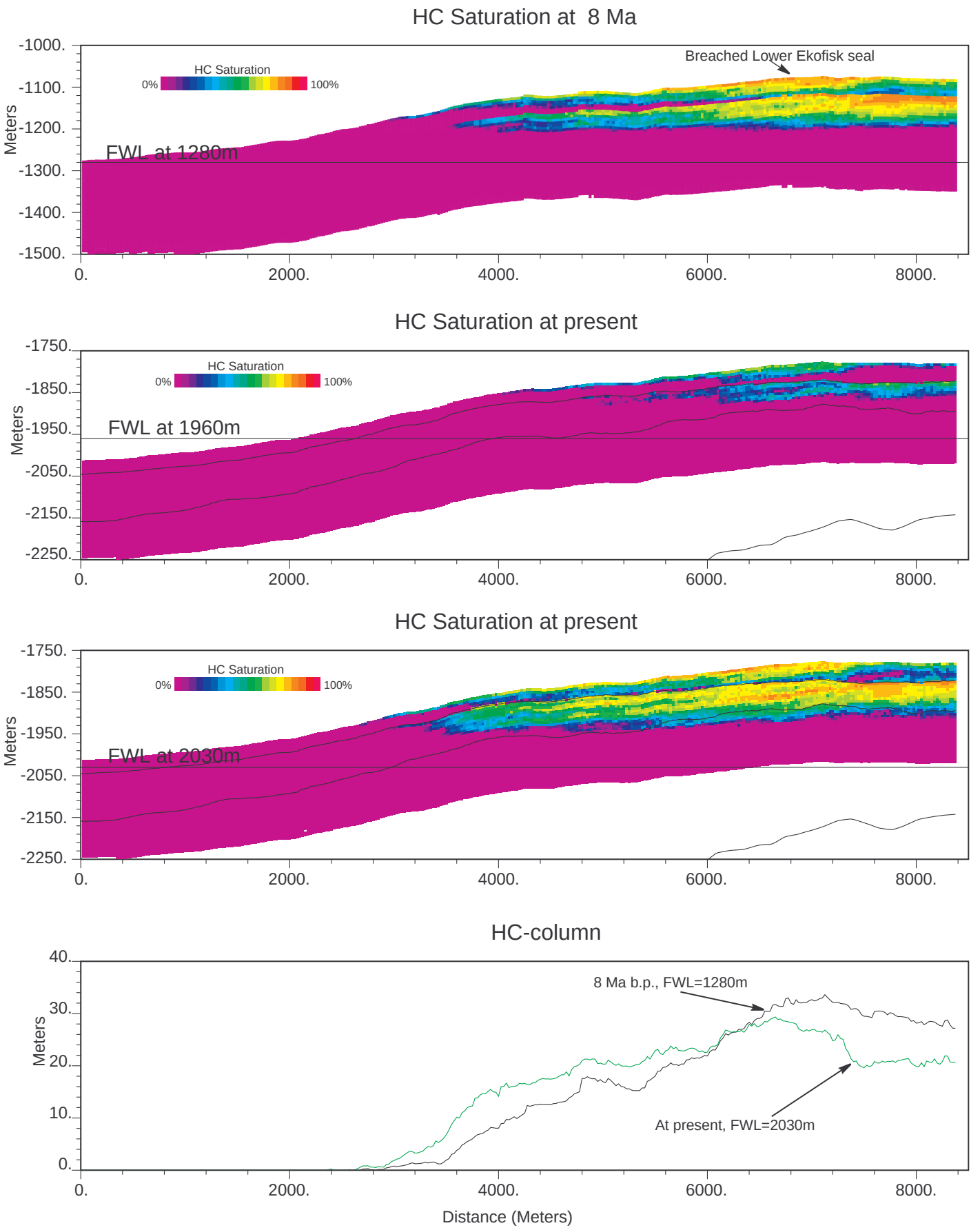
HC Saturation at 8 Ma
HC Saturation
0%
100%
Breached Lower Ekofisk seal
FWL at 1280m
Meters
-1000.
-1100.
-1200.
-1300.
-1400.
-1500.
0.
2000.
4000.
6000.
8000.
HC Saturation at present
HC Saturation
0%
100%
FWL at 1960m
Meters
-1750.
-1850.
-1950.
-2050.
-2150.
-2250.
0.
2000.
4000.
6000.
8000.
HC Saturation at present
HC Saturation
0%
100%
FWL at 2030m
Meters
-1750.
-1850.
-1950.
-2050.
-2150.
-2250.
0.
2000.
4000.
6000.
8000.
HC-column
8 Ma b.p., FWL=1280m
At present, FWL=2030m
Meters
40.
30.
20.
10.
0.
0.
2000.
4000.
6000.
8000.
Distance (Meters)

Fig. 49

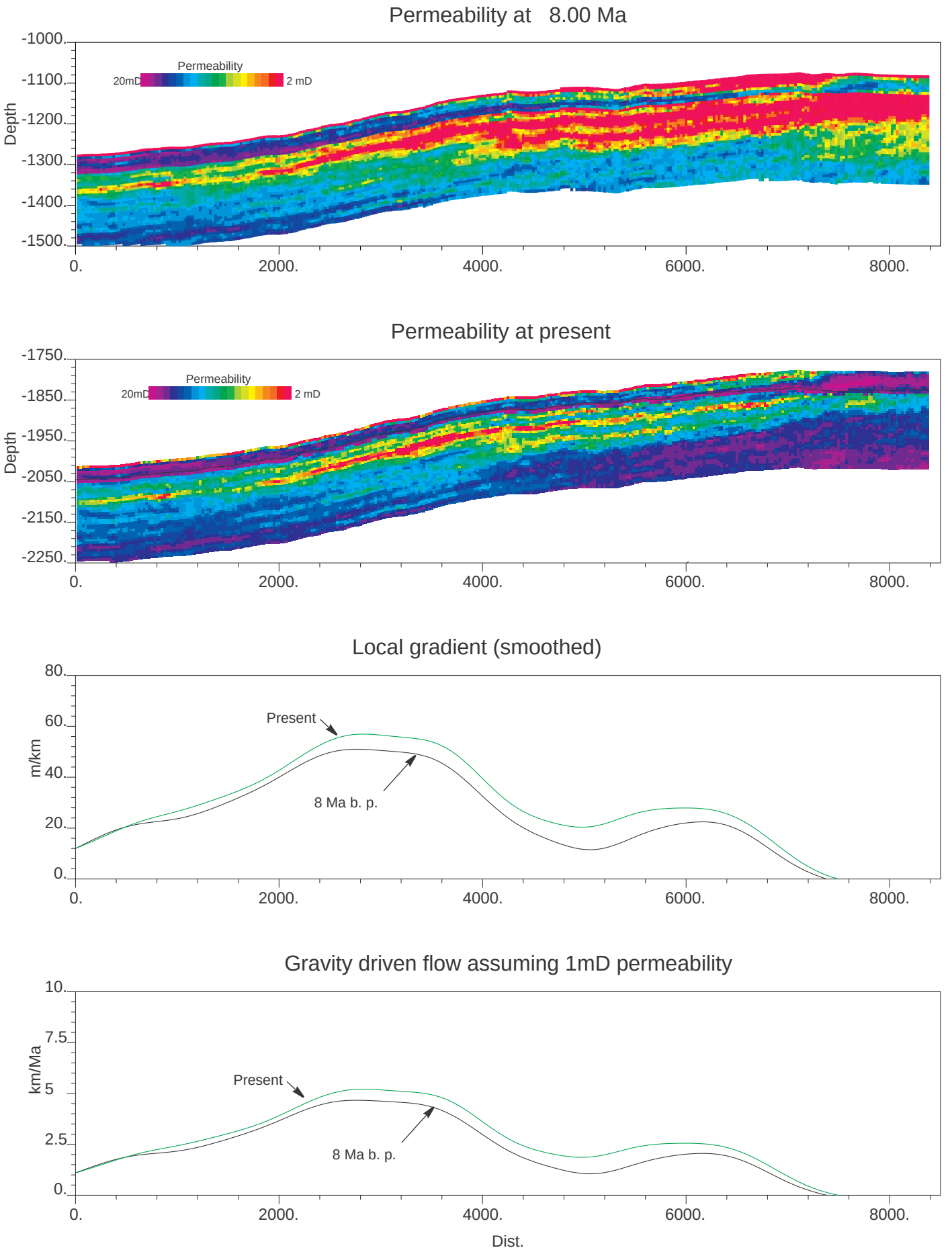
Permeability at 8.00 Ma
Permeability
20mD
2 mD
Depth
-1000.
-1100.
-1200.
-1300.
-1400.
-1500.
0.
2000.
4000.
6000.
8000.
Permeability at present
Permeability
20mD
2 mD
Depth
-1750.
-1850.
-1950.
-2050.
-2150.
-2250.
0.
2000.
4000.
6000.
8000.
Local gradient (smoothed)
m/km
80.
60.
40.
20.
0.
Present
8 Ma b. p.
0.
2000.
4000.
6000.
8000.
Gravity driven flow assuming 1mD permeability
km/Ma
10.
7.5
5
2.5
0.
Present
8 Ma b. p.
0.
2000.
4000.
6000.
8000.
Dist.

Fig. 50

7. References:

Andersen, C., Bidstrup, T., Dahl, B., Ineson, J. R., Lomholt. S., Møller, J. J., Skaarup, N. & Thomsen, E. 1998: EFP94: Sekundær migration i Central Truget. Danmark og Grønlands Geologiske Undersøgelse Report 1998/51.

Britze, P., Japsen, P. and Andersen, C., 1995(a): The Danish Central Trough: Top Chalk and the Post Chalk Group. Two-way time and depth, thickness and interval velocity, Geological Survey of Denmark, Map Series, 47, 1:200,000, 2 p., 4 maps.

Britze, P., Japsen, P. and Andersen, C., 1995(b): The Danish Central Trough: Base Chalk and the Chalk Group Two-way time and depth, thickness and interval velocity. Geological Survey of Denmark, Map Series, 48, 1:200,000, 2 p., 4 maps.

Engstrøm, F. 1995: A new method to normalize capillary pressure curves. International Symposium of the Society of Core analysts, San Francisco, 1995, SCA no. 9535, 12p.

Frederiksen, S., Nielsen, S.B., and Balling, N. 2001: Post-Permian evolution of the Central North Sea: a numerical model. Tectonophysics, 343, 185-203.

Frykman, P. 2001: Geodynamic and petrophysical modelling in the Kraka area. Danmark og Grønlands Geologiske Undersøgelse Report 2001/125, 23 p.

Gemmer,L., Nielsen, S. B., Huuse, M., and Lykke- Andersen, H. (submitted): Post-mid Cretaceous eastern North Sea evolution inferred from 3-D dynamic modelling. Tectonophysics.

Gradstein & Ogg 1996: A Phanerozoic timescale. Episodes, 19 (1,2).

Japsen, P. 1998: Regional velocity-depth anomalies, North Sea Chalk; a record of overpressure and Neogene uplift and erosion. American Association of Petroleum Geologists, Bulletin 82, 2031-2074.

Japsen, P. 1999: Overpressured Cenozoic shale mapped from velocity anomalies relative to a baseline for marine shale, North Sea. Petroleum Geoscience, 5, 321-336.

Japsen, P., 2000: Fra kridthav til Vesterhav, Nordsøbassinets udvikling vurderet ud fra seismiske hastigheder. Geologisk tidskrift, 2, 36 p.

Jensen, P. K., Holm, L. \& Thomsen, E. 1985: Modelling burial history, temperature and maturation. - In B. M. Thomas et al. (ed.): Petroleum Geochemistry in Exploration of the Norwegian Shelf. Proceedings of a NPF conf. - Graham & Trotman, PP. 145 - 153.

Kristensen, L., Dons, T., Maver, K. G. and Schiøler, P. 1995: A multi-disciplinary approach to reservoir subdivision of the Maastrichtian chalk in the Dan Field (Danish North Sea). American Association of Petroleum Geologists, Bull. 79(11).

Megson, J. & Hardman, R. 2001: Exploration for and development of hydrocarbons in the Chalk of the North Sea: a low permeability system. Petroleum Geoscience, 7, 3-12.

Michelsen, O., Thomsen, E., Danielsen, M., Heilmann-Clausen, C., Jordt, H., and Laursen, G. V. 1998: Cainozoic sequence stratigraphy in the Eastern North Sea. SEPM spec. publ. 60, 91-118.

Nielsen, L. H. & Japsen, P. 1991: Deep wells in Denmark 1935 – 1990. Danmarks geologiske Undersøgelse, Serie A, 31.

Sclater, J. G. and Christie, P. A. F. 1980: Continental stretching: an explanation of the post-mid-Cretaceous subsidence of the Central North Sea basin. - Jour. of Geoph. Res., vol. 85, no. b7., pp. 3711-3739.

Tredgett, P. and Mooney, P. 1995:: Data processing report of contiguous area. Migration project. 3D survey. Western Geophysical Company, 01/04-1995 (GEUS file no. 12967).

Thomasen, J. B. & Jacobsen, N. L. 1994: Dipping fluid contacts in the Kraka Field, Danish North Sea. SPE paper 28435, 763-772.

Vejbæk, O. V. 2000: Semi regional correlation of Maastrichtian and Danian reservoir units. Preliminary study, Contiguous Area, Confidential. Danmark og Grønlands Geologiske Undersøgelse Report 2000/70, 45 p.

Vejbæk, O. V. 2002: Reservoir characterization of the Roar Gas Field, Danish North Sea. Petroleum Geoscience, 2002, 8(1), 71-87.

Vejbæk, O. V. & Andersen, C. 2001: Post mid-Cretaceous inversion tectonics in the Danish Central Graben – regionally synchronous tectonic events?, Bull. Geol. Sec. Denmark (in press).

Williams, G.L., Brinkhuis, H., Bujak, J., Damassa, S., Hochuli, P.A., de Verteuil, L. & Zevenboom, D., 1998. In Hardenbol, J., Thierry, J. Farley, M.B., Jacquin T., de Graciansky, P.C. & Vail, P.R. Mesozoic and Cenozoic sequence chronostratigraphic framework of European basins. Society for Sedimentary Geology, Special Publication 60.